DISSERTATION

ENERGY TRANSFER INTERACTIONS WITH SINGLE MOLECULE PHENOMENA IN SMALL CLUSTERS OF QUANTUM DOTS

Submitted by

Kevin James Whitcomb

Department of Chemistry

In partial fulfillment of the requirements

For the Degree of Doctor of Philosophy

Colorado State University

Fort Collins, Colorado

Fall 2014

Doctoral Committee:

Advisor: Alan Van Orden

Elliot Bernstein
Nancy Levinger
Eugene Chen
Martin Gelfand

ABSTRACT

ENERGY TRANSFER INTERACTIONS WITH SINGLE MOLECULE PHENOMENA IN SMALL CLUSTERS OF QUANTUM DOTS

This dissertation describes the observed interactions between energy transfer in small clusters of nominally monodisperse semiconductor nanocrystals (quantum dots, QDs) and single molecule phenomena such as fluorescence intermittency (blinking) and antibunching. The relevant literature on energy transfer between QDs has typically invoked the Förster energy transfer mechanism to explain the observations in ensemble measurements. The size dispersion in QDs results in a dispersion in the electronic and optical properties of QDs due to size dependent confinement effects on photogenerated carriers. This size dispersion is thought to be the reason for energy transfer among nominally monodisperse QDs as in the single molecule work in this dissertation.

The single molecule measurements in this dissertation were done using confocal microscopy and correlated atomic force microscopy (AFM). The experimental setup is described in detail. Confocal microscopy is used to excite a small region on a surface of sparsely deposited QDs or QD clusters. This allows for observation of individual QDs or individual clusters at a time. The fluorescence from these samples is collected through the microscope objective and spatially filtered using confocal techniques, i.e. spatially filtering the fluorescence with a pinhole. The excitation region can be correlated with a nanoscale topographical image using the light that is backscattered through the microscope objective by an atomic force microscope tip. This provides an additional method for distinguishing individual QDs from QD clusters. Methods for setup, alignment, maintenance of the instruments used will be described with sample preparation and practical measurement considerations.

The interaction of energy transfer and QD blinking will be discussed in detail. The major findings are that the mechanism of energy transfer does not affect the individual blinking properties of QDs in a

cluster, nor does the close proximity of other quantum dots. The findings will also show evidence that an individual QD governs the fluorescence state of the cluster through energy transfer. The clusters in this work were primarily identified and analyzed using fluorescence properties. The threshold in clusters is not as obvious as in individual QDs so an intensity threshold is set using a model of energy transfer that sets a threshold based on the lifetime. The findings impact future studies of QD clusters and applications that utilize QDs in close proximity to each other.

The interaction of energy transfer and photon antibunching will also be discussed in detail. A simple model of energy transfer will be used to model the degree of antibunching in small clusters of QDs. The degree of antibunching observed in QD clusters is more characteristic of an individual emitter than multiple emitters which is a surprising find because it indicates that all QDs interact through energy transfer even in small nominally monodisperse aggregates. This work was done with correlated AFM to be sure that one QD or QD cluster is observed at a time. It is extremely important that only one emitter is in the excitation region because multiple independent emitters confound the analysis of antibunching and the observation of antibunching from multiple emitters heavily impacts single molecule study of QDs. Antibunching is thought to be the single definitive evidence that a single emitter is being probed but this is not so in the case of close proximity QDs even if the QDs are nominally the same size.

DEDICATION

To my family and friends that shaped me and to my mentors that guided me.

TABLE OF CONTENTS

Chapter 1

Introduction to Quantum Dots and Energy Transfer between Quantum Dots

This chapter will provide background information on colloidal quantum dots, the Förster energy transfer mechanism, literature background on ensemble measurements of quantum dot Förster energy transfer systems, and single molecule measurements on small aggregates of nanocrystals. Many ensemble measurements have found good agreement with experimental data and the Förster mechanism as an explanation for the fluorescence and fluorescence lifetime changes in films of different size quantum dots and of nominally monodisperse quantum dot films. Our work mostly corroborates these findings except that energy transfer in the systems we observe is surprisingly efficient, as evidenced by our antibunching work. Very little single molecule work has been done on small aggregates of nanocrystals and the findings on nanorods are very different from our observations of quantum dots. Our single molecule measurements are valuable because single molecule techniques can observe phenomena such as blinking and antibunching that ensemble measurements can't. Single molecule measurements can also observe the interaction of these single molecule phenomena and the energy transfer between quantum dots. Our experiments reveal strong evidence of energy transfer even among very small clusters of quantum dots (2-10) that are nominally monodisperse. The Förster mechanism requires some overlap between the emission of the donor and the absorbance of the acceptor so it is surprising that even among small clusters of nominally monodisperse quantum dots we observe evidence of efficient energy transfer. Recent work has challenged the validity of the Förster mechanism standard assumptions and may have implications for the efficiency of energy transfer that we see. This chapter will provide context with our experimental findings and ensemble measurements of energy transfer between quantum dots.

1.1 Quantum Dots

Colloidal semiconductor nanocrystals (NCs), often called quantum dots (QDs, quasispheres) or quantum rods (nanorods) are nanometer sized NCs with dimensions on the order of their bulk material's exciton Bohr radius. Colloidal NCs have stabilizing ligands on the surface that prevent the semiconductor surfaces from contacting each other and clumping into a bulk material. Quantum dots have optical and electronic properties that are size dependent, that is, the band-gap is effectively a function of NC size.[1-3] This is primarily a result of confinement effects on holes and electrons in a charged or excited NC. This effect occurs in semiconductor materials because the Fermi level occurs between bands. When the material absorbs a photon an electron-hole carrier pair forms and quickly relaxes to an excitonic state. The electron in the conduction band and hole in the valence band are essentially particles trapped in a semiconductor spherical well with the surface of the NC acting as the walls. Often there is a ZnS or other high band gap material shell around the NC raising this barrier helping to keep the carriers confined to the NC (Figure 1.1). The confinement effect adds energy to the band gap proportional to $1/R^2$ with R as the NC radius. The energy added is basically the energy term for the particle in a square well energy with n = 1 as the ground state. The higher energy states, analogous to n = 2,3, etc. are imposed on the band structure as well, but fast relaxation through phonon modes results in emission from the band edge only (Figure 1.2). The increase in the band gap from confinement is also affected by the effective mass of the confined carrier. Additional energy terms considered are the loss of solvation energy (increase in energy) and the effect of having the oppositely charged carriers closer together (decrease in energy). These terms are thought to be proportional to 1/R and do not contribute to the band-gap increase as heavily as the confinement energy. This confinement effect is not observed in metals because the Fermi level occurs within a band where there is a high density of states and the energy differences between these states is very small so even extreme confinement has little effect on the optical properties.[4] Insulators do not show confinement effects as semiconductor NCs do because the photoexcited electron is already confined to the orbital it occupies so confinement of the material around it has little effect.[4]

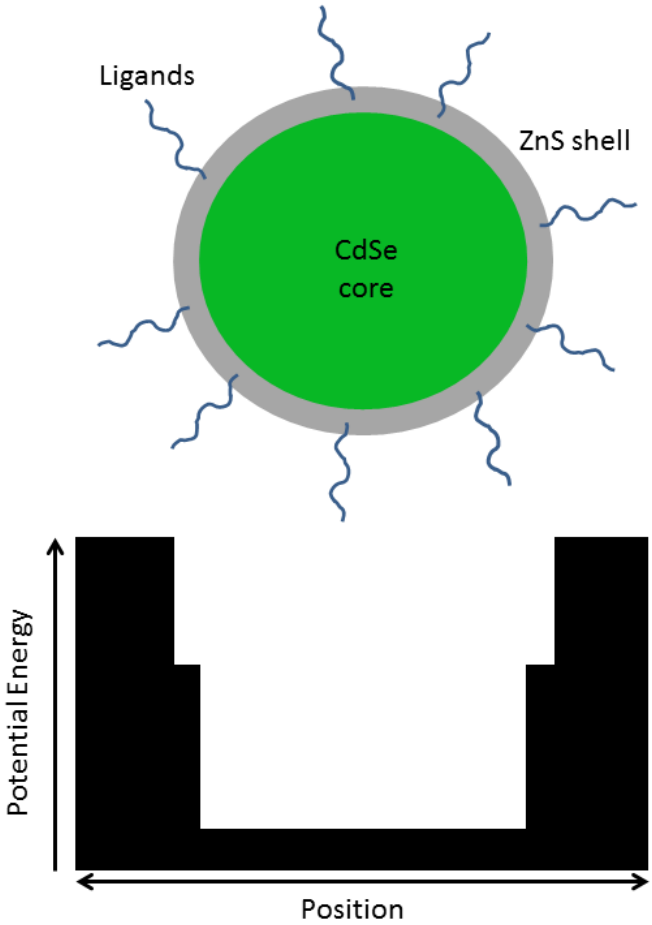

Figure 1.1: Schematic of a CdSe/ZnS core(green)/shell(grey) quantum dot with ligands (top) and schematic of a potential energy well (bottom) that a carrier such as a hole or electron would experience. This is similar to the particle in a square well potential that results in the states seen in Figure 1.2.

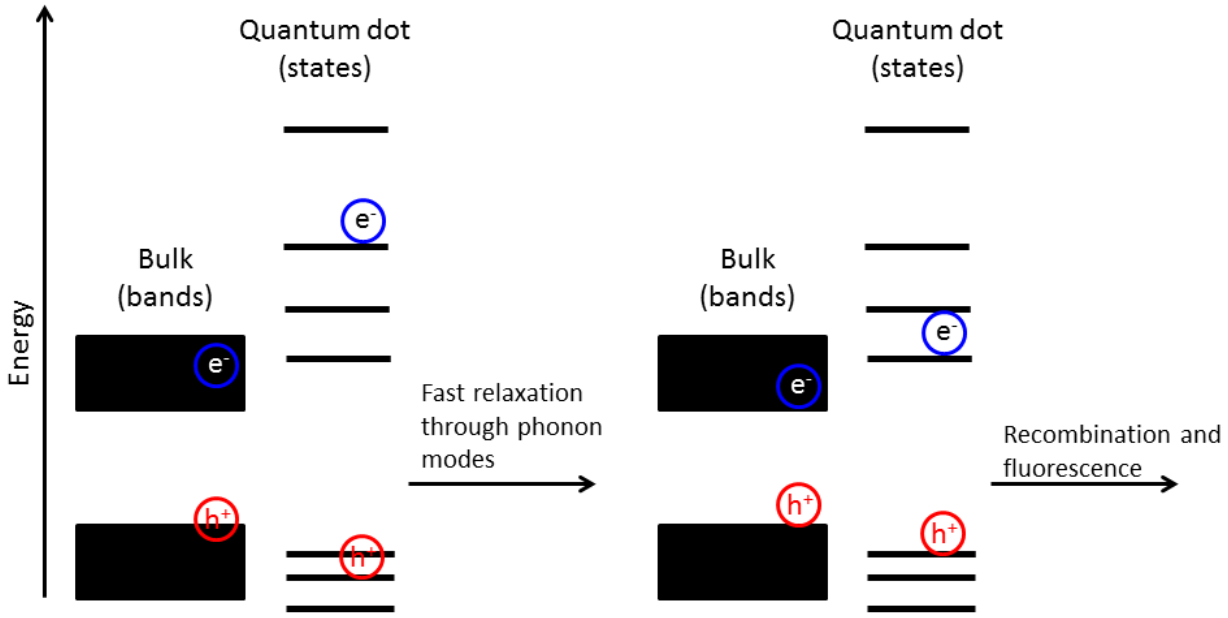

Figure 1.2: Schematic of the bands in a semiconductor (bulk) and states in a quantum dot after initial absorption of a photon (left) and after fast relaxation through phonon states to the band edge (right). Bands and states are not to scale.

There are several applications that utilize the size dependent properties of NCs such as light harvesters in solar materials,[5,6] photon detectors,[7,8] lasing media,[9-11] and biological imaging.[12] Colloidal QDs are relatively easily synthesized and deposited as films Applications, such as photovoltaics, can easily utilize colloidal QDs as opposed to embedded QDs or epitaxially grown QDs. Colloidal QDs can be dispersed easily in organic or aqueous solutions depending on the surface ligand, which keeps the QDs separate. The ligand can be exchanged with chemically different ligands which allow the QD to be dispersed in a variety of polar or non-polar solvents depending on the ligand polarity. The ligand can also be used to functionalize the QD for labeling applications. Because colloidal QDs have found many applications (vs non-colloidal QDs), my research has been exclusively on colloidal QDs and embedded and epitaxially grown QDs will not be discussed. Many applications that utilize QDs also have the nanocrystals in close proximity, such as in films, which allows for the possibility of energy transfer and other interactions between QDs. My research focuses on the interaction of single molecule phenomena and these interactions.

1.2 Förster Resonance Energy Transfer

Energy transfer between QDs and dyes,[13-15] as well as between different sized QDs[16-26] has been well studied using ensemble techniques. Often these experiments are designed such that the QD is the donor to an acceptor such as a dye or another larger QD. Because QDs have tunable emission properties, the QD can be synthesized such that its emission overlaps well with the acceptor absorption which allows for efficient non-radiative energy transfer via the Förster mechanism. Such systems are engineered Förster resonance energy transfer (FRET) systems. The FRET mechanism can be rationalized as the donor transferring an excitation by inducing a dipole in the acceptor. Most work on energy transfer between QDs has been well described by the FRET mechanism. A useful way to characterize FRET is the Förster radius, which is the distance between donor and acceptor at which it is equally likely for transfer to the acceptor to occur rather than other decay processes on the donor. The Förster radius[20]

$$R_0 = \left(\frac{9\eta\kappa^2 J}{128\pi^5 n^4}\right)^{\frac{1}{6}}$$ Equation 1.1

where R_0 is the Förster radius, η is the emission quantum yield of the donor, κ is the orientation factor for the two dipoles, n is the index of refraction of the material between the two dipoles, and J is the overlap between the normalized emission of the donor $D_{(\lambda)}$ and the absorption spectrum of the acceptor $A_{(\lambda)}$

$$J = \int \lambda^4 D_{(\lambda)} A_{(\lambda)} d\lambda$$ Equation 1.2

The FRET efficiency can be determined from the change in the relative donor and acceptor emission, change in donor fluorescence lifetime, and or from the center to center distance between the donor and acceptor. Each of these methods presents certain challenges. The efficiency can be determined from the donor emission if an emission spectrum can be collected from the pure donor and donor-acceptor system and the donor and acceptor are spectrally well separated. Assuming that all donor fluorescence quenching is a result of the energy transfer, the efficiency is

$$E_{Fl} = 1 - \frac{F_{DA}}{F_D}$$ Equation 1.3

where E_{Fl} is the FRET efficiency from fluorescence, F_{DA} is the fluorescence of the donor in the presence of an acceptor, and F_D is the fluorescence of the pure donor. Determining the FRET efficiency from donor fluorescence lifetime requires a fast time resolved signal, but otherwise is straightforward and can be determined from

$$E_\tau = 1 - \frac{\tau_{DA}}{\tau_D} = 1 - \frac{k_E}{k_E + k_T}$$ Equation 1.4

where E_τ is the efficiency from lifetime, τ_{DA} is the fluorescence lifetime of the donor in the presence of an acceptor, and τ_D is the fluorescence lifetime of the donor alone, k_E is the emission rate, and k_T is the transfer rate. This expression does not account for non-radiative decay rates. The transfer efficiency can be calculated from the distance between donors and acceptors; however, this is difficult because the

distances are typically less than 10 nm. Often FRET efficiency, determined by other means, is used to extract the distance between donor and acceptor, r, using a known Förster radius and Equation 1.5.

$$E_{FRET} = \frac{1}{1+\left(\frac{r}{R_0}\right)^6} \qquad \text{Equation 1.5}$$

This expression applies to the FRET mechanism, however, Equation 1.3 and 1.4 can be applied to any energy transfer mechanisms as long as the loss of donor fluorescence or the change in donor lifetime can be attributed to energy transfer alone. The expression for efficiency from the donor lifetime is particularly useful to our single molecule experiments where the spectra of acceptors and donors are not well resolved and very difficult to obtain due to low fluorescence signal.

1.3 Van Orden Group Research on Quantum Dot Clusters

My work has focused on single molecule measurements of small clusters of CdSe/ZnS core shell QDs. These measurements have revealed strong evidence of energy transfer among nominally monodisperse QDs (NMQDs). Yu et al.[27] first observed a faster decay in the intensity autocorrelation in clusters of NMQDs that was distinct from single QDs and well separated groups of QDs. Atomic force microscopy correlated with confocal microscopy was used to distinguish individual QDs from clusters in this experiment. Large fluctuations of cluster fluorescence were observed and termed "enhanced blinking" in this work. The fluorescence of individual QDs fluctuates (blinks) between fluorescent and completely dark states but the cluster seemingly blinked much like an individual QD instead of blinking like a group of individual QDs. Shepherd et al.[28] used similar techniques with time correlated single photon counting to observe the fluorescence lifetime during these enhanced blinking events and found a correlation between intensity and fluorescence lifetime. This led to the energy transfer model as an explanation of the blinking behavior.

The model assumes that the size dispersion among the QDs leads to band gap differences among the QDs in the cluster that allow for energy transfer among small clusters of NMQDs.[28] The lowest

energy QD in the cluster (the acceptor) can receive energy from any QD with a higher band gap (donors). When the acceptor goes into the *off* state, i.e. blinks off, any energy transferred to the acceptor is lost. Emission that comes from donors before transfer is observed but is low intensity because the transfer rate is much faster than the emission rate in QDs by about a factor of 6-10. The transfer rate can be approximately determined from the decreased fluorescence lifetime during *low* fluorescence states as described by Equation 1.4. The high fluorescence state emission primarily comes from the acceptor and so has the fluorescence lifetime of the acceptor. In Shepherd's work we were able to observe donor and acceptor emission in one experiment without spectral resolution because of the blinking of the acceptor. Two main assumptions made for the energy transfer model in Shepherd's work were that energy transfer only occurs from higher band gap QDs to lower and that the blinking statistics of the individual members of the cluster were unaffected.

In my work on QD cluster blinking[29] the assumption of independent and unaltered QD blinking in a cluster was tested. Chapter 3 contains a full discussion of individual QD and QD cluster blinking statistics and blinking memory. The fluorescence states of the cluster are controlled by the acceptor. When the acceptor is in the *on* state the cluster exhibits high emission and long lifetime and is in the *high* state. When the acceptor is in the *off* state the cluster exhibits low emission and short lifetime and is in the *low* state. Long fluorescence trajectories of clusters revealed that clusters show the same power law blinking for *high* and *low* states just as individual QDs exhibit in the *on* and *off* states for short events. Shorter truncation times were observed for both *high* and *low* states, but this was attributed to the Poisson noise at the *high*/*low* threshold. *High*/*low* cluster blinking showed blinking memory (correlations between events) that was characteristic of individual QDs. In my work on cluster blinking, I also observed lifetime blinking that had the characteristics of individual QD blinking which further supported the hypotheses that the acceptor controls the cluster blinking.

Finally, I have published a paper on antibunching observed in small clusters of NMQDs discussed in detail in Chapter 4.[29] Fluorescence is antibunched when there is a lowered probability of

observing two photons from a photon source simultaneously. Individual QDs exhibit photon antibunching because two excitations on one QD annihilate each other via fast Auger processes. A small cluster of QDs exhibits antibunched fluorescence because all members of the cluster can transfer energy to a lower band gap QD in the cluster. Most excitations end up on the acceptor, so multiple excitations transferred to the acceptor annihilate each other. The degree of antibunching in clusters is less than in individual QDs because there is a chance of emission before transfer but a cluster shows antibunching to a degree that is more consistent with a single emitter than multiple emitters which is somewhat surprising. We were able to predict the degree of antibunching using the fluorescence decay of the cluster, which is how we obtained transfer rates previously, and the energy transfer model.

Our single molecule experiments have shown evidence of energy transfer in small clusters of NMQD, but more than that, we observe the interaction of the single molecule properties of QDs with energy transfer.[28-30] Blinking and antibunching are only directly observable with single molecule techniques, and therefore, the effects of energy transfer on these phenomena are only observable with single molecule techniques. We will discuss ensemble measurements of energy transfer in designed systems of QD donor and acceptors, ensemble measurements of energy transfer between NMQDs and single molecule measurements of small aggregates of NMQDs and provide context with our previous work and my contributions to the field.[28-30]

1.4 Ensemble Measurements of FRET Designed Systems of Quantum Dot Solids

Much work has been done investigating FRET donor-acceptor systems in QD solids. These experiments have been done on large assemblies of QDs where the QDs are mixed into solid film of acceptors and donors,[16-20] or in a layer of donors organized with a layer of acceptors.[21-26] The calculations of the theoretical energy transfer rate from FRET match experimental data well in most cases, and match predicted picosecond transfer times in layered structures which is thought to be the theoretical limit in these systems.[22,24]

In reports by Kagan et al. mixed films of CdSe QD donors and acceptors were made and analyzed by small angle x-ray scattering and high resolution scanning electron microscopy.[16,17] The authors extracted the distance between QDs using the form factor obtained from the small angle x-ray scattering experiments. Energy transfer efficiency (FRET) calculations were done in part by comparing the fluorescence from a pure donor solid to a mixed solid of donors and acceptors. A Förster radius of 4.7 nm from energy transfer between 3.85 nm and 6.2 nm diameter QDs was obtained for room temperature experiments. These experiments indicate that random dipole orientations and nearest neighbor interactions are sufficient to explain the magnitude of the Förster radius in this system. The authors did not need to invoke multipole interactions or aligned dipoles to explain their findings.

Another work by Lunz et al.[19] has indicated that interactions beyond nearest neighbor need to be considered. This was based on the fluorescence decay of the donor in a 2 dimensional film of CdTe QD donors and acceptors. The authors calculated a Förster radius of 3.6 nm with 1.9 nm diameter (524 nm emission) donor QDs and 3.5 nm diameter (617 nm emission) acceptor QDs. This Förster radius was in agreement with the observed fluorescence decay with the assumption of random dipole orientations but including energy transfer interactions from QDs further than the nearest neighbor. This transfer from further (or outer shell) QDs was assumed because acceptor emission showed increasing enhancement with lower acceptor to donor ratios that continued even at very low acceptor to donor ratios, indicating that the acceptor was receiving energy from beyond nearest neighbors. Otherwise the enhancement would saturate when the acceptor was on average completely surrounded by donors. Crooker et al.[21] and Acherman et al.[22] (both of the Klimov group) came to the same conclusion based on the rate of energy transfer in films of monodisperse QDs. They found that the energy transfer extends from one or two QDs beyond the nearest neighbor (2^{nd} or 3^{rd} "shell" of donors). It is possible, given the surprising energy transfer efficiency among NMQDs we observe, that energy transfers to neighboring QDs and then to the acceptor rather than directly from QDs further away. The degree of antibunching we observe in small clusters[30] supports the idea of highly efficient energy transfer among NMQDs.

Recently work on a mixed film of CdSe/ZnS core/shell quantum dots with very careful measurements on donor-acceptor distance and experimental error propagation by Mork et al.[20] have reported experimental energy transfer rates that are an order of magnitude higher than theory predicts for random dipole interaction. The authors suggest that dipole alignment and multipole interactions could account for the large transfer rates. This result may help explain another energy transfer phenomenon in QD solids: the energy transfer among nominally monodisperse QDs. Conversely, the energy transfer among QDs of the same size may help explain the seemingly large transfer rates observed. The authors in this study compared the emission rate of QD donors in solution, instead of a solid of pure donors, to the mixed film of donors and acceptors. This effectively neglects energy transfer from donor QDs to other donor QDs that we observe and use to explain the fluorescence behavior of small clusters. This does not account for all of the nearly tenfold discrepancy in the FRET rate they observe.

1.5 Ensemble Measurements of FRET Among Nominally Monodisperse Nanocrystal Solids

Several groups have observed signatures of energy transfer in ensemble measurements of NMQDs.[21,22,31-36] Colloidal synthesis of QDs samples have unavoidable size dispersion, which results in a dispersion of the band gaps of the QDs because the confinement effects are size dependent. This dispersion in band gap energy is typically used to explain the energy transfer seen in films or aggregates of NMQDs.

The work of Crooker et al.[21] suggests that energy transfer can occur from one QD to another with a band gap disparity of 55 meV based on the fluorescence decay as a function of emission energy in CdSe QD films. The authors found that the calculated emission decay as a function of emission energy only fit experimental data when limiting transfer from donor QDs to acceptor QDs with a band gap at least 55 meV lower. Several works have shown a shift in the emission of NMQDs in films or small aggregates of about 15-30 meV.[16,21,31] The full width at half maximum of the photoluminescence signal from a sample is indicative of the energy dispersion and is typically of the order of 100 meV. As a result, any NMQD

sample with QDs in close proximity can exhibit energy transfer. It should be noted, however, that the luminescence spectrum of an individual QD inherently broad[37] and the spectra of individual QDs also changes under illumination.[38] This raises the question; are the identities of the donors and acceptors static? If the emission energy fluctuates in an individual QD then the identity, and therefore position of the acceptor, may also change. Fluorescence measurements on a small cluster of known geometry would be able to answer this question.

Koole et al.[32,33] studied NMQD molecules causing aggregation by adding linker molecules (e.g. 1,6 hexane dithiol) to a solution of CdTe NMQDs. These linker molecules bind to the surface of QDs to link the QDs together. The authors looked at the emission and absorption spectra of these aggregates as they increased the cross linker amount which created larger aggregates as confirmed by TEM measurements. The authors observed the characteristic red shift in fluorescence emission and fluorescence quenching in the larger QDs. The authors reported electronic coupling in smaller QDs in their earlier work.[32] The electronic coupling was inferred from the red shift in the absorption spectrum, which does not occur in samples where energy transfer is the only interaction. Energy transfer does not change the electronic properties of the donor QDs, so the absorption is unaffected. The emission red shifts because energy transfers to lower band gap QDs and emits from there at lower energy than if the excitation had stayed on the higher band gap QD. In later work by Koole et al. this absorption shift was found to be an effect of the ligand.[33] However, energy transfer was observed with several different ligands, several linker concentrations, and several QD sizes in the latter study.[33] Evidence of energy transfer was observable even at lower linker concentrations where dimers were at their highest concentration. This indicates that energy transfer occurs efficiently between most NMQDs even though earlier work has indicated that a substantial 55 meV difference is needed.[21] In our experiments, we observe evidence of energy transfer in all clusters of NMQDs even in small clusters where donor-acceptor possibilities are limited.[28-30]

Energy transfer has also been observed from ensemble measurements of small chains of NMQDs[31] synthesized from CdTe QDs. It should be noted that the total fluorescence intensity decreases and fluorescence lifetime shows a new shorter component in these chains that is not observed after breaking the chains up by sonication or in solutions of non-aggregated QDs.[31] The reduction in fluorescence intensity has also been observed in QD films and QD aggregates in solution.[16,32,33] The changes in fluorescence intensity and lifetime are inferred to be a result of energy transfer to non-fluorescent QDs[16,21,31] but this is only inferred because individual QD fluorescence fluctuations are only observable in single molecule experiments. We observe clearly the interaction of energy transfer and fluorescence blinking in single molecule experiments.[28,29] The single molecule properties of individual QDs themselves have been well studied which include fluorescence intermittency (blinking),[39-51] blinking memory,[52,53] spectral drift,[38] and photon antibunching.[54-59] In the context of interparticle interactions, very little single molecule work has been done on aggregates of nominally monodisperse nanoparticles.[27-29,60-62]

1.6 Single Molecule Measurements on Nominally Monodisperse Nanocrystal Assemblies

Interestingly, the changes observed in aggregates of CdSe/ZnS core/shell quantum dots (QDs)[27-29,62] are markedly different from the changes observed in CdSe/ZnSe/ZnS core/doubleshell nanorod aggregates.[60,61] The intensity autocorrelation function can be used in these systems as a gauge to how fast the intensity is changing over time. Wang et al.[60,61] have reported work on nanorods that has investigated fluorescence of nominally monodisperse aggregates of nanorods correlated with transmission electron microscopy. This correlated measurement allowed the authors to count the number of particles in the aggregates and correlate the number of nanorods to the fluorescence properties of the cluster. The authors found a slower decay in the autocorrelation with increasing nanorod number and longer *on* state times, longer truncation times for the *on* state, and no significant change in the *off* state distributions.[60,61] Our work on QDs has investigated the fluorescence properties of small QD clusters with time correlated single photon confocal microscopy correlated with atomic force microscopy. We have shown faster autocorrelation decay with clustering, evidence of energy transfer among the QDs in nominally

monodisperse aggregates, and blinking statistics with *on* and *off* state times were typically shorter, showing a shorter truncation time compared to individual QDs but otherwise very similar.[29] The blinking statistics of these two works may not be comparable because Wang et al.[60,61] set their *on*/*off* threshold using the noise of their detection electronics. They set the *on*/*off* threshold a number of camera dark count standard deviations above the background average, while we used the lifetime decay of the aggregate to set the threshold based on a model of energy transfer.[29]

It is likely that interactions between nanorods are not limited to FRET or energy transfer and may be separate all together given the differences in the blinking statistics and autocorrelation. This is even more likely when considering that the nanorod cores were 5.8 ± 0.3 nm in diameter and had an emission peak at 670. The bulk band gap of material (CdSe) is 1.7 eV,[63] equivalent to a 713 nm photon. Assuming a $1/R^2$ dependence of the confinement energy on the particle diameter, the size dispersion reported would result in single digit meV differences between nanorods in their sample. This small difference in energy does not exclude the possibility of energy transfer, but does make it less significant when considering the findings of Crooker et al.[21] were that the difference in QDs band gaps may need to be up to 55 meV for the spectral overlap required for energy transfer. The degree of interaction has been reported in ensemble measurements to be dependent on the QD size with less interaction between larger QDs.[16,32,33] However, other interactions may not be as dependent on the spectral overlap, such as the charge trapping/detrapping possibilities and exciton realignment noted by Wang et al.[61] in their work. The relationship between low confinement and low dispersion may explain why nanorods show different effects upon aggregating than QD aggregates and little evidence of the effects energy transfer observed by our group.

The work of Kang et al.[62] primarily focuses on the effects of photobleaching in dimers of CdSe/ZnS core/shell QDs that were separated from monomers and other aggregates via an electrospray technique. Their work contains many of the signatures of energy transfer between NMQDs. The authors were able to obtain time dependent photoluminescence (PL) spectra, intensity trajectories, and lifetime trajectories of aggregates with relatively good certainty in the number of QDs in the aggregate. The time

dependent normalized PL spectra of a dimer shows that when one QD photooxidizes to the point where its emission is noticeably blue shifted, only one peak maximum is observed at a time in the normalized PL spectra. If we interpret the high emission intensity from one QD and low emission from the other as evidence of energy transfer, the results observed can be rationalized as emission from the acceptor when it is in the *on* state (high red shifted emission) and low blue shifted emission is donor emission when the acceptor is in the *off* state. The energy from the donor is quickly transferred to the acceptor, explaining the low intensity and blue shift. When the acceptor is in the *off* state, any energy transferred to it is lost and no acceptor emission is observed. Emission can occur from the donor but it is low intensity because the transfer rate is typically much faster than emission in QDs. This donor emission will be blue shifted and only visible in a normalized PL spectra when the acceptor is in the *off* state as seen in the report from Kang et al.[62]

Kang et al.[62] also studied blinking in their experiments finding different statistics for different phases of photooxidation induced by high excitation intensity. Before any evidence of photooxidation they observed power law blinking statistics in dimers with long truncation times: nearly pure power law for the duration of the experiment. After individual QDs had begun to photooxidize, they observed an increase in the power law exponent. After initial photooxidation of one QD in a dimer, a much shorter truncation time was observed in the blinking statistics. It is difficult to compare these results to our work[29] because it is not clear how an *on*/*off* threshold was set and only the statistics for *on* states are reported.

1.7 Conclusions from Single Molecule Studies of Energy Transfer in Quantum Dots

Energy transfer has been observed in several systems of QDs including those with designated donors and acceptors as well as in close proximity nominally monodisperse QDs. The Förster resonance energy transfer mechanism has been used to explain the observed phenomena in ensemble measurements.[16,17,19,22-25] Single molecule measurements have been able to detect signs of energy transfer in small clusters of QDs as well as the interaction of single molecule phenomena with energy transfer

such as the enhanced blinking in clusters[27-29] as well as antibunching in QD fluorescence.[30] Our work supports the conclusions made by others on the decrease overall fluorescence of QD aggregates; that energy transfers to QDs in the *off* state.[16,31-33] There is also much support for the observation of energy transfer in close proximity nominally monodisperse QDs even in small clusters with few donor acceptor possibilities.[31-33] This could partially explain the results in QD films that require energy transfer from outer "shells" of donors[19,21,22] as transfer through donor QDs to designed acceptor QDs may not have been considered, and instead, long range transfer from further donors was implicated. The energy transfer observed among monodisperse QD aggregates is surprisingly efficient given the antibunching we observe and the evidence that a band gap difference of 55 meV is needed[21] for energy transfer. The findings of Mork et al.[20] may help explain this as they observed a FRET rate much higher than predicted by random dipole interactions.

Chapter 1 References

(1) Brus, L. E. On the Development of Bulk Optical-Properties in Small Semiconductor Crystallites. *J. Lumin.* **1984**, *31-2*, 381-384.

(2) Brus, L. E. Electron Electron and Electron-Hole Interactions in Small Semiconductor Crystallites - the Size Dependence of the Lowest Excited Electronic State. *J. Chem. Phys.* **1984**, *80*, 4403-4409.

(3) Rossetti, R.; Ellison, J. L.; Gibson, J. M.; Brus, L. E. Size Effects in the Excited Electronic States of Small Colloidal Cds Crystallites. *J. Chem. Phys.* **1984**, *80*, 4464-4469.

(4) Alivisatos, A. P. Semiconductor clusters, nanocrystals, and quantum dots. *Science* **1996**, *271*, 933-937.

(5) Nozik, A. J.; Beard, M. C.; Luther, J. M.; Law, M.; Ellingson, R. J.; Johnson, J. C. Semiconductor Quantum Dots and Quantum Dot Arrays and Applications of Multiple Exciton Generation to Third-Generation Photovoltaic Solar Cells. *Chem. Rev.* **2010**, *110*, 6873-6890.

(6) Kamat, P. V. Quantum Dot Solar Cells. The Next Big Thing in Photovoltaics. *J. Phys. Chem. Lett.* **2013**, *4*, 908-918.

(7) Konstantatos, G.; Clifford, J.; Levina, L.; Sargent, E. H. Sensitive Solution-Processed Visible-Wavelength Photodetectors. *Nat. Photonics* **2007**, *1*, 531-534.

(8) Clifford, J. P.; Konstantatos, G.; Johnston, K. W.; Hoogland, S.; Levina, L.; Sargent, E. H. Fast, Sensitive and Spectrally Tuneable Colloidal Quantum-Dot Photodetectors. *Nat. Nanotechnol.* **2009**, *4*, 40-44.

(9) Klimov, V. I.; Mikhailovsky, A. A.; Xu, S.; Malko, A.; Hollingsworth, J. A.; Leatherdale, C. A.; Eisler, H. J.; Bawendi, M. G. Optical Gain and Stimulated Emission in Nanocrystal Quantum Dots. *Science* **2000**, *290*, 314-317.

(10) Malko, A. V.; Mikhailovsky, A. A.; Petruska, M. A.; Hollingsworth, J. A.; Htoon, H.; Bawendi, M. G.; Klimov, V. I. From Amplified Spontaneous Emission to Microring Lasing Using Nanocrystal Quantum Dot Solids. *Appl. Phys. Lett.* **2002**, *81*, 1303-1305.

(11) Chen, Y. J.; Herrnsdorf, J.; Guilhabert, B.; Zhang, Y. F.; Watson, I. M.; Gu, E. D.; Laurand, N.; Dawson, M. D. Colloidal Quantum Dot Random Laser. *Opt. Express* **2011**, *19*, 2996-3003.

(12) Wang, Y. C.; Hu, R.; Lin, G. M.; Roy, I.; Yong, K. T. Functionalized Quantum Dots for Biosensing and Bioimaging and Concerns on Toxicity. *ACS Appl. Mater. Interfaces* **2013**, *5*, 2786-2799.

(13) Kim, H.; Ng, C. Y. W.; Algar, W. R. Quantum Dot-Based Multidonor Concentric FRET System and Its Application to Biosensing Using an Excitation Ratio. *Langmuir* **2014**, *30*, 5676-5685.

(14) Hoffman, J. B.; Choi, H.; Kamat, P. V. Size-Dependent Energy Transfer Pathways in CdSe Quantum Dot-Squaraine Light-Harvesting Assemblies: Forster versus Dexter. *J. Phys. Chem. C* **2014**, *118*, 18453-18461.

(15) Claussen, J. C.; Hildebrandt, N.; Susumu, K.; Ancona, M. G.; Medintz, I. L. Complex Logic Functions Implemented with Quantum Dot Bionanophotonic Circuits. *ACS Appl. Mater. Interfaces* **2014**, *6*, 3771-3778.

(16) Kagan, C. R.; Murray, C. B.; Bawendi, M. G. Long-range resonance transfer of electronic excitations in close-packed CdSe quantum-dot solids. *Phys. Rev. B* **1996**, *54*, 8633-8643.

(17) Kagan, C. R.; Murray, C. B.; Nirmal, M.; Bawendi, M. G. Electronic Energy Transfer in CdSe Quantum Dot Solids. *Phys. Rev. Lett.* **1996**, *76*, 1517-1520.

(18) Guo, L.; Krauss, T. D.; Poitras, C. B.; Lipson, M.; Teng, X. W.; Yang, H. Energy Transfer Between Colloidal Semiconductor Nanocrystals in an Optical Microcavity. *Appl. Phys. Lett.* **2006**, *89*, 061104.

(19) Lunz, M.; Bradley, A. L.; Chen, W. Y.; Gun'ko, Y. K. Two-Dimensional Forster Resonant Energy Transfer in a Mixed Quantum Dot Monolayer: Experiment and Theory. *J. Phys. Chem. C* **2009**, *113*, 3084-3088.

(20) Mork, A. J.; Weidman, M. C.; Prins, F.; Tisdale, W. A. Magnitude of the Forster Radius in Colloidal Quantum Dot Solids. *J. Phys. Chem. C* **2014**, *118*, 13920-13928.

(21) Crooker, S. A.; Hollingsworth, J. A.; Tretiak, S.; Klimov, V. I. Spectrally Resolved Dynamics of Energy Transfer in Quantum-Dot Assemblies: Towards Engineered Energy Flows in Artificial Materials. *Phys. Rev. Lett.* **2002**, *89*, 186802.

(22) Achermann, M.; Petruska, M. A.; Crooker, S. A.; Klimov, V. I. Picosecond Energy Transfer in Quantum Dot Langmuir-Blodgett Nanoassemblies. *J. Phys. Chem. B* **2003**, *107*, 13782-13787.

(23) Franzl, T.; Koktysh, D. S.; Klar, T. A.; Rogach, A. L.; Feldmann, J.; Gaponik, N. Fast energy transfer in layer-by-layer assembled CdTe nanocrystal bilayers. *Appl. Phys. Lett.* **2004**, *84*, 2904-2906.

(24) Franzl, T.; Shavel, A.; Rogach, A. L.; Gaponik, N.; Klar, T. A.; Eychmuller, A.; Feldmann, J. High-Rate Unidirectional Energy Transfer in Directly Assembled CdTe Nanocrystal Bilayers. *Small* **2005**, *1*, 392-395.

(25) Kim, D.; Okahara, S.; Nakayama, M.; Shim, Y. Experimental verification of Forster energy transfer between semiconductor quantum dots. *Phys. Rev. B* **2008**, *78*, 153301.

(26) Moreels, I.; Justo, Y.; Raino, G.; Stoferle, T.; Hens, Z.; Mahrt, R. F. Impact of the Band-Edge Fine Structure on the Energy Transfer between Colloidal Quantum Dots. *Advanced Optical Materials* **2014**, *2*, 126-130.

(27) Yu, M.; Van Orden, A. Enhanced Fluorescence Intermittency of CdSe-ZnS Quantum-Dot Clusters. *Phys. Rev. Lett.* **2006**, *97*, 237402.

(28) Shepherd, D. P.; Whitcomb, K. J.; Milligan, K. K.; Goodwin, P. M.; Gelfand, M. P.; Van Orden, A. Fluorescence Intermittency and Energy Transfer in Small Clusters of Semiconductor Quantum Dots. *J. Phys. Chem. C* **2010**, *114*, 14831-14837.

(29) Whitcomb, K. J.; Ryan, D. P.; Gelfand, M. P.; Van Orden, A. Blinking Statistics of Small Clusters of Semiconductor Nanocrystals. *J. Phys. Chem. C* **2013**, *117*, 25761-25768.

(30) Whitcomb, K. J.; Geisenhoff, J. Q.; Ryan, D. P.; Gelfand, M. P.; Van Orden, A. Photon Antibunching in Small Clusters of CdSe/ZnS Core/Shell Quantum Dots. *J. Phys. Chem. B* **2014**, *Article ASAP*.

(31) Tang, Z. Y.; Ozturk, B.; Wang, Y.; Kotov, N. A. Simple preparation strategy and one-dimensional energy transfer in CdTe nanoparticle chains. *J. Phys. Chem. B* **2004**, *108*, 6927-6931.

(32) Koole, R.; Liljeroth, P.; Donega, C. D.; Vanmaekelbergh, D.; Meijerink, A. Electronic Coupling and Exciton Energy Transfer in CdTe Quantum-Dot Molecules. *J. Am. Chem. Soc.* **2006**, *128*, 10436-10441.

(33) Koole, R.; Luigjes, B.; Tachiya, M.; Pool, R.; Vlugt, T. J. H.; Donega, C. D. M.; Meijerink, A.; Vanmaekelbergh, D. Differences in cross-link chemistry between rigid and flexible dithiol molecules revealed by optical studies of CdTe quantum dots. *J. Phys. Chem. C* **2007**, *111*, 11208-11215.

(34) Clark, S. W.; Harbold, J. M.; Wise, F. W. Resonant Energy Transfer in PbS Quantum Dots. *J. Phys. Chem. C* **2007**, *111*, 7302-7305.

(35) Bose, R.; McMillan, J. F.; Gao, J.; Rickey, K. M.; Chen, C. J.; Talapin, D. V.; Murray, C. B.; Wong, C. W. Temperature-Tuning of Near-Infrared Monodisperse Quantum Dot Solids at 1.5 μm for Controllable Forster Energy Transfer. *Nano Lett.* **2008**, *8*, 2006-2011.

(36) Williams, K. J.; Tisdale, W. A.; Leschkies, K. S.; Haugstad, G.; Norris, D. J.; Aydil, E. S.; Zhu, X. Y. Strong Electronic Coupling in Two-Dimensional Assemblies of Colloidal PbSe Quantum Dots. *ACS Nano* **2009**, *3*, 1532-1538.

(37) Empedocles, S. A.; Norris, D. J.; Bawendi, M. G. Photoluminescence spectroscopy of single CdSe nanocrystallite quantum dots. *Phys. Rev. Lett.* **1996**, *77*, 3873-3876.

(38) Neuhauser, R. G.; Shimizu, K. T.; Woo, W. K.; Empedocles, S. A.; Bawendi, M. G. Correlation between fluorescence intermittency and spectral diffusion in single semiconductor quantum dots. *Phys. Rev. Lett.* **2000**, *85*, 3301-3304.

(39) Kuno, M.; Fromm, D. P.; Hamann, H. F.; Gallagher, A.; Nesbitt, D. J. Nonexponential "Blinking" Kinetics of Single CdSe Quantum Dots: A Universal Power Law Behavior. *J. Chem. Phys.* **2000**, *112*, 3117-3120.

(40) Kuno, M.; Fromm, D. P.; Hamann, H. F.; Gallagher, A.; Nesbitt, D. J. "On"/"Off" Fluorescence Intermittency of Single Semiconductor Quantum Dots. *J. Chem. Phys.* **2001**, *115*, 1028-1040.

(41) Shimizu, K. T.; Neuhauser, R. G.; Leatherdale, C. A.; Empedocles, S. A.; Woo, W. K.; Bawendi, M. G. Blinking Statistics in Single Semiconductor Nanocrystal Quantum Dots. *Phys. Rev. B* **2001**, *63*, 205316.

(42) Kuno, M.; Fromm, D. P.; Johnson, S. T.; Gallagher, A.; Nesbitt, D. J. Modeling Distributed Kinetics in Isolated Semiconductor Quantum Dots. *Phys. Rev. B* **2003**, *67*, 125304.

(43) Knappenberger, K. L.; Wong, D. B.; Romanyuk, Y. E.; Leone, S. R. Excitation Wavelength Dependence of Fluorescence Intermittency in CdSe/ZnS Core/Shell Quantum Dots. *Nano Lett.* **2007**, *7*, 3869-3874.

(44) Pelton, M.; Smith, G.; Scherer, N. F.; Marcus, R. A. Evidence for a Diffusion-Controlled Mechanism for Fluorescence Blinking of Colloidal Quantum Dots. *Proc. Natl. Acad. Sci. U. S. A.* **2007**, *104*, 14249-14254.

(45) Frantsuzov, P.; Kuno, M.; Janko, B.; Marcus, R. A. Universal Emission Intermittency in Quantum Dots, Nanorods and Nanowires. *Nat. Phys.* **2008**, *4*, 519-522.

(46) Frantsuzov, P. A.; Volkan-Kacso, S.; Janko, B. Model of Fluorescence Intermittency of Single Colloidal Semiconductor Quantum Dots Using Multiple Recombination Centers. *Phys. Rev. Lett.* **2009**, *103*, 207402.

(47) Lee, S. F.; Osborne, M. A. Brightening, Blinking, Bluing and Bleaching in the Life of a Quantum Dot: Friend or Foe? *ChemPhysChem* **2009**, *10*, 2174-2191.

(48) Rosen, S.; Schwartz, O.; Oron, D. Transient Fluorescence of the Off State in Blinking CdSe/CdS/ZnS Semiconductor Nanocrystals Is Not Governed by Auger Recombination. *Phys. Rev. Lett.* **2010**, *104*, 157404.

(49) Vela, J.; Htoon, H.; Chen, Y. F.; Park, Y. S.; Ghosh, Y.; Goodwin, P. M.; Werner, J. H.; Wells, N. P.; Casson, J. L.; Hollingsworth, J. A. Effect of Shell Thickness and Composition on Blinking Suppression and the Blinking Mechanism in 'Giant' CdSe/CdS Nanocrystal Quantum Dots. *J. Biophotonics* **2010**, *3*, 706-717.

(50) Zhao, J.; Nair, G.; Fisher, B. R.; Bawendi, M. G. Challenge to the Charging Model of Semiconductor-Nanocrystal Fluorescence Intermittency from Off-State Quantum Yields and Multiexciton Blinking. *Phys. Rev. Lett.* **2010**, *104*, 157403.

(51) Galland, C.; Ghosh, Y.; Steinbruck, A.; Sykora, M.; Hollingsworth, J. A.; Klimov, V. I.; Htoon, H. Two Types of Luminescence Blinking Revealed by Spectroelectrochemistry of Single Quantum Dots. *Nature* **2011**, *479*, 203-207.

(52) Stefani, F. D.; Zhong, X. H.; Knoll, W.; Han, M. Y.; Kreiter, M. Memory in Quantum-Dot Photoluminescence Blinking. *New J. Phys.* **2005**, *7*, 197.

(53) Volkan-Kacso, S.; Frantsuzov, P. A.; Janko, B. Correlations Between Subsequent Blinking Events in Single Quantum Dots. *Nano Lett.* **2010**, *10*, 2761-2765.

(54) Lounis, B.; Bechtel, H. A.; Gerion, D.; Alivisatos, P.; Moerner, W. E. Photon Antibunching in Single Cdse/Zns Quantum Dot Fluorescence. *Chem. Phys. Lett.* **2000**, *329*, 399-404.

(55) Michler, P.; Imamoglu, A.; Mason, M. D.; Carson, P. J.; Strouse, G. F.; Buratto, S. K. Quantum Correlation Among Photons from a Single Quantum Dot at Room Temperature. *Nature* **2000**, *406*, 968-970.

(56) Messin, G.; Hermier, J. P.; Giacobino, E.; Desbiolles, P.; Dahan, M. Bunching and Antibunching in The Fluorescence of Semiconductor Nanocrystals. *Opt. Lett.* **2001**, *26*, 1891-1893.

(57) Santori, C.; Pelton, M.; Solomon, G.; Dale, Y.; Yamamoto, E. Triggered Single Photons From a Quantum Dot. *Phys. Rev. Lett.* **2001**, *86*, 1502-1505.

(58) Zwiller, V.; Blom, H.; Jonsson, P.; Panev, N.; Jeppesen, S.; Tsegaye, T.; Goobar, E.; Pistol, M. E.; Samuelson, L.; Bjork, G. Single Quantum Dots Emit Single Photons at a Time: Antibunching Experiments. *Appl. Phys. Lett.* **2001**, *78*, 2476-2478.

(59) Nair, G.; Zhao, J.; Bawendi, M. G. Biexciton Quantum Yield of Single Semiconductor Nanocrystals from Photon Statistics. *Nano Lett.* **2011**, *11*, 1136-1140.

(60) Wang, S.; Querner, C.; Fischbein, M. D.; Willis, L.; Novikov, D. S.; Crouch, C. H.; Drndic, M. Blinking Statistics Correlated with Nanoparticle Number. *Nano Lett.* **2008**, *8*, 4020-4026.

(61) Wang, S. Y.; Querner, C.; Dadosh, T.; Crouch, C. H.; Novikov, D. S.; Drndic, M. Collective Fluorescence Enhancement in Nanoparticle Clusters. *Nat. Commun.* **2011**, *2*, 364.

(62) Kang, H.; Clarke, M. L.; Lacerda, S. H. D.; Karim, A.; Pease, L. F.; Hwang, J. Multimodal Optical Studies of Single and Clustered Colloidal Quantum Dots for the Long-Term Optical Property Evaluation of Quantum Dot-Based Molecular Imaging Phantoms. *Biomed. Opt. Express* **2012**, *3*, 1312-1325.

(63) Liu, X.; Furdyna, J. K. Optical dispersion of ternary II-VI semiconductor alloys. *J. Appl. Phys.* **2004**, *95*, 7754-7764.

Chapter 2

Experimental Methods and Procedures for Single Molecule Measurements

This chapter is dedicated to the experimental methods used in my work and the general use and operation of the instruments. This chapter will describe the experimental setup and the components used to collect fluorescence from individual quantum dots as well as quantum dot clusters and collect correlated atomic force microscopy images of the excitation area. These are difficult experiments requiring frequent alignment and maintenance. The main challenge for optical experiments is to obtain enough fluorescence from the sample using an objective with high numerical aperture to collect fluorescence at a wide angle and very efficient avalanche photodiodes that are capable of detecting single photons at high efficiency. The objective also focuses excitation light to a diffraction limited spot on the surface. The difficulty of the optical experiments is compounded by the inclusion of the atomic force microscopy elements. The task of collecting atomic force microscopy data of nanoparticles that are ~3nm presents additional challenges to the experiment. This chapter will discuss in detail the data collection from the avalanche photodiodes and photon counting hardware and the limitations of this hardware. The optical alignment procedures and recommended frequency of maintenance will be detailed. The basic setup and tuning of the atomic force microscope will be described and procedures for correlating the atomic force microscope with the fluorescence collection region discussed. The preparation of suitable substrates for single molecule fluorescence measurements and correlated atomic force microscopy measurements will be discussed as well. Preparation of solutions of individual quantum dots and small quantum dot clusters will be described along with procedures for depositing these solutions onto suitable substrates for optical and atomic force microscopy. Finally, collection of data from individual quantum dots will be described.

2.1 Description of the Experimental Setup

The experimental diagram is depicted in Figure 2.1. The excitation source is a 453 nm pulsed laser system PDL 800-B driver and LDH-P-C 450B laser head (PicoQuant, Berlin, Germany). The laser operates typically at 0.1 mW at the aperture and 10 MHz pulse rate. The excitation beam is passed through an M-20× objective (Newport, Jessup, Maryland) into a mode locked 5405-XP optical fiber (Thorlabs, Newton, New Jersey) to select the 0,0 mode of the laser, which has one maximum. The efficiency through the fiber is typically ~25%. The beam is then collimated by an infinity corrected Achro 10× 0.40 numerical aperture collimating objective (Leica, Solms, Germany). This should form a beam that does not spread or collapse for ~5 m and is approximately 6.5 mm in diameter. The excitation beam passes through a 50/50 mirror and an HQ440/90m bandpass (Chroma, Rockingham, Vermont) laser cleanup filter to optically filter the 453 nm laser light. The beam then encounters a Z450rdc dichroic mirror (Chroma, Rockingham, Vermont) at 45° which reflects the excitation beam into the microscope objective. Ideally the beam should slightly overfill the back of the objective. The microscope objective is a 1.4 numerical aperture 40× infinity corrected Zeiss Fluar oil immersion objective (Zeiss, Oberkochen, Germany) and serves to focuses the beam to a diffraction limited spot ~0.5 µM diameter. The spot size is calculated using the radius of the Airy disc, $r_{airy} = (1.22\lambda)/(2NA)$ where λ is the wavelength and NA is the numerical aperture of the objective. This spot is focused on the top surface of the sample substrate which is scanned with a model NIS-30 SC-100/208 piezo scanning stage (Nanonics, Jerusalem, Israel) to create a 20 × 20 µm fluorescence map. The intensity in the excitation region for fluorescence measurement is typically attenuated to 15-30 W/cm^2 at the surface or ~50 nW average power for the full beam just before the microscope objective. After a fluorescence map has been created, a point of interest such as a quantum dot (QD) is selected and positioned in the excitation region. The stage is moved to maximize the fluorescence from the point. Fluorescence that is excited by the excitation spot is collected through the microscope objective and passes through the dichroic to a tube lens in the microscope that focuses the fluorescence onto a 50 µm pinhole, which spatially filters the fluorescence. The fluorescence is then split

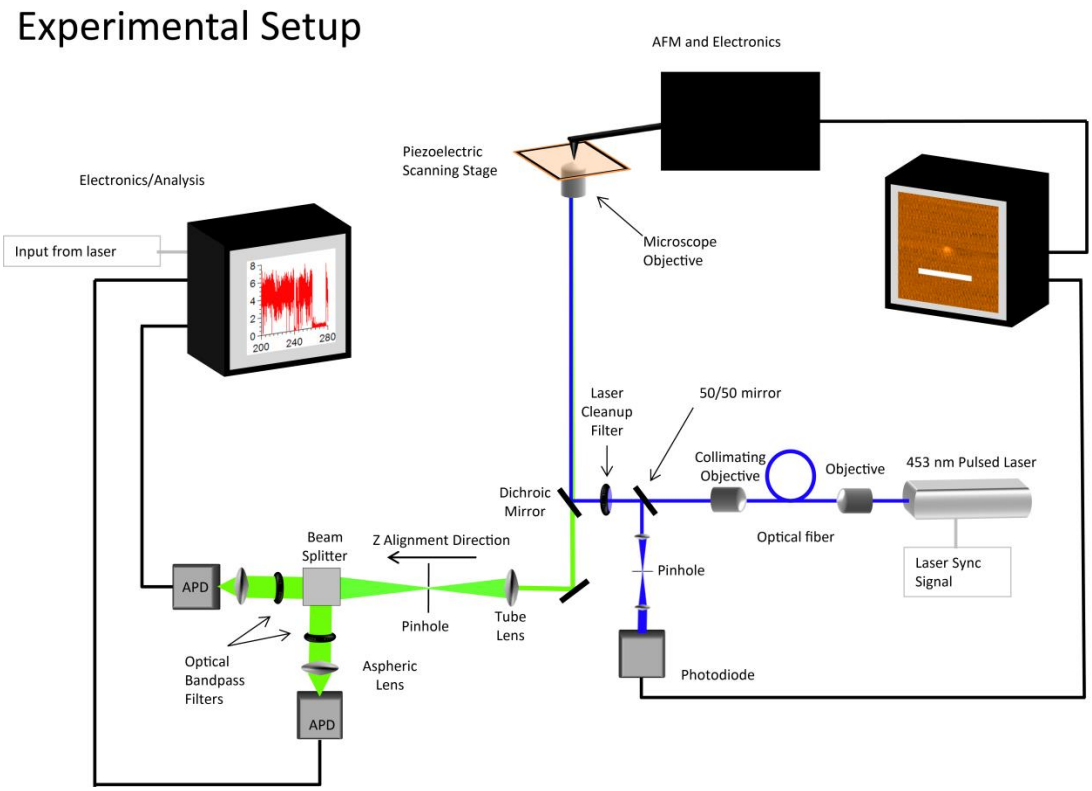

Figure 2.1: Experimental diagram of the instrument used for AFM correlated fluorescence measurements.

with a 50/50 beamsplitter through D565/40m bandpass filters (Chroma, Rockingham, Vermont) onto two avalanche photodiodes (APDs) by aspheric lenses. The APDs are τ-SPAD 50 detectors (PicoQuant, Berlin, Germany) and output a TTL (Transistor-Transistor Logic) pulse to a router connected to the Time Harp 200 photon counting hardware (PicoQuant, Berlin, Germany) for collection of fluorescence data. The detectors are also capable of outputting a NIM (Nuclear Instrumentation Module) pulse which is similar to the laser sync signal. The laser sync signal is an output of NIM pulses whenever light pulses are generated. This sync signal is used in collecting fluorescence lifetimes. The signal passes through a variable delay box to the photon counting hardware. The delay is used to time the laser sync pulses with photon arrivals because there is a delay between the electronic sync signal and detector TTL pulse.

After fluorescence measurements are completed, an atomic force microscope can be used to observe the topography of the surface. The Bioscope II atomic force microscope (AFM) Dimension head (Digital Instruments) is mounted above the scanning stage. The excitation beam should be unattenuated (20 μW after the fiber) to observe the AFM backscatter, as the photodiode for the backscatter detection is not extremely sensitive. The APDs should be turned off as they could be damaged at this excitation intensity. After fluorescence measurements are completed, the AFM is engaged by bringing the AFM tip within 0.5 mm of the surface and beginning the auto approach procedure with the AFM software Nanoscope V5.12 software (Digital Instruments). The AFM tips are OTESPA model AFM probes with 40 N/m force constant and 270-350 kHz tapping frequency (Bruker, Camarillo, CA). Typically a 5-10 μm scan is collected to find the excitation region. When the AFM tip passes over the excitation region more excitation light is reflected back through the objective. This light hits the dichroic mirror at 45° and passes through the laser cleanup filter to the 50/50 mirror. The backscattered light is then focused onto a 100 μm pinhole to spatially filter the backscatter and then focused onto a photodiode. The photodiode signal is sent to a Stanford Research Systems SR844 RF lock-in amplifier. The lock-in amplifier amplifies signal at the tapping frequency of the AFM tip, enhancing only signal that is backscattered by the tip. This amplified signal is collected with the topographical data from the AFM measurement with

the Nanoscope V5.12 software to create correlated concurrent topographical and backscatter images (Figure 2.2). The magnitude of the lock-in filtered backscatter signal depends on the intensity of the backscattered beam, size/shape of the AFM tip, and phase of the lock-in amplifier.

2.2 Data Collection and Hardware Limitations

This section will describe the photon detection electronics and their limitations such as the resolution and dead times. The time-tagged time-resolved reverse start stop electronics are described with the different data acquisition schemes for the standard setup and Hanbury Brown-Twiss interferometer configurations that can be used with the hardware.

The stage software and data collection software cannot concurrently use the photon counting hardware so the stage software detection should be disabled before opening the data collection software; Symphotime V. 5.3.2.2 (PicoQuant, Berlin, Germany). The data collection software and photon counting hardware create time-tagged time-resolved (t3r files) data files. The data is stored in such a way that the photon arrivals relative to a laser sync pulse, as well as the photon arrival relative to a system clock are both collected. This data storage scheme allows for a reconstruction of the intensity trace as well as nanosecond scale lifetime data that can be parsed to examine the lifetime of portions of the trace or even individual photon bins in a fluorescence trajectory. The hardware also operates in a reverse stop start method so that data is only taken if a photon starts the clock and the laser sync output stops the clock. The photon counting hardware requires ~100 ns to prepare for another event so coincident events occurring with the "dead time" are not recorded. The setup can be configured to work around this but this requires sacrificing other data.

The system can be set up as a Hanbury-Brown Twiss interferometer which can measure antibunching and collect correlated photon histograms. This is done by replacing the laser sync output with the NIM pulse from one of the detectors through a ~100 ns delay. The TTL output of that detector should be disconnected. This configuration only records photons that arrive within the time window

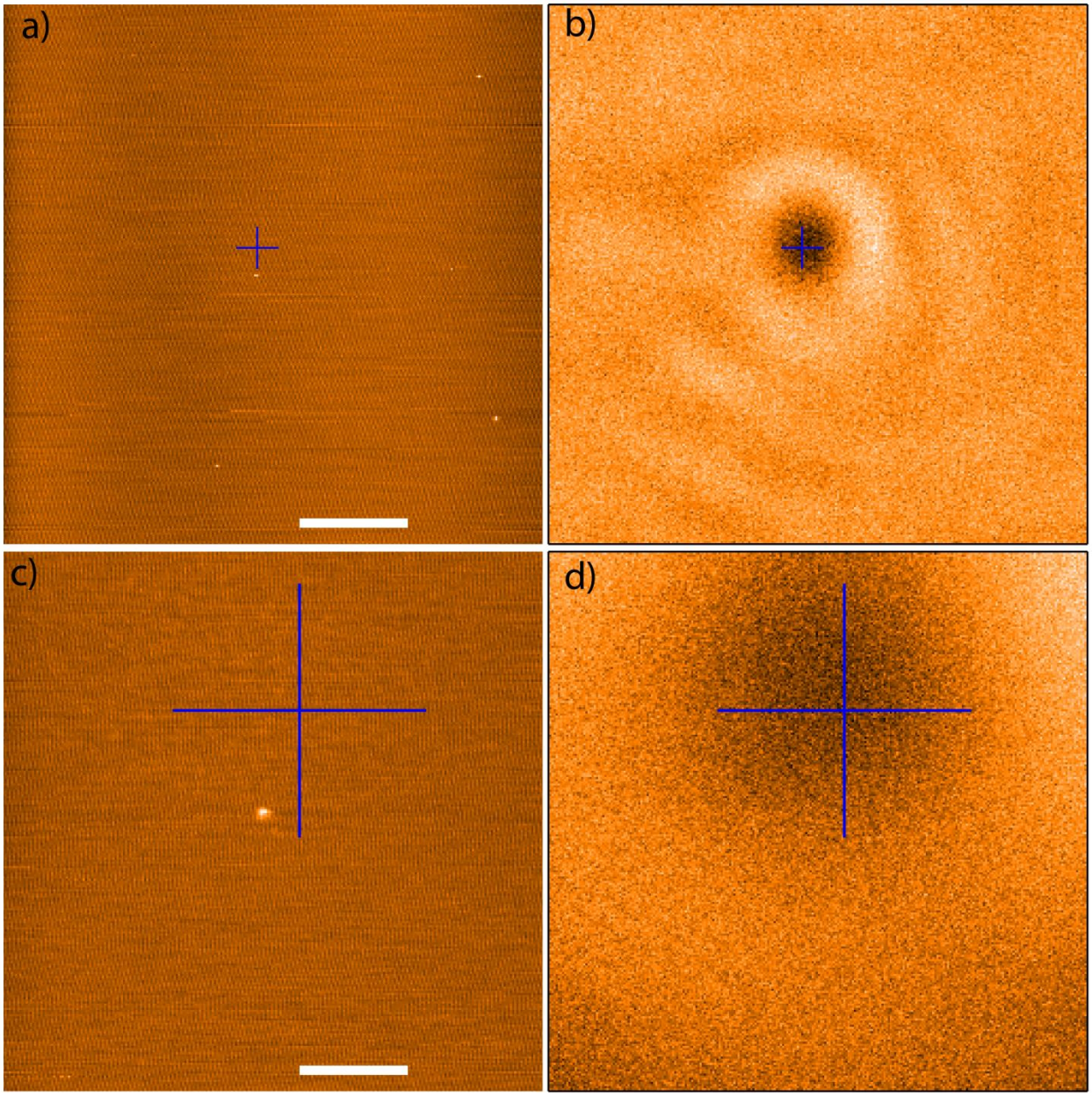

Figure 2.2: Correlated topographical images (left) and excitation region backscatter (right). The topographical region in a (scale bar 1 μm) is correlated with the backscatter image in b. The topographical image in c (scale bar 200 nm) shows a cluster of QDs in the excitation region d and is a smaller scale image of the a-b pair. The blue markers show the same point in a-b and c-d. Section 2.5 shows how to correlate the microscope to obtain images like these.

determined by the resolution of the photon counting hardware. The hardware has a limited amount of memory, ~4000 points, to log times. If the resolution of the hardware is set to .144 ns, then the time window for the card is ~ 570 ns. Because the system can only log coincident events, the majority of the intensity data is lost and lifetime data cannot be collected directly. The lifetime data can be obtained from fitting the correlated photon histogram but this histogram is heavily weighted toward higher intensity data. Data from low intensity signals does not contribute significantly to the correlated photon histogram so the lifetime data of relatively low intensity events is difficult to obtain in this configuration.

The APDs also have dead times of ~200 ns. If a second photon arrives at the detector within the dead time after the first photon it is not possible for the detector to trigger again within that time. The resolution of the lifetime measurements are currently limited by the APDs. The laser pulse is ~70 ps, the photon counting hardware resolution can be set to 32 ps, but the APD response time full width at half maximum (FWHM) is typically 0.5 ns.

2.3 Optical System Alignment Procedures and Maintenance

The following section contains procedures for aligning the confocal microscope for fluorescence measurements. Procedures are presented in the order in which they need to be completed or in working order and the frequency at which they should be done is stated.

The mode selecting fiber should be cut using a S90R ruby fiber cutter (Thorlabs, Newton, New Jersey). The plastic coating needs to be removed exposing ~2 cm of the bare glass fiber from each end of a ~30 cm fiber. Each end needs to be cleaved cleanly. An end of the stripped fiber should be taped to a clean surface and pulled taught. While the fiber is pulled taught a fiber cutter is used to nick the exposed glass fiber. When the fiber is nicked, it should break and leave a clean flat end. If this is done correctly, light that comes out will be symmetrical and circular. The fiber should not need to be re-cut or cleaned unless it has been damaged or soiled. The fiber is delicate but should not typically come into contact with anything. The excitation beam should be aligned into the fiber each day it is used. The laser beam out of

the laser aperture is reflected by steering mirrors into an M-20× objective (Newport, Jessup, Maryland) that focuses the beam into the fiber. The objective and fiber need to be positioned to maximize the efficiency through the fiber. The angle and position of the incoming beam can also be adjusted with the steering mirrors to increase the efficiency through. For a beam that is not inherently 0,0 mode, 25-30% efficiency through the fiber should be achievable.

Collimation of the beam should not need to be adjusted on a routine basis and should be stable for weeks/months. The end of the fiber should be mounted in front of the Achro 10× 0.40 numerical aperture collimating objective and positioned near the focal point of the objective using a mount. The objective should remain fixed in one position, pointed toward the steering mirrors. To collimate the beam, the fiber is pointed into the objective and the beam coming out is measured right at the exit and at a far distance (~5 m) from the collimating objective using a mirror to reflect the beam to a far point. The beam should also be traced to make sure that it does not focus at any point between the two measurements. The goal is to make sure the beam is the same size at all points, and thus is collimated by adjusting the distance between the fiber and objective by adjusting the mount of the fiber.

The collimated beam is steered into the microscope with two steering mirrors to adjust the symmetry and position of the excitation region. The symmetry of the excitation region should be checked each day the microscope is used and adjusted accordingly. The 50/50 mirror and laser cleanup optical filter should be in place so that their effect on the beam position is accounted for. The goal of this alignment is to direct the excitation beam straight into the objective from the dichroic mirror such that the reflection of the excitation region from the surface of a glass coverslip (observed by a camera) is a symmetric pattern. The objective is moved above and below the surface to check this symmetry. If the spot on the surface is not circular or exhibits astigmatism the fiber may not be clean or properly cut. Some astigmatism is acceptable. The steering mirrors should be adjusted to position the excitation region in the center of the camera and to change the angle of approach such that the reflection from slightly above the surface is nearly identical to the reflection from slightly below.

The Z alignment of the fluorescence spatial filter pinhole should not need to be frequently adjusted and should be stable for months. It will need to be adjusted anytime the collimation changes. The Z direction will be designated as the propagation of the fluorescence signal. The X and Y directions are orthogonal to this direction (Figure 2.1). This alignment is completed using a dilute solution of QDs and fluorescence correlation spectroscopy (FCS). This alignment also requires that some light be correctly aligned into the APDs through the pinhole. This may require using a solid film of QDs on a cover slip to produce light visible to the eye that can be aligned into the inactive APDs before attempting this alignment. A dilution of 1:1000 of the stock 5 mg/mL QD solution should be prepared in an organic solvent, such as toluene (see QD solutions preparation). A 100 µL aliquot of this solution should be placed in a specialized sample container. This container is made of a 1 mL clear shell vial, part number 66015-702 (VWR, Radnor, Pennsylvania) that is open at both ends and affixed to a coverslip with dried sodium silicate (Fisher Scientific, Batavia, Illinois) such that a coverslip window into the solution is available. The QD solution is added to the container and is sealed. Immersion oil (oil objectives only) is applied to the glass window and placed above the objective. The excitation beam should then be focused deep into the solution with excitation power ~50 nW. The pinhole X and Y position should be adjusted to maximize fluorescence received by the APDs. Each APD X and Y position should be adjusted to further maximize the fluorescence received. Several iterations of alignment between the pinhole and detectors should be made before proceeding. Once the fluorescence is at a relative maximum for both APDs a 5 minute measurement should be collected with the Symphotime software. An autocorrelation analysis should be performed on this data to obtain an FCS curve. This correlation vs t (time) curve should be fit to the function $(1/(1+t/\tau_d))(1/N)$ where τ_d is the diffusion time and N is the number of emitters in the probe region on average. When the pinhole is well aligned in the X, Y, and Z directions, the τ_d will be at a minimum and the fluorescence will be at a maximum. It is more reliable to use the τ_d for this alignment instead of the intensity. The Z of the detectors should be adjusted to maximize fluorescence after some progress has been made minimizing the τ_d. The pinhole Z positon should be adjusted by a small amount for each iteration and the X and Y position of the pinhole and detectors should also be adjusted after each

pinhole Z position adjustment. The τ_d should about 500 μs in a toluene solution with a 50 μm pinhole for a suitable alignment. The τ_d is sensitive to anything that effects the diffusion through the excitation region. The excitation region is at its smallest at the focal point of the objective, and therefore, the smallest τ_d and most fluorescence are obtained when the pinhole is exactly at the focal point of the tube lens because only light from the focal point of the objective makes it through the pinhole. The detector Z position should be adjusted one more time to produce a steep left hand edge (fluorescence rise signal) in the fluorescence decay histogram. The limit of the steepness is dictated by the response time of the detector.

The APD detectors and pinhole (fluorescence spatial filter) X and Y should be aligned each day that the instrument is used. For this alignment, a small amount of severely attenuated laser light is used. The band pass filters should be replaced with neutral density filters with an optical density of 2 (a factor of 100 reduction for the whole visible spectrum) and the laser intensity into the microscope should be ~5 μW. The excitation beam should be focused onto the surface of a glass coverslip using the camera. The reflection off of the surface is used to align the pinhole and detectors. The pinhole X and Y positions should be adjusted to maximize the signal. When the excitation laser is focused tightly onto the center of the active area in the APD, the response from the APD is the fastest, i.e. the FWHM of the APD response to the laser is at a minimum. The X and Y positions for each detector should be adjusted to minimize the FWHM of the response to the laser. Once this has been completed, a 1 min measurement of this response should be collected as the instrument response function (IRF, Figure 2.3). This is the final alignment for fluorescence measurements and the instrument is ready to collect fluorescence data when the 560 nm bandpass filters are back in place.

2.4 Atomic Force Microscope Maintenance and Operation

This section describes the suitable parameters used for the AFM and brief troubleshooting information for common problems encountered. This section should allow a user to properly set up the

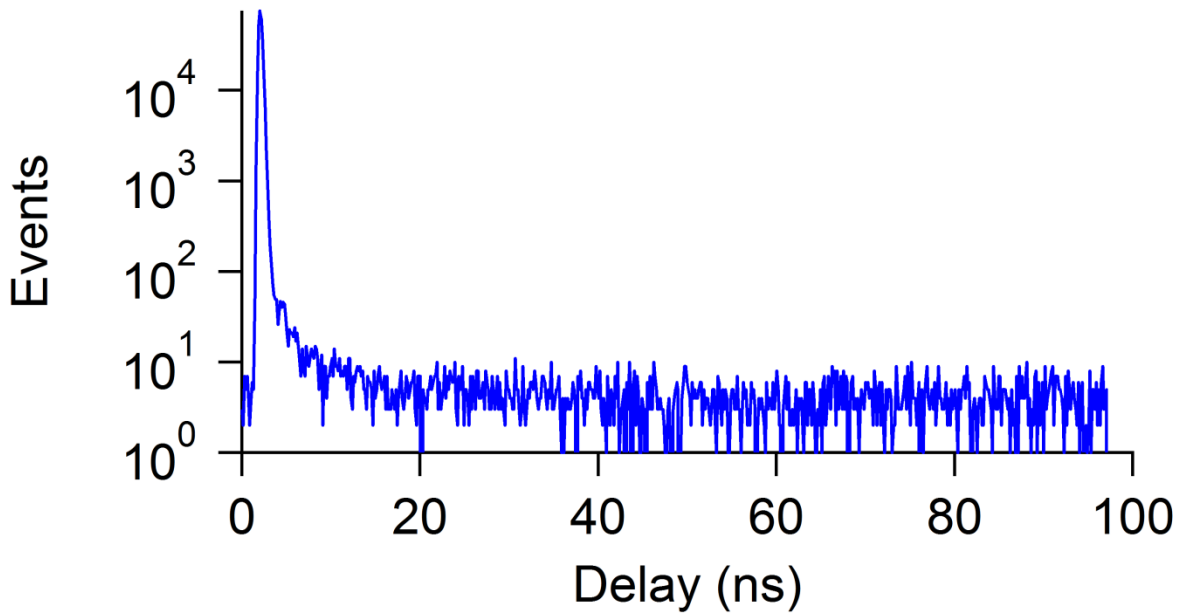

Figure 2.3: Instrument response function (IRF) of the optical system. A small amount of laser light is allowed to reach the detectors to observe the fastest response of the system. Typically the width of the IRF peak is limited by the time resolution of the detectors. Smaller peaks can be seen approximately 3 ns after the main peak. These are reflections in the system.

AFM and tune a new tip as well as identify when a tip needs to be replaced or scan settings need to be adjusted.

The AFM is mounted above the piezo scanning stage. The instrument is operated with Nanoscope V5.12 software (Digital Instruments) in tapping mode. The AFM tips should be changed whenever artifacts are seen in observations of glass coverslips (Figure 2.4) or if a suitable tune cannot be found for the tip (discussed later). A fresh tip is mounted in the tip holder using the AFM tip holder mount. The tip holder is placed in the mount inverted. A sliding metal chip holds the AFM cantilever in place in the holder. A fresh tip should be placed in the groove on the tip holder and secured with the sliding metal chip. The tip holder can now be placed on the piezo stack of the AFM.

Once the tip holder is mounted on the piezo stack the red AFM laser needs to be aimed at the very end of the cantilever where the deflection is highest using the knobs on top of the AFM head. When the laser is nearly aimed correctly a red dot will appear on the window on the AFM head. There is a dot that appears if the laser is aimed too far toward the base of the cantilever. This is a false positive and can be identified by its non-responsiveness to the lateral aiming direction (the direction perpendicular to the length of the cantilever). When in the correct position, the lateral movement of the spot in the AFM head window is fast. The correct position for the laser on the cantilever is as far out toward the tip of the cantilever while maintaining a "sum signal" of ~2 which is displayed by the software. The sum signal is the total amount of signal received by the AFM photodiodes. There are 4 split diodes that monitor the position of the deflected laser beam. When the laser is aimed correctly at the end of the cantilever, the directing knobs (side of the AFM head) are use to aim the deflected laser into the center of the diodes. Most importantly the vertical deflection should be below 0.1 V.

The system must be tuned to the resonant frequency of the cantilever. This frequency can be found from the software auto tune function. The software will scan through a range of frequencies to find the maximum oscillation response and offset from the maximum. The software monitors the oscillation in

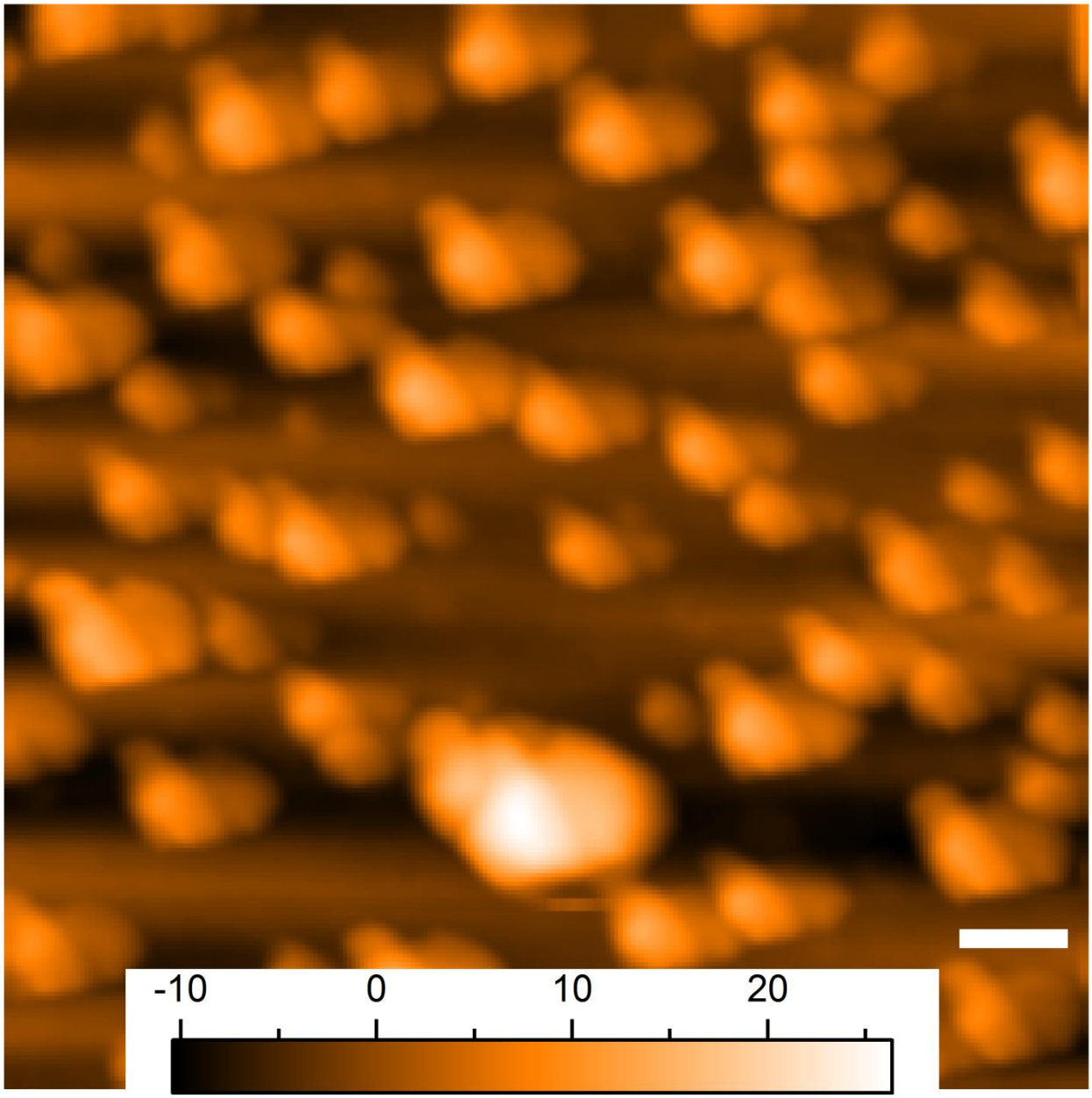

Figure 2.4:AFM image of a glass coverslip showing a tip artifact. A repeating shape on a glass coverslip is the damaged tip's shape. The scale bar is 100 nm and color scale in nm.

the vertical deflection and displays the root mean square (RMS) of the oscillation amplitude. The amplitude that the software tunes to is set by the user in the software (2 V for QD measurements) and is called the setpoint amplitude. The drive amplitude is the voltage that the piezos are driven to achieve the setpoint amplitude. If a tip is mounted correctly, it should have a drive amplitude of 50-150 mV. A drive amplitude of up to 250 mV can be used but efforts should be made to remount the tip if this is the case.

The AFM obtains topographical information by scanning the tip over a surface and adjusting the height in response to a decrease in the amplitude of the oscillation. The feedback gains for measurements of QDs should be set very low (0.15 integral gain, 4.0 proportional gain). If gains are too high, the tip will oscillate over the surface with a high amplitude (sinusoidal noise) because the instrument is adjusting too much for small changes. If the gains are too low, the tip will not adjust the height quickly enough when passing over sudden changes in height creating what will look like streaking in the direction (fast scan axis) of the scan because the instrument is not responding fast enough.

To engage the tip and collect an image from a surface the tip should be lowered to just above the surface (less than 0.5mm) and allowed to approach the surface using the software auto-approach. The tip is most likely to be crashed during the manual lowering. The software will lower the tip until a point where the free oscillation amplitude is sufficiently interrupted. This should take less than 5 minutes. A large scan (5-10 μm) should be taken first. Large scans typically have a parabolic error, i.e. the swing of the instrument causes a flat surface to look like a parabola. The instrument is reliably measuring a surface if the trace and retrace of a line match each other well. If the line scans in two directions deviate, the instrument is likely not actually responding to a surface. This is most apparent in large scans. Small scans (500 nm) suffer from drift and must continuously be adjusted to keep small objects of interest in the measurement area. A glass coverslip is an easy to observe surface to troubleshoot AFM issues. The surface of a coverslip typically has several large and small features and, as a result, can't be used for QD AFM measurements. However, if these features are observable with none of the previous mentioned errors, they AFM should be in good working order. Often it is difficult to distinguish between AFM

instrument issues and sample issues so coverslips provide an easy to measure surface for the instrument. In addition, if all objects on a glass coverslip surface have a non-circular shape, the tip has likely been damaged and the shape viewed is the shape of the damaged AFM tip (Figure 2.4).

2.5 Correlating the Atomic Force Microscope with the Excitation Region

This section will describe how to obtain correlated images as in Figure 2.2. The alignment of the backscatter, initial and final positioning of the microscope near the excitation region, and adjusting the phase to find the backscatter spot will be described.

The backscatter alignment into the photodiode through the pinhole is straightforward. While the excitation beam is focused on a glass coverslip, the reflected beam (off the surface and 50/50 beamsplitter) is sent through 2 focusing lenses onto the photodiode. Using an oscilloscope and the photodiode, the intensity of the light should be maximized by adjusting the position of the photodiode into the focal point of the 2^{nd} lens. When this is maximized, the 100 μm pinhole is placed at the focal point of the 1^{st} lens. Adjust the pinhole X and Y positions to maximized light through the pinhole.

A low magnification microscope objective should be used to begin the alignment of the AFM with the excitation region. This will allow a wider view to observe the position of the AFM cantilever relative to the excitation region on the system camera. Two positioning knobs on the AFM (near the stage) move the AFM head relative to the surface and microscope objective. The AFM head should be lowered to just above the surface. A light should be used to illuminate the cantilever and surface from above so that the shadow of the cantilever is visible on the surface. The positioning knobs are used to position the tip of the cantilever shadow near the excitation region. The AFM should then be engaged on the surface and the scan size set to 1 μm or less. If the position of the cantilever tip is not directly over the excitation, retract the AFM tip and position it just above the surface again and move the head using the positioning knobs closer to the excitation region. When the AFM tip touches down close to the reflection of the laser spot, withdraw the AFM and replace the wide view objective with the microscope objective

used for fluorescence measurements. If the excitation region is within 10 μm of the 0,0 X Y offset point of the AFM, the rest of the alignment can be done using the backscatter signal. A concurrent topographical and backscatter image should be collected (10 μm). If the backscatter spot is found, set the offset positions of the AFM to center the backscatter spot. If the spot cannot be found, the phase should be adjusted 45-90° to make sure the phase was not ~90° from the signal resulting in no backscatter signal.

2.6 Sample Substrate Preparation

This section will describe the properties of suitable substrates for optical measurements, AFM measurements and how to prepare these substrates. The pre-measurement treatment of the mica surface for AFM will also be described.

There are several key aspects of sample preparation for successful measurements using confocal microscopy. The substrate or surface on which the QDs are deposited needs to be clean, thin, transparent, and flat on the micrometer scale. Glass coverslips fit these requirements well, particularly Fisher Finest 12-548C. The substrate must be clean so that the top surface does not have fluorescent unknowns that interfere with the measurement and the bottom surface does not foul the immersion oil or the objective. The substrate must be thin such that the objective can focus on the top surface. High numerical aperture objectives typically have very low working distances (approx 200 μm) so focusing on the surface of a thicker substrate will not be possible. The substrate must be transparent to both the excitation beam as well as the emission signal of the sample. Absorption or reflection of either reduces signal. The surface must be relatively flat on the micrometer scale for optical measurements so that different portions of the sample are not too far from the focused excitation beam, i.e. one part of the measurement will be at a higher point that the other and will not receive equal excitation and will suffer from poor collection. Atomic force measurements require much higher flatness as will be discussed in this section.

Samples prepared for correlated AFM measurements require a very thin mica substrate that is affixed to a glass coverslip described above. Large slides of mica ~10 × 10 mm^2 can be cut into thinner

smaller chips of mica. These are cut from a bulk slide of muscovite grade V1 mica (TED Pella, Redding, California) with a sharp implement such as a razor blade. Mica is used because it is extremely flat and relatively transparent. The mica should be cut such that it does not appear to have a yellow or brown color. If the mica has a visible yellow or brown color it is too thick but can be thinned after being affixed to a glass coverslip. The glass coverslip and mica chip should be cleaned with spectrophotometric grade methanol (Alfa Aesar, Ward Hill, MA) and dried. Optical adhesive should be applied in very small amounts to the class coverslip (less than 10 µL) and shaped to match the shape of the mica chip to be affixed. The UV Norland 81 (Norland Optical, Cranbury, New Jersey) can be used. The flattest side of the mica chip (no visible fractures or breaks) should be placed face down onto the adhesive. The coverslip and chip should then be heated over a hotplate to wick the adhesive out to all sides of the chip. The mica chip and glass coverslip should then be cured with a UV lamp for ~30 minutes with the mica chip facing up. The substrate should then be exposed to intense visible light (white light) for 30 minutes as well to bleach the mica and adhesive. This will result in less optical noise during measurements. These prepared surfaces should be stored on clean lens paper or Kim wipes, glass side down.

Immediately before deposition of QDs on the mica, the surface of the mica should be freshly cleaved with tape and treated with 3-aminopropyltriethoxy silane (APTES). The APTES should be stored in a refrigerator in a sealed bag to keep it from air exposure while not in use. Tape is applied to the surface of the mica and removed to pull off a thin layer leaving a fresh cleaved clean mica surface behind. The mica pulled off by the tape should be flat, smooth, and unbroken. This can be done multiple times to a single mica substrate. This cleaving method can also be used to thin mica substrates that were prepared too thick. The freshly cleaved mica is then placed in a vacuum desiccator with 30 µL of heated APTES and evacuated of air for ~15 minutes. This treatment will apply a submonolayer of APTES to the mica that allows QDs and QD clusters to “stick” to the surface. The APTES can be observed with AFM (Figure 2.5). After the mica has been treated with APTES it should be used within 1-2 hours and stored in a container with a lid on top of lens paper or Kim Wipes to prevent dust from settling on the surface.

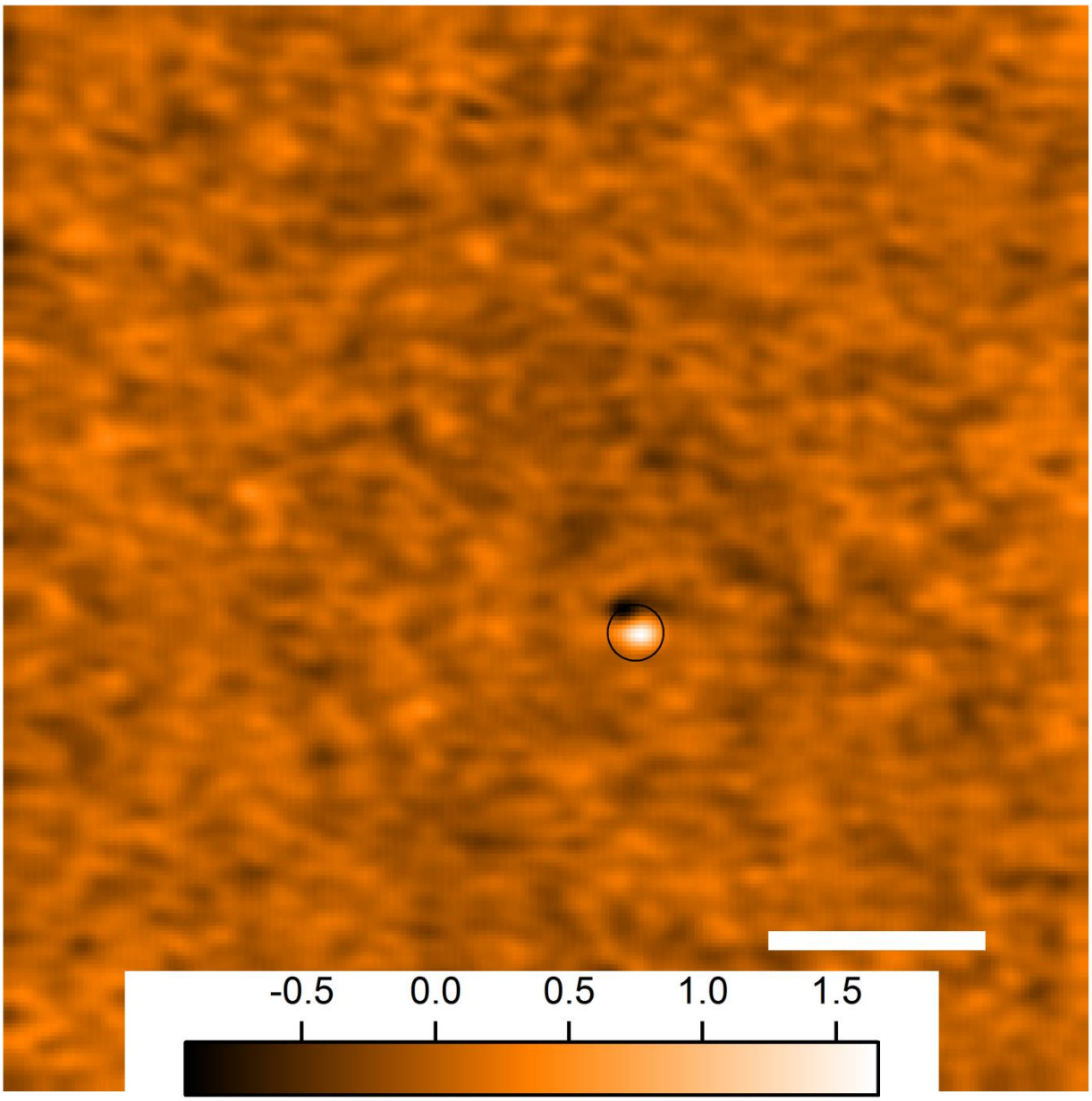

Figure 2.5: An AFM image of an APTES treated mica surface with a quantum dot (circled). The APTES makes an irregular very low pattern that can only observed with low gains and a system in good working order. Bare mica, in comparison, is featureless and flat on the angstrom scale. The scale bar is 100 nm and color scale in nm.

2.7 Deposition of Quantum Dot Samples on a Substrate

This section will describe the preparation of QD solutions for dispersal on suitable substrates and the factors that affect the surface coverage. The solutions must be kept clean and free of contaminants and dust, particularly from plastic surfaces. This section will also describe deposition of the solutions on suitable substrates using a spin coater.

Solutions of 560 nm emission CdSe/ZnS core/shell QDs (Ocean Nanotech, Springdale, AR) for depositing onto a substrate for measurements should be made in spectrophotometric grade solvents, e.g. toluene. Quantum dots with organic capping ligands will disperse in most non-polar organic solvents. Autoclavable caps and glass should be used whenever possible when handling/storing solvents for these solutions. Caps that are not solid plastic should be avoided as they can contaminate the solution and affect fluorescence properties with the adhesives used to hold the cap together. Autoclavable caps do not have such adhesives. Plastic containers and pipette tips will contaminate the solution with dust which will affect AFM measurements. The stock solution of QDs should be kept cold but not below 0° C and as isolated from air as can reasonably be achieved. This QD solution is typically ~5 mg/mL. Two ~1:1,000 dilutions should be made into 1 mL of spectrophotometric grade solvent using a 1 µL glass capillary for a total dilution of 1:1,000,000. This solution should be used for deposition onto a substrate immediately (within 0.5 hours). Quantum dot clusters are made by adding a small amount of methanol (5-10 µL) to 1 mL of a higher concentration QD sample (4:1,000,000 instead of 1:1,000,000 QD dilution) and allowing the mixture to sit for ~10 minutes. These parameters may depend on the solvent used and particular concentration/age of the sample so they should be taken as starting points to obtain reasonably sized clusters. The described solution preparation should produce a sample of individual QDs or clusters (depending on the solution) suitable for single molecule experiments if the following deposition procedure is used.

The substrate should be mounted in the KW-4A spin coater (Chemat, Northridge CA). The spin coater should be set to quickly ramp to 5000 rpm and spin for 30 s. Approximately 30 µL of the solution described previously can be placed in the center of the substrate and spun or deposited as the substrate spins at its maximum rate. The former method will result in higher coverage than the latter. Generally, the latter method of deposition on a spinning substrate should be used. Once the sample has come to a complete stop it should be stored in a container with a lid on top of clean lens paper or Kim Wipes. This sample should be examined within 1-2 hours.

2.8 Sample Measurements

This section will briefly describe a fluorescence measurement of well separated QDs on a surface using the instrument. Starting points for sample coverage, scan size, and other troubleshooting are discussed.

Quantum dot coverage on the sample surface should be low enough to ensure that only one QD will be in the probe region (approx 0.5 µm) and the system has a low probability of drifting near another QD. This includes non-fluorescent QDs that will be detected in atomic force microscopy AFM measurements. Typically five QDs/clusters in a $20 \times 20\ \mu m^2$ scan is a good starting point. The surface coverage is affected by three main factors; QD concentration in the deposition solution, amount deposited on the substrate, and deposition method. An "activation" scan should be performed on each area observed. This is a high power scan ($6\ kW/cm^2$) that has the effect of "turning on" QDs and bleaches unwanted signal on the surface. The detectors should not be on for this scan. Typically, QDs become brighter and more stable after one activation scan, however, multiple high power scans will bleach the QDs so only one activation scan should be performed per area. A fluorescence map of the area should be made to find QDs/QD clusters at a laser intensity of ~50 nW ($15\ W/cm^2$). This intensity will allow for long measurements of QDs with little probability of bleaching the sample. The stage software measurement should be stopped when the Symphotime software is needed for time-tagged time resolved

measurements. The Symphotime oscilloscope can be used to keep the stage centered on the point of interest. A slight position adjustment should be considered every 5 min depending on the offsets of the stage. Higher offsets suffer from faster stage drift, even if the stage software hold position function is used.

Chapter 3

Quantum Dot Cluster Blinking

This chapter is based on work published in the Journal of Physical Chemistry C titled "Blinking Statistics of Small Clusters of Semiconductor Nanocrystals" in which I was the lead author in this work with co-workers Duncan Ryan, Martin Gelfand, and Alan Van Orden. Figures, tables, and text are adapted with permission from American Chemical Society. Copyright 2013 American Chemical Society. In this work I designed an experiment to observe the blinking statistics of quantum dots and quantum dot clusters to test the assumption that the blinking statistics of the cluster are governed by the blinking of a single quantum dot and that these blinking statistics are not altered by the close proximity of neighboring quantum dots in a cluster. I prepared samples of individual quantum dots and clusters, recorded time-tagged time resolved fluorescence from these samples for long durations, and devised a scheme to identify clusters in mixed samples of individual quantum dots and clusters of quantum dots. I also devised a method to set a threshold consistent with the energy transfer model and used this threshold to analyze the blinking of clusters that do not have an obvious threshold. We found that the blinking of individual quantum dots in the cluster was unaltered by the presence of nearby quantum dots and the energy transfer mechanism does not interact with the blinking mechanism in a way that would alter these properties. These findings apply broadly to optoelectronic applications that utilize quantum dots in close proximity such as in films and are affected by the *off* state of quantum dots. The observation of relatively unaltered blinking in clusters indicates that quantum dots in films would also blink normally. This chapter will also discuss a brief summary of what I believe to be the most important current research on the topic of individual quantum dot blinking.

3.1 Quantum Dot Blinking

With a few exceptions,[1-3] the fluorescence intensity of an individual quantum dot (QD) under constant illumination exhibits intermittency:[4-14] it is either in an *on* state, corresponding to high quantum

efficiency, or in an *off* state, consistent with zero emission within experimental uncertainty. This behavior is often termed blinking. In the *off* state, QDs continue to absorb light[15] and the absence of fluorescence is due to fast nonradiative decay; but the details of that process (or processes) are a subject of active investigation.[10,14,16-20] One feature of QD blinking, which is distinct from the blinking behavior of other fluorophores such as molecular dyes, is that the *on*/*off* event times follow power law probability distributions, that is, the probability of observing an event of duration t is proportional to t^{-m} where m is a constant, usually about 1.5. Both *on* and *off* events follow this distribution over a broad range of times.[4] At the longest times deviations from power law behavior, particularly for the *on* intervals, are sometimes observed and termed "truncation." [6,9] This power law behavior is surprising because it indicates that there are multiple or fluctuating rates for to and from the *off* state. In contrast, a single rate transition to the *off* state would result in an exponential probability distribution of *on* times as in triplet blinking. A fluctuating rate would result in the power law behavior observed,[5] but it is difficult to determine the mechanism for the fluctuation and, as will be discussed, what exactly the *off* state is.

Another characteristic of QD blinking is correlation between event durations.[8,13] The durations of *on* events show positive correlation with *on* event times and negative correlation with *off* event times. These correlations are strongest for subsequent events and typically decay slowly over many events. Likewise, *off* event durations show analogous correlations. These correlations are termed blinking memory.

It is well understood that the origin of blinking in QDs involves the surface of the QD. Adding a wide band gap shell to the QD[6] and surface ligand coverage[21,22] have severe impacts on the truncation time (roll-off time) in QD *on* statistics. The known successful methods to eliminate QD blinking have all involved the surface; either adding a giant shell[3] to move the surface far from the core or annealing[2] the QD to create a smooth boundary between the shell and QD core surface. The involvement of the surface in the luminescence of QDs is logical because, in nanocrystals, the ratio of surface to volume is very high

and much of the "bulk" of the nanocrystal is in close proximity to the surface. Nevertheless, the mechanism of QD blinking has not yet been unambiguously identified.

For a long time, the prevalent model of blinking was the Efros-Rosen model, in which the excited QD loses one of the photogenerated carriers and becomes charged.[23] This carrier was thought to go to a trap state on the QD surface or into the environment.[24] The charged QD core would be much less luminescent because fast Auger recombination involving the extra charge quenches fluorescence. An excitation on the QD would transfer energy to the additional carrier quickly, sending an electron higher into the conduction band or a hole down into the valence band depending on which carrier initially escaped the QD. The carriers relax quickly through phonon states to the band edge and the energy is lost to phonons. The Efros-Rosen model for power law blinking in QDs, although well known, has fallen out of favor as the understanding of the charged QD has developed. It is important to discuss this further because the charging model is still invoked as the blinking mechanism in QDs.[25-27]

Electronic force microscopy was used to observe QDs under several illumination conditions and found that the charging behavior of QDs was difficult to reconcile with the observed *off* state.[18] The electronic force microscopy measurement was able to determine how long QDs remain charged and under what illumination conditions they become charged. The study found that QDs with ZnS shells become charged very infrequently and that when QDs without shells become charged, they remain so for minutes to hours. Both of these findings indicate that charging does not play a major role in the power law blinking of QDs. While the ZnS shell increases the truncation time of the *on* state statistics, it does not eliminate blinking as much as the shell eliminated charging in this study and although the *off* state can last for long periods due to its power law nature, minutes to hours are not typical *off* times.

Another challenge to the Efros-Rosen model comes from the luminescence of the charged state itself. Two studies have indicated that the luminescence of the charged state is much higher than the *off* state that is observed.[17,19] In one study,[19] the biexciton yield of individual QDs was measured. The

biexciton state is essentially a doubly excited QD with four charges (two electrons and two holes) and the biexciton yield is the yield of 2nd photons that emit from the biexciton state; i.e. the probability of observing two photons from a double excitation. While the probability to observe the 2nd photon is very low, it is non-zero. The authors of these studies have determined that the biexciton yield may be as much as 10 times brighter than the *off* state observed. In another study on the luminescence of charged QDs,[17] the trion state of the QD was studied. A trion is essentially a charged QD that has absorbed a photon and has an exciton (hole and electron) for a total of three charges, hence, trion. The authors of this study also found that the lifetime of the trion would result in a photon yield that is too high to be the observed *off* state. Given the lack of charging in ZnS shelled QDs, the duration of the charged state observed,[18] and the fluorescence of charged or biexciton states,[17,19] it is very unlikely that the charged QD is the observed *off* state in the power law blinking observed in nanocrystals.

Further insight on the blinking mechanism in QDs comes from work that has successfully prevented blinking from occurring.[2,3] Ghosh et al.[3] synthesized so called "giant" QDs with 10-20 nm thick CdS shells on CdSe cores that exhibited no blinking. This is thought to be a quasi-type II structure in which the electron is delocalized over the whole core/shell structure while the hole is confined to the core. The type II structure combined with the size of the shell had the effect of extending the fluorescence lifetime and also had significant effects on blinking. The authors noted a correlation between particle volume, the length of the fluorescence lifetime, and the fraction of non-blinking QDs. Preparations of larger QDs exhibited longer fluorescence lifetimes and higher fractions of non-blinking QDs. Nearly all QDs were non-blinking with a fluorescence lifetime of 65 ns or higher. The work of Wang et al.[2] demonstrated non-blinking QDs created by annealing the core (CdSe) and shell (ZnS) together. The authors believe that this created a smooth potential energy curve between the core and shell instead of a sudden potential energy jump with the sudden transition between the two materials. Effectively there is no core surface because of the annealing and the material continuously changes composition. The common aspect between both non-blinking QD preparations is the lack of access to the surface, particularly for the

hole carrier. In giant QDs, the electron wavefunction is thought to extend throughout the entire nanocrystal while the hole is still confined to the core. This could effectively limit recombination at the outer interface of the CdS shell. In the annealed QDs, the surface is a high band gap ZnS with the core surface effectively erased to make a smooth transition to the shell material, which the carriers would not have the energy to access so they remain in the core material without access to the surface. Given that blinking is so heavily affected by the QD surface, this lack of access to the surface may explain why these QDs do not blink.

One of the most important studies on QD blinking to date is the single molecule fluorescence measurements by Galland et al.[14] on QDs in an electrochemical cell. This study revealed two types of luminescence blinking on CdSe/CdS core/large shell QDs. These are similar to the giant non-blinking QDs but not so large that blinking is eliminated. The authors identify A and B type blinking. The A type *off* state is negatively charged QD with a lower fluorescence lifetime and exponential *on*/*off* state statistics similar to the truncation in the *on* state observed.[6] The B type blinking has the power law *on/off* statistics observed in all nanocrystals[10] with a no change in lifetime relative to the *on* state. The authors were able to eliminate the different types of blinking with electrochemical control. A slight positive charge (0.6 V) eliminates A type blinking by preventing excess negative charge resulting in neutral QDs. The B type blinking can be eliminated with a slight negative cell potential (-1.0 V) which the authors conclude fills trap states on the QD surface with electrons, preventing hot photoexcited electrons from going into these states. The B type blinking can also be eliminated in QDs with larger shells which puts the surface further from the core of the QD so that tunneling to these states cannot occur, according to Galland et al.[14]

These studies, taken together, indicate that power law QD blinking involves the surface of the QD, likely the trap states on the surface, and that charging of the QD may play a role in the roll-off time observed in the *on* state statistics. These conclusions are supported by the studies indicating that the charge state is not the *off* state observed because the charged states are too luminescent[17,19] and too long lived.[18] Blinking is eliminated in QDs with giant shells that put the surface far from the hole carrier in the

core,[3] and in annealed QDs which have a smooth transition to a high band gap material shell,[2] effectively putting surface states out of reach energetically. Finally, the power law blinking in CdSe/CdS core/large shell QDs can be turned off with a slight negative potential that fills surface states with electrons and the exponential blinking that results from charging can be suppressed with a slight positive potential prevents negative charging of QDs.[14] Despite this wealth of information, it is still not unambiguously known how the power law blinking statistics arise in nanocrystal blinking and work is still ongoing, as not all models are based on QD charging but still lack strong evidence.[22,28,29]

3.2 The Energy Transfer Model and Blinking in Quantum Dot Clusters

Previous work using confocal fluorescence microscopy correlated with atomic force microscopy (AFM) revealed that small clusters of close proximity (<10 nm) CdSe/ZnS core/shell QDs had fluorescence intensity autocorrelations that could be distinguished both from those of individual QDs and of several individual, isolated QDs within the confocal region.[30] Further AFM correlated studies with lifetime data revealed that intervals of low emission intensity from clusters were correlated with intervals of short fluorescence lifetime.[31] The latter observation led us to propose a minimal model for the energy dynamics in a QD cluster, in which we introduced a single rate for nonradiative energy transfer from any QD to one with a smaller gap. These differences in band gap result from the innate size dispersion in the samples used to make the clusters. Our model assumes that the *on/off* blinking of individual QDs as well as the radiative decay rate in the *on* state are not strongly affected by the presence of neighboring QDs in a cluster. With just the energy transfer rate and the number of QDs in a cluster as parameters, this model accounts for the experimental observations.

When the QD with the smallest energy gap, which we denote the acceptor, is *on*, the fluorescence intensity is relatively high and the lifetime is close to the single QD radiative lifetime. When the acceptor is *off*, the fluorescence intensity is relatively low and the lifetime is much shorter. Note that when the acceptor is *off*, there will still be emission from other QDs in the cluster that are in the *on* state, but both

the intensity and lifetime are significantly reduced compared to times when the acceptor is *on* since radiative decay in any QD other than the acceptor competes primarily with energy transfer to the acceptor. The *on* and *off* states of the acceptor should thus correspond to two distinct states for the cluster, which we denote *high* and *low,* with high intensity and long lifetime corresponding to the *on* state of the acceptor and the low intensity and short lifetime corresponding to the *off* state of the acceptor.

The present work is concerned with testing the prediction that QD clusters undergoing energy transfer will exhibit two-state *high*/*low* blinking, while at the same time testing the assumption that the *on/off* blinking statistics of a QD are unaffected by its presence in a cluster. If the statistical properties of blinking by the acceptor are unaffected by its presence in the cluster, then *high/low* blinking should have the same statistical properties as *on/off* blinking. Note that within both the *high* and *low* states there can be considerable variation of intensity, due to *on/off* blinking of members of the cluster other than the acceptor.

In the present work we have collected long (20 min) fluorescence trajectories from single QDs and clusters of QDs using single molecule confocal microscopy with pulsed excitation and time tagged photon collection. Clusters of quasi-spherical, approximately 3-nm-diameter CdSe/ZnS core/shell QDs stabilized with octadecylamine ligands in toluene were formed by adding methanol to cause aggregation as in previous work.[30,31] After a short time, the solution was spin cast on a glass surface. These samples result in a mixture of individual QDs and clusters dispersed at the solid/air interface which are fully resolved by the confocal microscope. We use the intensity autocorrelation and fluorescence decay histograms to distinguish clusters from individual QDs. A key challenge is to operationally define *high* and *low* emission for the purpose of analyzing blinking statistics of the clusters. For any individual QD the intensity histogram has a well-defined gap between the peaks associated with the *on* state and the *off* state. For clusters, the intensity histograms show considerable variability, and it is not obvious where one should place a threshold between *high* and *low* emission states. We have devised two schemes for

high/low discrimination, one which sets an objective intensity threshold by analyzing the intensity-lifetime distribution, and another based on lifetime trajectories.

We have found that the *high*/*low* blinking of QD clusters shows the power law distribution for both *high* and *low* event durations, and also blinking and correlations and memory, similar to what is observed in individual QDs. These observations are consistent with our model's prediction of acceptor-dominated emission and are consistent with the assumption that the acceptor retains the blinking characteristics of an individual QD.

3.3 Experimental Methods Specific to Work on Quantum Dot Cluster Blinking

Octadecylamine stabilized CdSe-ZnS core-shell colloidal nanocrystals with an emission peak at 560 nm were purchased from Ocean Nanotech (QSO-560) at a concentration of 5.6 mg/mL in toluene. To prepare individual QDs for optical study, the stock solution was diluted to 30 ng/mL in spectrophotometric grade toluene (Sigma-Aldrich, St. Louis MO) and 40 μL was spin cast onto a glass coverslip using a KW 4A spin coater at 5000 rpm (Chemat, Northridge, California). QD clusters were prepared by diluting the stock solution in toluene to 110 ng/mL, adding 5 μL of methanol (Fisher, Fair Lawn New Jersey) to 1 mL of solution, allowing the mixture to sit for approximately 5 minutes and then spin casting. Samples for correlated optical/AFM measurements were dispersed on APTES (Sigma-Aldrich, St Louis, Missouri) treated freshly cleaved high grade mica (TED Pella, Redding, California) that was glued to a glass coverslip with low fluorescence optical adhesive (Norland Optical, Cranbury New Jersey).

The QD-coated coverslips were mounted onto a piezoelectric x-y scanning stage model NIS-30 SC-100/208 (Nanonics, Jerusalem Israel) attached to a Zeiss Axiovert 2TV inverted microscope to collect fluorescence data. Samples were excited with a 453 nm pulsed laser diode system, PDL 800-B driver and LDH-P-C 450B laser head, (PicoQuant, Berlin Germany) at 10 MHz, <100ps pulse width, and ~50 nW average power. Light was focused through a Zeiss Fluar 1.3NA/40□ oil immersion objective to form a

0.45-μm-diameter probe region at the top glass/air interface of the coverslip. Fluorescence was collected through the same objective and filtered with a Z450rdc dichroic beamsplitter (Chroma, Rockingham, Vermont) and D565/40m bandpass filters (Chroma, Rockingham Vermont). Spatial filtering was done with a 50 μm pinhole positioned at the focal point of the microscope. The fluorescence was split and focused onto two τ-SPAD-50 avalanche photodiode detectors (Picoquant, Berlin, Germany). The detector signals were output to a Time Harp 200 time correlated single photon counting card (Picoquant, Berlin, Germany).

Samples were raster scanned using in house programmed software to generate a fluorescence map. Sample coverage was about 5 individual QDs or clusters per 20×20 μm^2 scan area, ensuring the presence of a single QD or cluster in the probe region. The stage was moved to maximum fluorescence over a QD/QD cluster. Fluorescence data was collected for 20 min to obtain sufficient data for statistical analysis of blinking. Intensity traces were binned at 10 ms. Lifetime traces and fluorescence lifetime intensity distributions (FLIDs) were generated with 100 ms bins. Fluorescence lifetime histograms, intensity traces, and autocorrelations were processed by PicoQuant's Symphotime (v. 5.3.2.2) software. Blinking statistics were generated with in-house software programmed in Igor Pro 6.

Correlated atomic force microscopy (AFM) measurements were done immediately after the corresponding fluorescence measurement for some samples. An AFM image was acquired near the region of excitation (within 10 μm) using a Digital Instruments Bioscope AFM in tapping mode with Bruker OTESPA AFM probes (~42 N/m spring constant). When the AFM probe scanned over the focused laser spot on the surface, backstattered light was reflected through the objective at the frequency of the AFM probe oscillation. This backscatter was reflected by a 50/50 mirror, focused onto a 100 μm pinhole, and collected by a photodiode. A lock-in amplifier (Stanford Research Systems SR844 RF) amplified the signal at the tapping frequency and created a backscatter image. This method allows us to image the excitation region with the AFM and generate the corresponding topography image concurrently.[32]

3.4 Blinking of Quantum Dot Clusters Compared to Individual Quantum Dots

Prior to detailed analysis of fluorescence data it is essential to have confidence that the detected photons are coming from either an individual QD or a small cluster of QDs in the confocal region. In previous work we found that the clusters of QDs, in comparison to isolated QDs, showed faster decay of the intensity autocorrelation function and enhancement of the short lifetime component in a biexponential fit to the fluorescence decay histogram. These effects were only observed in QD clusters that were close packed (<10 nm) as confirmed by correlated AFM.[30,31] In the present work, we use these differences in the fluorescence properties to confidently distinguish QD clusters from individual QDs. To establish specific thresholds in these fluorescence characteristics, we prepared dilutions of QD samples in pure toluene in which only individual, isolated QDs would be present. We obtained autocorrelation functions (Figure 3.1b) and fluorescence decay histograms (Figure 3.1c) from these samples. We then defined two parameters for the purpose of distinguishing individual QDs and clusters of QDs in the methanol treated samples. The first, the roll-off time τ_R, is the lag time at which the intensity autocorrelation decays to half its value averaged over 0.1 to 1 ms. A smaller τ_R is observed in clusters than in individual QDs. The second parameter is the short lifetime component in the fluorescence lifetime decay histogram which we fit to a biexponential form

$$Ae^{-t/\tau_S} + Be^{-t/\tau_L} \qquad \text{Equation 3.1}$$

where τ_S and τ_L are the short and long lifetimes. The short lifetime component is then defined as $f_S = A/(A+B)$. Our previous studies found that clusters have a much greater f_S than individual QDs.[31] Figure 3.1a shows the distribution of τ_R and f_S found in samples prepared from pure toluene and from methanol treated solutions. We use the minimum τ_R and the maximum f_S obtained from individual QDs in the pure toluene samples as thresholds: emitters with $\tau_R < 2.0$ s and $f_S > 16\%$ are presumed to be clusters. As anticipated, some individual QDs are found in the methanol-treated samples. Note the absence of emitters with $\tau_R < 2.0$ s and $f_S < 16\%$, or with $\tau_R > 2.0$ s and $f_S > 16\%$: thus our classification scheme is

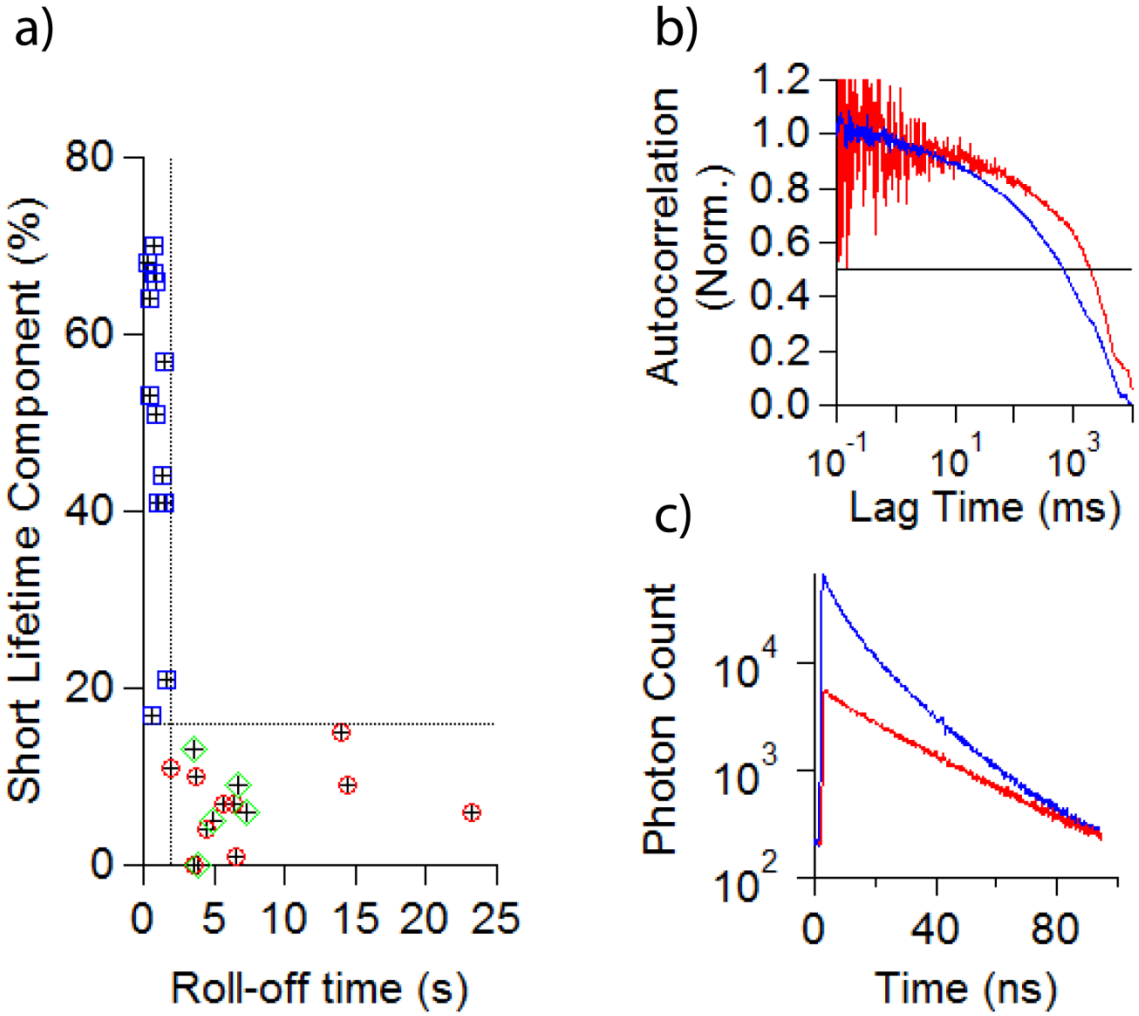

Figure 3.1: Distinct fluorescence behaviors used to distinguish individual QDs from clusters of QDs. (a) Scatter plot of short lifetime component in the fluorescence decay histogram versus autocorrelation roll off time. The plot includes QD solutions prepared without methanol, and therefore, no clustering (red circles), individual NCs found in methanol-treated samples (green diamonds), and clusters (blue squares). The dotted lines are the thresholds used for differentiating clusters from individual NCs. Note the absence of emitters in the lower left and upper right regions. (b) Normalized autocorrelation functions for an individual NC (red line) and a cluster (blue line). The marker illustrates the threshold used to determine the roll off time. (c) Fluorescence decay histograms for an individual NC (red line) and a cluster (blue line).

robust. Clusters are approximately 3-7 QDs in size based on fluorescence intensity compared to individual QDs.

Clusters and individual QDs also exhibit distinct behavior in fluorescence lifetime–intensity distributions (FLIDs). Figure 3.2 shows representative FLIDs and intensity trajectories for an isolated, individual QD (Figure 3.2a); a group of QDs that are sufficiently separated to be considered individual QDs rather than elements of a cluster (Figure 3.2b, and see remark in Methods); and a QD cluster (Figure 3.2c). These particular examples were confirmed by correlated AFM experiments, also shown in the figure. The individual, isolated QD shows a single FLID peak at the typical QD lifetime (~25 ns) and at the intensity of its *on* state. The FLID for the group of non-interacting QDs shows a wider distribution in intensity, from the independent *on*/*off* switching of each QD, but essentially the same lifetime distribution at every intensity. The FLID for the cluster is quite different, with evident positive correlation between intensity and lifetime. The FLID from each cluster has its own particular form depending, presumably, on the detailed arrangement of QDs in the cluster. A variety of FLIDs are shown in figure 3.3. However, all cluster FLIDs share the characteristics of shorter lifetimes (less than the lifetime of an individual QD) at lower intensities together with a broad distribution of intensities. According to our model, low-intensity, short-lifetime features in cluster FLIDs are associated with times when the acceptor is *off*, while the broad distribution of intensities is associated with *on/off* blinking of the other QDs.

To obtain the blinking statistics of individual QDs and QD clusters we must distinguish *on*/*off* and *high/low* states, respectively. For an individual QD this is simple: an intensity histogram is generated and the first minimum in the histogram is chosen as the cutoff intensity. In our experiments, a bin time of 10 ms leads to an intensity threshold of about 0.5 kHz.

Clusters have multiple intensity levels within the *high* and *low* states corresponding, presumably, to which subset of QDs in the cluster are in the *on* state besides the acceptor. There is no obvious, ubiquitous feature in the intensity histograms which facilitates the setting of an intensity threshold.

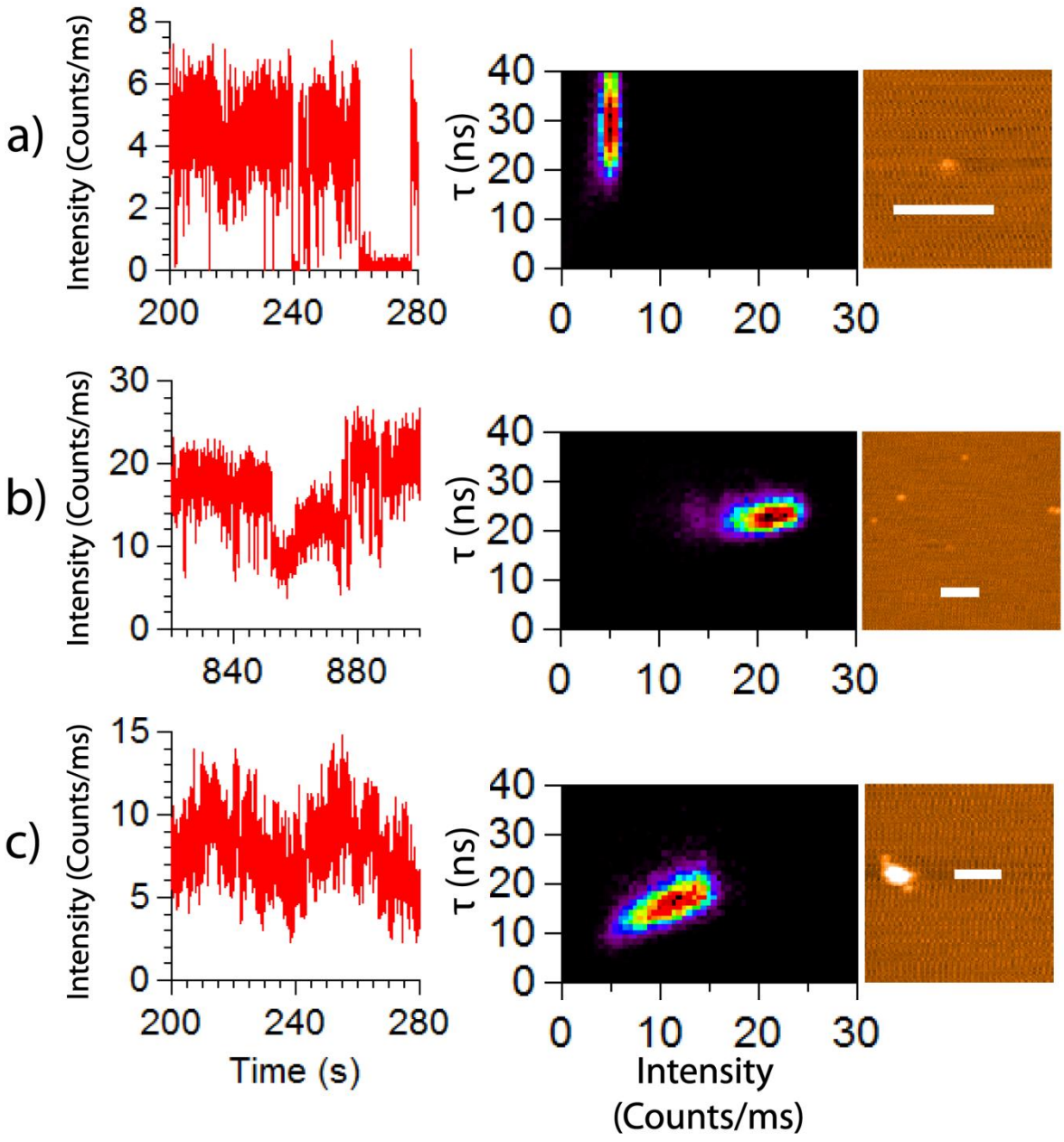

Figure 3.2: Fluorescence trajectories (left), fluorescence lifetime-intensity distributions (middle), and correlated AFM images (right, scale bar = 100 nm) for (a) an isolated individual QD, (b) several individual QDs in the optical probe region, and (c) a QD cluster. The excitation intensity was 30 W/cm^2 in (a) and (b) and 7.5 W/cm^2 in (c).

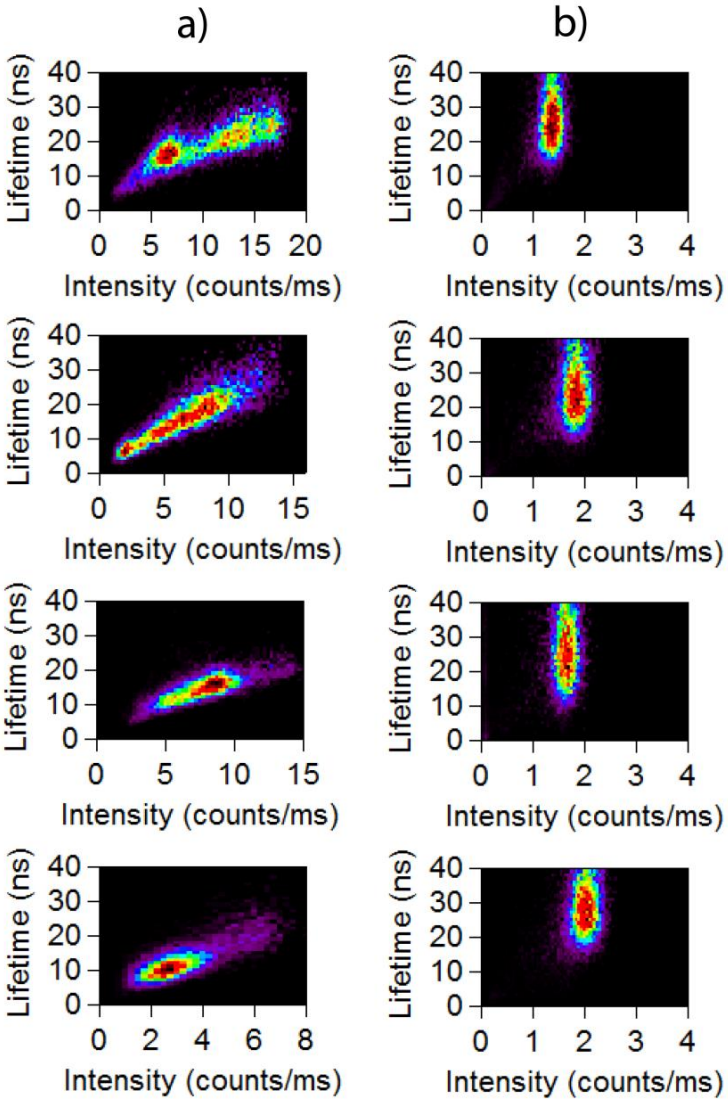

Figure 3.3: Sample FLIDs from clusters (column a) and individual QDs (column b). Clusters show very different shapes depending on the *on* times and presumably the geometry of the cluster.

However, our energy-transfer model predicts that *high* and *low* states have different lifetimes, and those lifetimes can be determined from the biexponential fit (Figure 3.4b) of the fluorescence decay histogram for the cluster. Then portions of the FLID (Figure 3.4a) associated with intermediate lifetimes are assumed to be artifacts of the binning. Therefore a cross section of the FLID is taken at the lifetime value $(\tau_S + \tau_L)/2$, which serves as a lifetime threshold (Figure 3.4a), and the location of the maximum in the FLID along this cross section serves as an intensity threshold (Figure 3.4d). This treatment allows us to consistently and objectively analyze the intensity trajectories in terms of *high/low* states for all clusters.

On and *off* times (*high* and *low* times) from individual QDs (QD clusters) are generated from 10-ms-binned intensity trajectories using the thresholds described above and collected into histograms of *on*/*off* (*high/low*) times. Probability densities were calculated from the histograms following the prescription of Kuno *et al*.[5]

$$P(t) = \frac{N_t}{N_{total}\left(\frac{t_{n+1}-t_{n-1}}{2}\right)} \qquad \text{Equation 3.2}$$

where N_t is the number events with duration t, N_{total} is the total events of the state for the trajectory, t_{n+1} is the duration of the next observed event, and t_{n-1} is the duration of the previously observed event. The probability densities were first fit to a power-law form

$$P(t) = Ct^{-m} \qquad \text{Equation 3.3}$$

Typical results for an individual QD and a cluster are shown in Figure 3.5; both show the widely reported[4,6,9] power-law behavior. Average values (± one standard deviation) for all fifteen individual QDs studied (Table 1) were $m = 1.55(\pm 0.20)$ for *on* states and $m = 1.86(\pm 0.20)$ for *off* states. The averages for all fourteen clusters (Table 2) were $m = 1.59(\pm 0.14)$ for *high* states and $m = 1.50(\pm 0.10)$ for *low*

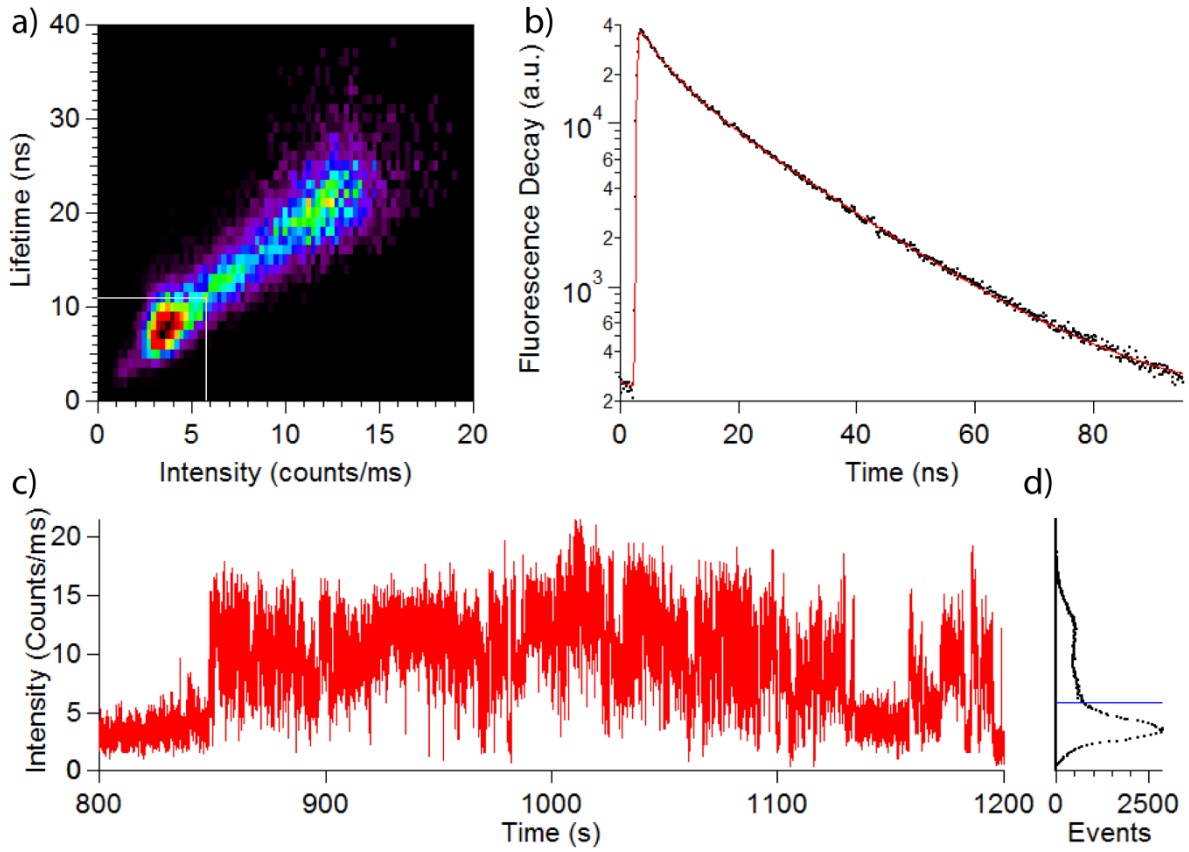

Figure 3.4: (a) Fluorescence lifetime-intensity distribution for an QD cluster, with horizontal and vertical lines at the lifetime and intensity thresholds for *high/low* blinking, as described in the text; (b) fluorescence decay histogram and bi-exponential fit with decay times of 4.6 ns and 17.3 ns; (c) partial intensity trace showing *high/low* blinking; and (d) intensity histogram with the *high*/*low* threshold indicated in blue. All parts of this figure were obtained from the same QD cluster.

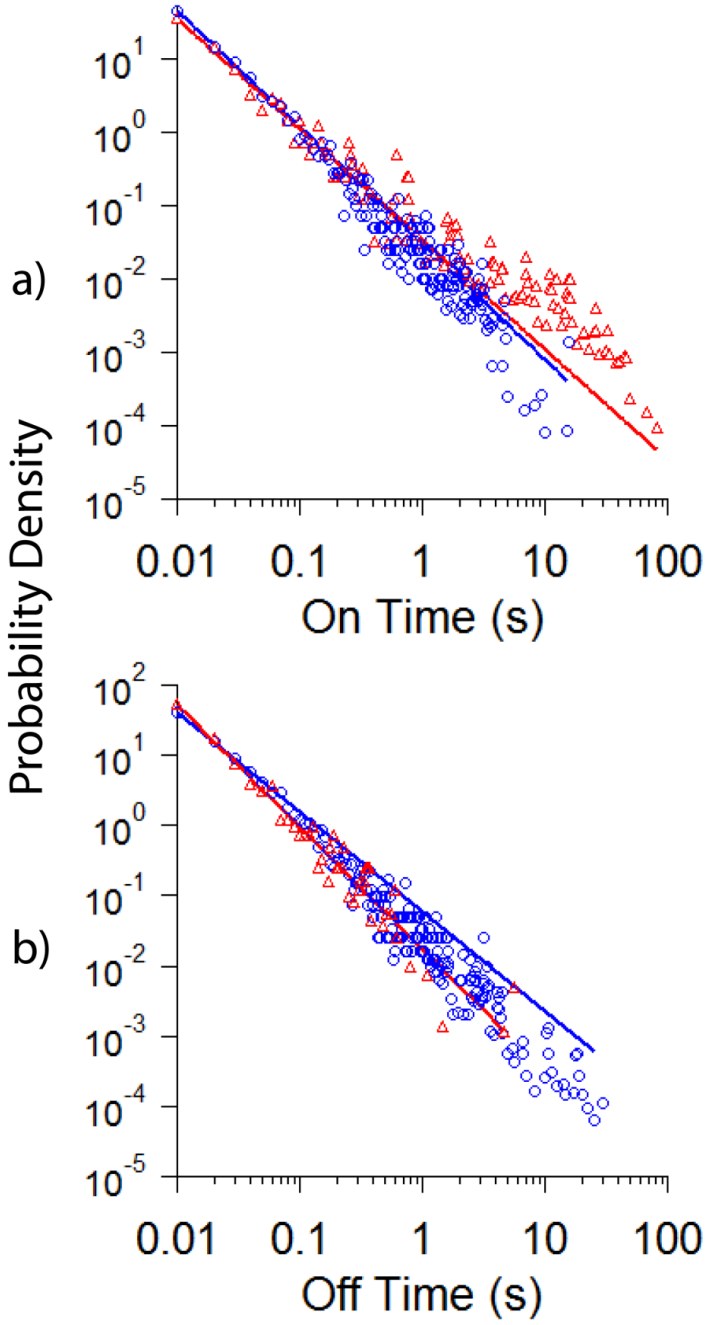

Figure 3.5: Blinking event probability distributions, with power law fits, of a typical individual QD (red triangles) and a cluster (blue circles) for (a) the *on* (m=1.50) and *high* (m=1.59) states and (b) the *off* (m = 1.74) and *low* (m=1.42) states.

Table 3.1: Properties of individual QDs: autocorrelation roll-off time, short-lifetime component of decay histogram, *on/off* intensity threshold, and blinking power-law exponents. Individual QDs in methanol were found in samples that also contained clusters.

Roll-Off Time (s)	τ_s (ns)	τ_l (ns)	Short Lifetime Component	Intensity Threshold (counts/ms)	Power Law Exponent	
Individual QDs with No Methanol					m On	m Off
3.7	2.3	24.1	10%	0.4	1.80	1.70
2.0	4.6	27.6	12%	0.6	1.50	1.73
14.5	2.8	26.2	8%	0.5	1.50	2.08
23.3	3.7	23.2	6%	0.6	1.53	1.91
6.4	4.8	33.1	7%	0.5	1.56	2.12
5.7	4.2	31.3	7%	0.5	1.96	1.46
4.5	4.9	24.5	4%	0.6	1.33	1.88
14	2.2	34.1	16%	0.6	1.79	1.60
6.6	8.9	26.9	1%	1.0	1.65	1.62
3.5	0.0	24.9	0.0%	0.5	1.24	2.20
Individual QDs in Methanol						
3.9	0.0	30.0	0%	0.6	1.51	2.14
7.2	4.5	28.0	6%	0.3	1.71	1.66
3.5	3.4	35.5	13%	1.3	1.40	1.74
6.7	6.9	28.5	9%	0.5	1.24	2.21
5	8.5	20.5	5%	0.5	1.59	1.91
				Average (all)	1.55 ±.20	1.86 ±.20

Table 3.2: Properties of QD clusters: autocorrelation roll-off time, short-lifetime component of decay histogram, *high/low* intensity threshold, blinking power-law exponents, and blinking truncation times.

Roll-Off Time (s)	Short Lifetime Component	τs (ns)	τl (ns)	Intensity Threshold (counts/ms)	Power Law Exponent		Truncation Time (s)	
					m On	m Off	On	Off
0.8	66%	6.6	15.7	6.0	1.52	1.52	0.58	0.29
0.6	17%	7.6	23.7	3.5	1.43	1.70	0.92	0.70
1.0	51%	4.9	14.7	7.3	1.63	1.46	0.69	0.66
0.7	67%	5.5	14.5	2.3	1.94	1.29	1.07	0.67
1.5	57%	4.4	12.0	7.0	1.76	1.42	0.92	0.76
1.1	41%	4.4	17.8	10.0	1.52	1.66	1.61	1.02
1.7	22%	4.4	25.0	7.0	1.6.0	1.46	0.40	0.48
0.5	53%	4.4	11.9	7.5	1.50	1.60	0.58	0.60
0.2	68%	7.7	16.6	3.0	1.68	1.35	0.56	0.55
1.4	41%	5.8	20.5	7.0	1.45	1.67	0.97	1.11
0.7	70%	4.8	16.2	11.3	1.71	1.39	0.52	0.68
1.4	44%	4.6	17.3	5.8	1.59	1.42	2.89	1.07
0.9	51%	7.2	20.5	5.8	1.50	1.53	1.33	1.04
0.5	64%	15.0	28.2	12.5	1.42	1.50	0.72	0.66
				Average	1.59±.14	1.50±.10		

states. Note that the fits are dominated by the data associated with short event times, and that the deviations from power law behavior at longer times will be discussed below. The key results are that power law behavior persists in clusters and the exponents observed for clusters are consistent with those for individual QDs, which supports one of the key assumptions of the energy transfer model.

We would like to note that the power law behavior is very robust and even in clusters; the selection of the threshold does not alter the behavior qualitatively. To demonstrate this robustness we present the blinking statistics of a cluster at several thresholds (Figure 3.6). The power law behavior is still evident and *m* values do not vary greatly. Some thresholds result in a higher apparent degree of truncation, which will be discussed below. Figures 3.7, 3.8, and 3.9 show the *on* and *off* distributions for several thresholds together with no offsets, further demonstrating the general robustness of the power-law behavior, but also the deviations of each state as the threshold varies.

Under the present experimental conditions, individual QDs did not show truncation in their power law blinking statistics. That was not the case for clusters. To account for truncation, probability densities were next fit to equation[9,33] 3.4

$$P(t) = Dt^{-m}\, e^{-t/t_c} \qquad \text{Equation 3.4}$$

where t_c is the cutoff time and m is fixed to the value previously determined. These fits for blinking data from clusters were clearly superior to the pure power-law fits (reducing χ^2 significantly), while fits to blinking data from individual QDs were hardly improved.

We postulate that the truncation in the power law statistics of clusters is primarily due to the fluctuations in the intensity of the *high* state. A similar truncation result can be achieved in individual QDs[34] if the threshold is set too high in the Poisson noise or too low in the detector noise. We believe this to be the dominant reason for the truncation because both *high* and *low* times are affected equally and the truncation is very dependent on bin size. An alternate explanation is that the energy transferred to the acceptor QD effectively increases the excitation intensity. This would result in shorter truncation time for

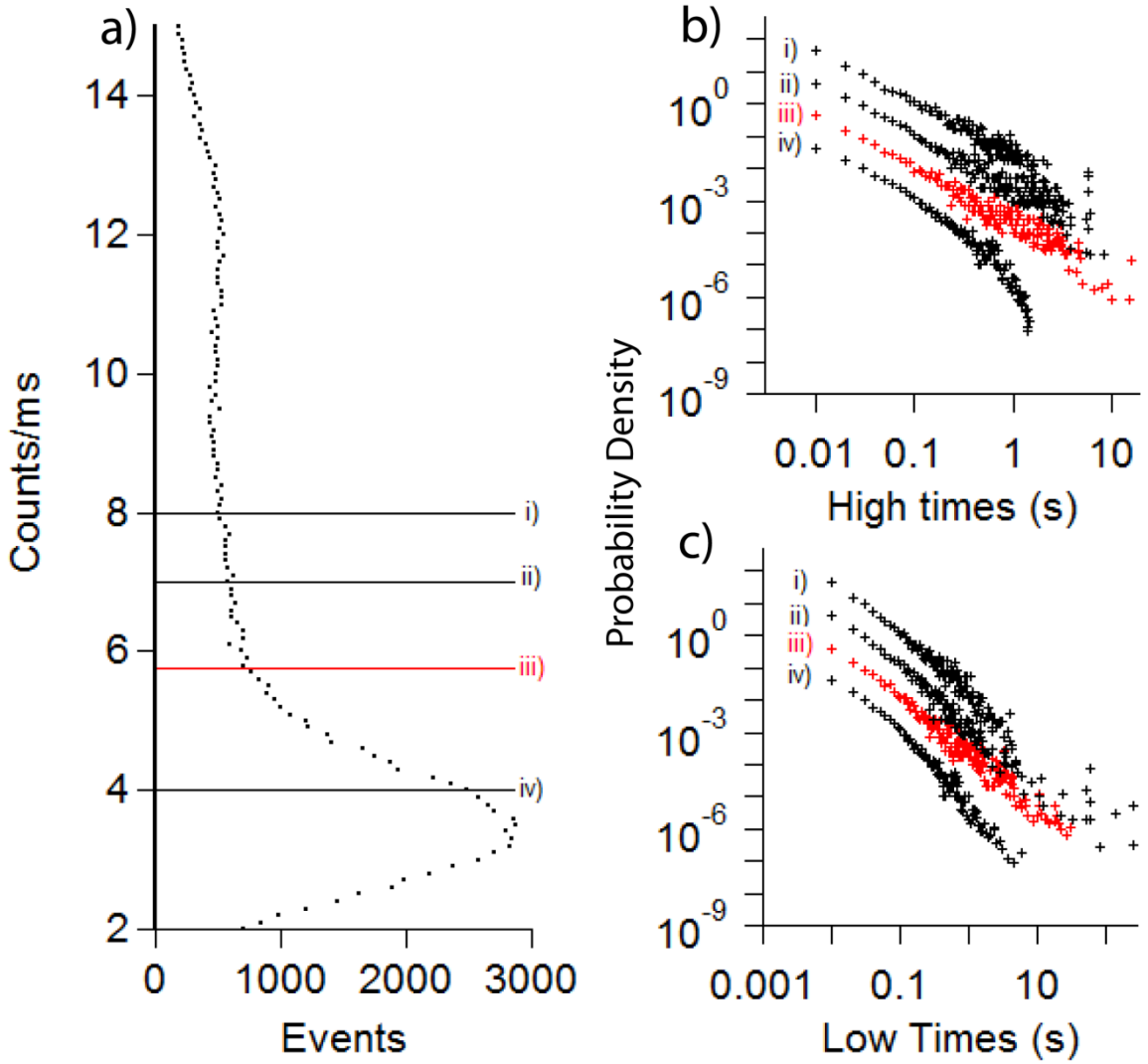

Figure 3.6: Blinking event probability distributions in a single QD cluster using different thresholds. (a) The intensity histogram with horizontal lines showing different thresholds. The red line corresponds to the threshold determined by our criterion. (b) Probability distributions for *high* event durations (offset vertically for clarity) using the thresholds indicated. The *m* values for thresholds i, ii, iii, and iv are 1.47, 1.59, 1.66, and 1.62 respectively. (c) Probability distributions for *low* event durations, again vertically offset. The *m* values for thresholds i, ii, iii, and iv are 1.48, 1.42, 1.39, and 1.53 respectively.

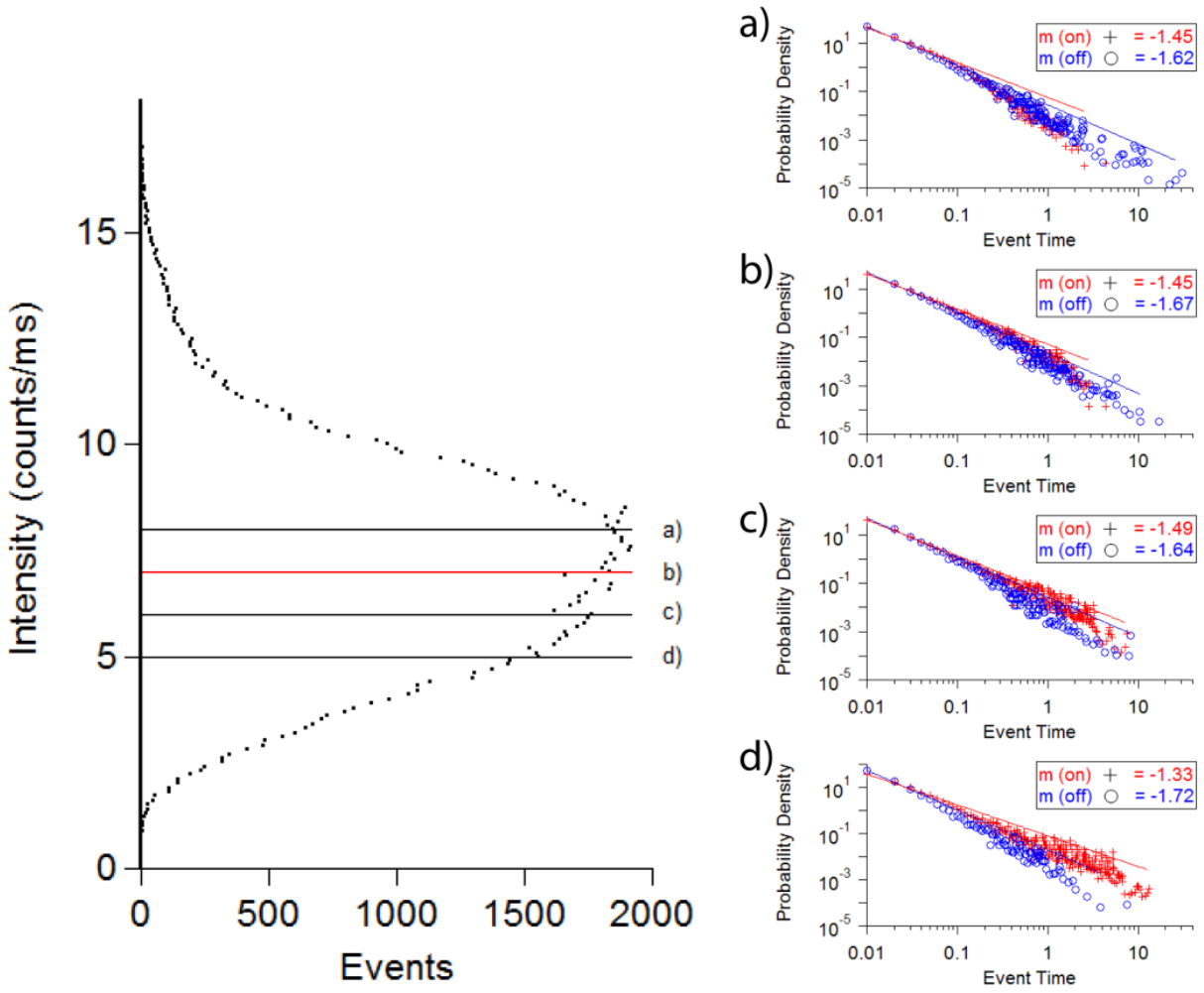

Figure 3.7: Cluster blinking statistics at several different *high*/*low* thresholds. Intensity histogram (left) and blinking statistics results (right). The red line indicates the threshold determined using the method detailed in the text. Other thresholds were chosen arbitrarily. Thresholds: a) 8 b) 7 c) 5.75 d) 5.

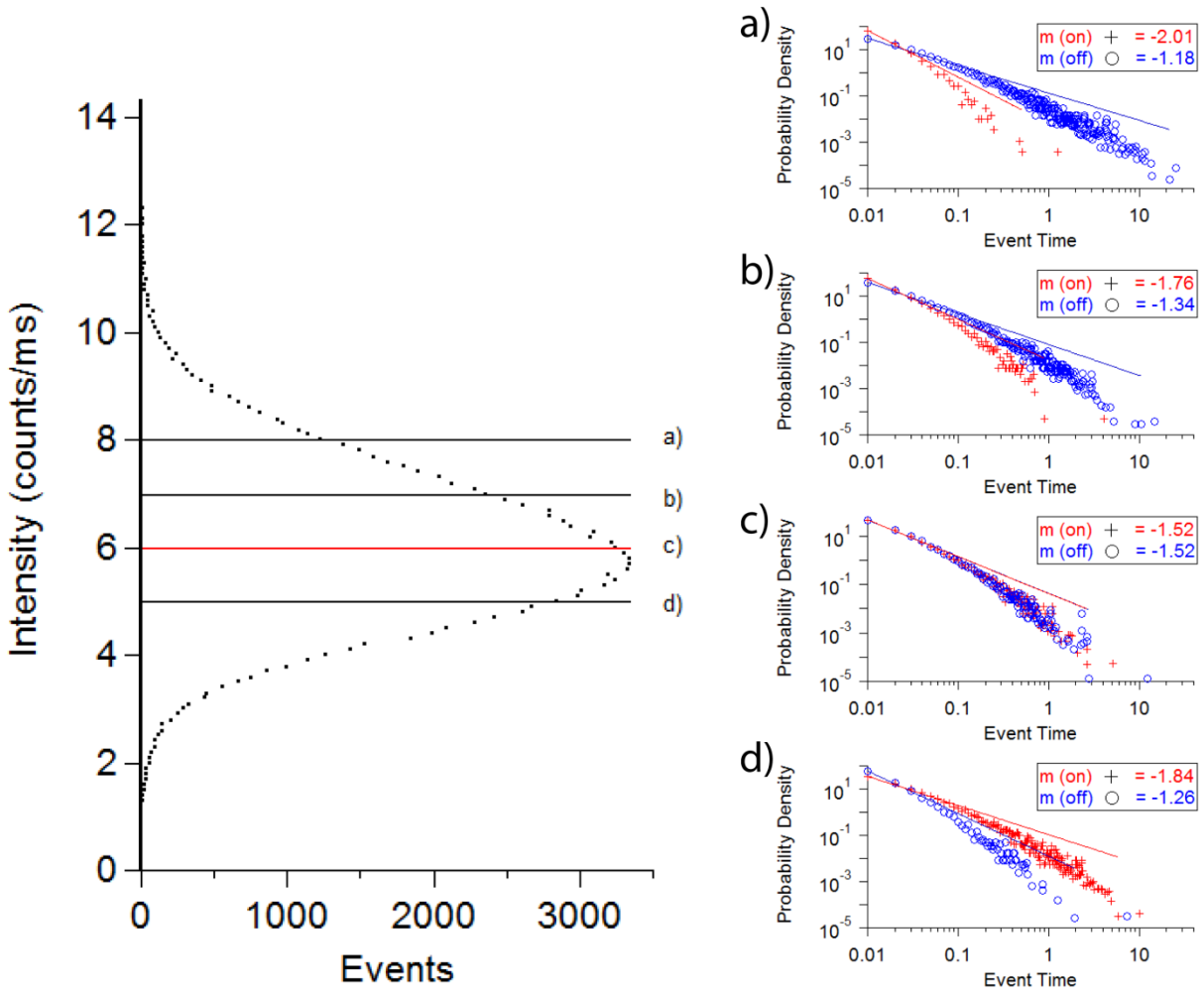

Figure 3.8: Cluster blinking statistics at several different *high*/*low* thresholds. Intensity histogram (left) and blinking statistics results (right). The red line indicates the threshold determined using the method detailed in the text. Other thresholds were chosen arbitrarily. Thresholds: a) 8 b) 7 c) 6 d) 5.

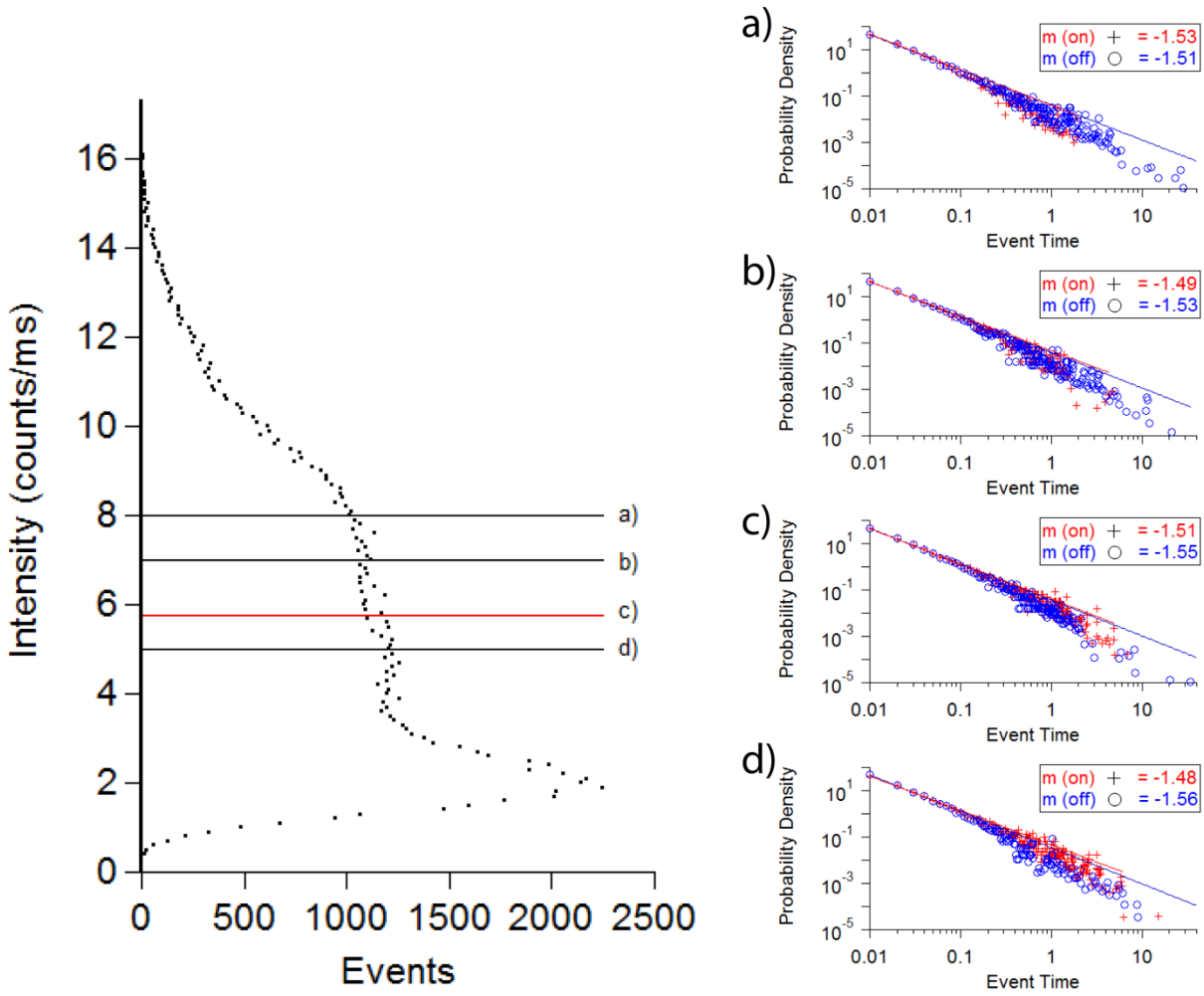

Figure 3.9: Cluster blinking statistics at several different high/low thresholds. Intensity histogram (left) and blinking statistics results (right). The red line indicates the threshold determined using the method detailed in the text. Other thresholds were chosen arbitrarily. Thresholds: a) 8 b) 7 c) 5.75 d) 5.

the *on* times of the acceptor but would not affect the *off* times equally.[6] Although we observe this truncation effect in clusters, the power law behavior is still evident at the shorter event durations.

Our second scheme to obtain blinking statistics from clusters is to analyze the intermittency in fluorescence lifetime trajectories. With time-tagged time-resolved correlated single photon counting, a fluorescence decay histogram can be generated for each photon data bin and fit to obtain a lifetime for the bin as long as there is enough photon data. With 100 ms bins, clusters yield enough photons in the *low* state to reasonably fit lifetime data and obtain a fluorescence decay lifetime for that bin. With this data, a lifetime trajectory can be constructed. The FLID shows that the *high* state is accompanied by long fluorescence decay lifetime and the *low* state with short fluorescence decay lifetime. Therefore, we can observe the *high*/*low* blinking (Figure 3.10) in the lifetime trajectories. The lifetime threshold used to obtain lifetime blinking data is the average of the two lifetimes, τ_S and τ_L, as described above. The results show power law blinking for *high* and *low* times similar to results from intensity blinking. The truncation time changes greatly using these traces and fits produce t_c values more than an order of magnitude longer than with intensity traces, usually in the range of seconds rather than a tenth of a second. This difference is likely due to larger bin size. In addition to the FLID data, the observation of power law blinking in lifetime trajectories is further evidence of the fluorescence state of the cluster being controlled by a single low band gap QD and supports the assumption that the blinking of QDs is unchanged by their presence in a cluster.

In addition to power law blinking, we have observed blinking memory in QD clusters (Figure 3.11 and 3.12). Other studies[8,13] have reported such correlations in individual QD blinking: an *on* event is likely followed by an *on* event of similar duration (i.e. short *on* event followed by another short *on* event). The result is a positive correlation between subsequent *on* event durations. The memory is also present for *off* events: an *off* event will likely be followed by an *off* event of similar duration. The correlation between the two different states, however, is negative: a short event of one state will likely be followed by a long event in the other state (Tables 3.3and 3.4). These correlations decay over many events in individual QDs.

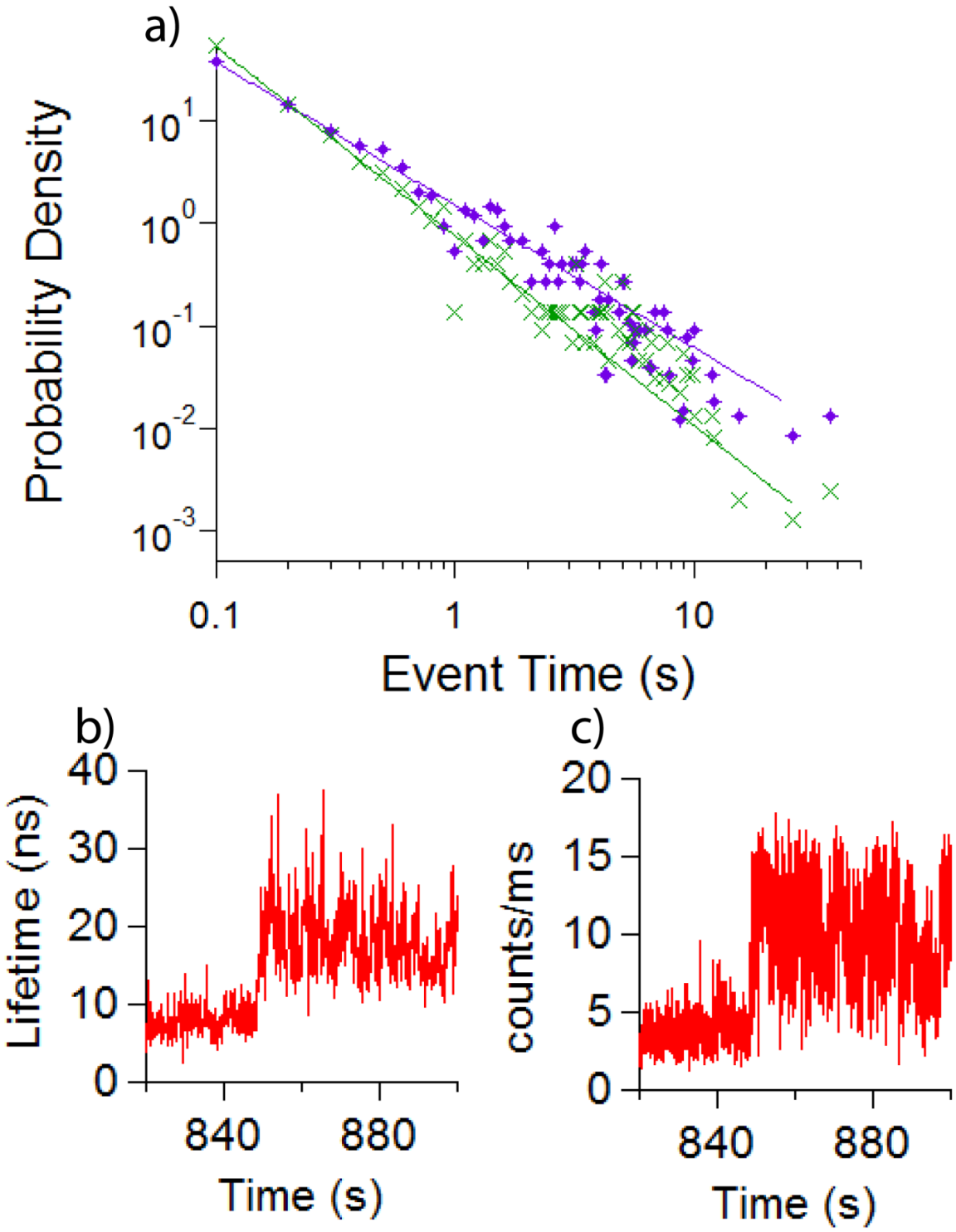

Figure 3.10: Lifetime blinking in a cluster. (a) Probability distribution of *high* (green ×) and *low* (purple +) intervals for a cluster, as obtained from a lifetime trajectory. The power law fits give m = 1.85 and 1.40 for *high* and *low* respectively. (b) A segment of the corresponding lifetime trajectory. Note that the *high/low* threshold is 10.95 ns. (c) The corresponding segment of the intensity trajectory.

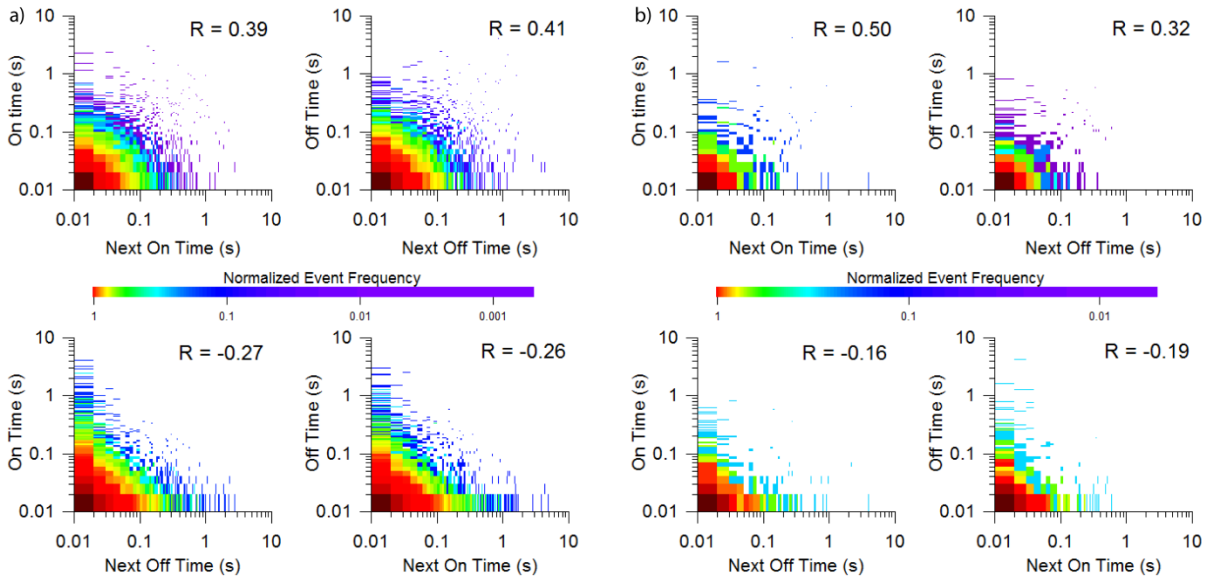

Figure 3.11: Two-dimensional histograms generated by plotting event duration vs. neighboring event duration for (a) a QD cluster and (b) an individual QD. The correlation coefficients displayed in the upper right corners were determined from the logarithm of event durations. Both clusters and individual QDs show positive correlation for nearest same states and negative correlation for different states.

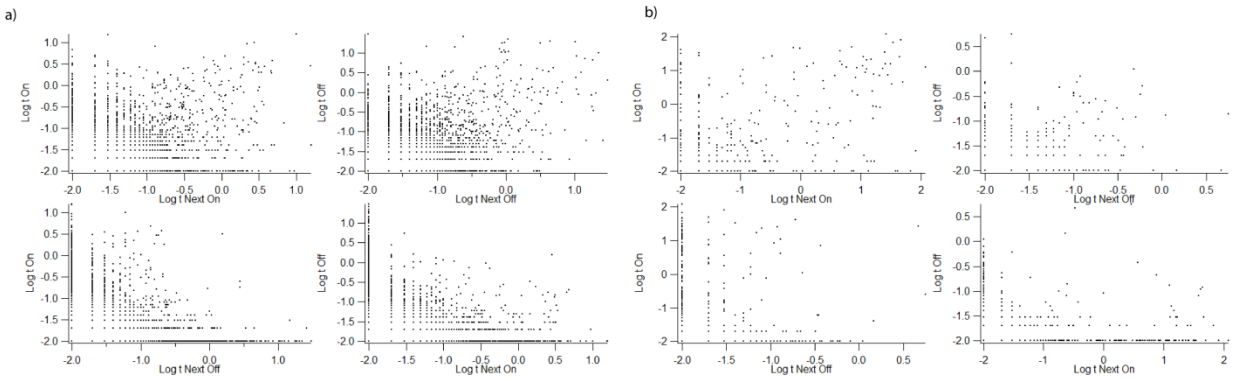

Figure 3.12: Black and white scatter plot version of Figure 3.11. Two-dimensional histograms generated by plotting event duration vs. neighboring event duration for (a) an NC cluster and (b) an individual NC. The log of the event times are plotted in this figure. See figure 3.11 for correlation coefficients**.**

Table 3.3: Correlation coefficients for nearest neighbor blinking event memory in individual QDs. Calculated from the log of event times.

Isolated QD	on-on	off-off	on-off	off-on
1	0.71	0.54	-0.27	-0.29
2	0.50	0.32	-0.16	-0.19
3	0.57	0.65	-0.32	-0.29
4	0.43	0.56	-0.26	-0.23
5	0.55	0.48	-0.19	-0.1
6	0.73	0.48	-0.37	-0.39
7	0.61	0.25	-0.06	-0.09
8	0.69	0.45	-0.29	-0.27
9	0.65	0.48	-0.13	-0.13
10	0.47	0.33	-0.04	0.02
11	0.54	0.51	-0.26	-0.21
12	0.60	0.44	-0.41	-0.43
13	0.47	0.35	-0.19	-0.18
14	0.45	0.59	-0.18	-0.17
15	0.46	0.65	-0.27	-0.29
Average	0.56	0.47	-0.23	-0.22
Standard Deviation	0.10	0.12	0.11	0.12

Table 3.4: Correlation coefficients for nearest neighbor blinking event memory in QD clusters. Calculated from the log of event times.

Cluster	on-on	off-off	on-off	off-on
1	0.34	0.32	-0.27	-0.28
2	0.38	0.31	-0.22	-0.23
3	0.38	0.38	-0.27	-0.28
4	0.43	0.56	-0.31	-0.32
5	0.39	0.50	-0.30	-0.30
6	0.50	0.39	-0.31	-0.32
7	0.27	0.38	-0.25	-0.25
8	0.34	0.33	-0.27	-0.28
9	0.31	0.33	-0.23	-0.23
10	0.36	0.42	-0.30	-0.28
11	0.29	0.40	-0.26	-0.27
12	0.39	0.41	-0.27	-0.26
13	0.35	0.30	-0.23	-0.23
14	0.36	0.27	-0.15	-0.18
Average	0.36	0.38	-0.26	-0.27
Standard Deviation	0.06	0.08	0.04	0.04

To quantify blinking memory in individual QDs and clusters we determine the linear correlation coefficients for *on-on*, *off-off*, *off-on* and *on-off* (in individual QDs) and *high-high* and *low-low*, *low-high* and *high-low* (in clusters) events from $\log t_{n,s}$ and $\log t_{n+1,s}$, where $t_{n,s}$ is the duration of the *n*th event of state *s* in a fluorescence trajectory. Typical event duration correlation histograms from which the correlation coefficients are calculated are shown in Figure 3.10. Results for all clusters and individual QDs are presented in Tables 3.3 and 3.4. Both clusters and individual QDs show positive correlations for events of the same type and weaker negative correlations for events of the opposite type, as was observed in other studies for individual QDs.[8,13] These results further support the assumption that the blinking of the acceptor is not substantially altered by its presence in a cluster.

We have also observed the decay of memory in QD clusters. In Figure 3.13 we plot the correlation coefficients determined for $\log t_{n,s}$ and $\log t_{n+x,s}$, as a function of *x*. The correlations persist in clusters for larger values of *x* than in isolated QDs. We believe this to be due to more frequent *high*/*low* switching in the clusters than *on/off* switching in individual QDs. We typically observe an order of magnitude more occurrences of *high/low* transitions in clusters than *on*/*off* transitions in individual QDs during a 20 min trajectory, which puts the memory decay of clusters approximately on the same *time* scale as individual QDs. While this is one of the few differences between individual QD blinking and cluster blinking, it does not represent a serious challenge to our model of cluster blinking because the blinking statistics/memory are dominated by the shorter event times.

Our studies of quasi-spherical CdSe/ZnS QD cluster conflict somewhat with recent studies of clusters of CdSe/ZnSe/ZnS nanorods by Wang *et al.*[35] Those authors observed longer average and maximum *on* times for nanorod clusters than for individual nanorods, and suggested that the blinking of nanorods in a cluster was significantly affected by interactions between nanorods. We believe that the observations of Wang *et al.* represent a different phenomenon which we do not observe in the small quasi-spherical QD clusters, and their observation of slower decay in the autocorrelation of aggregates is

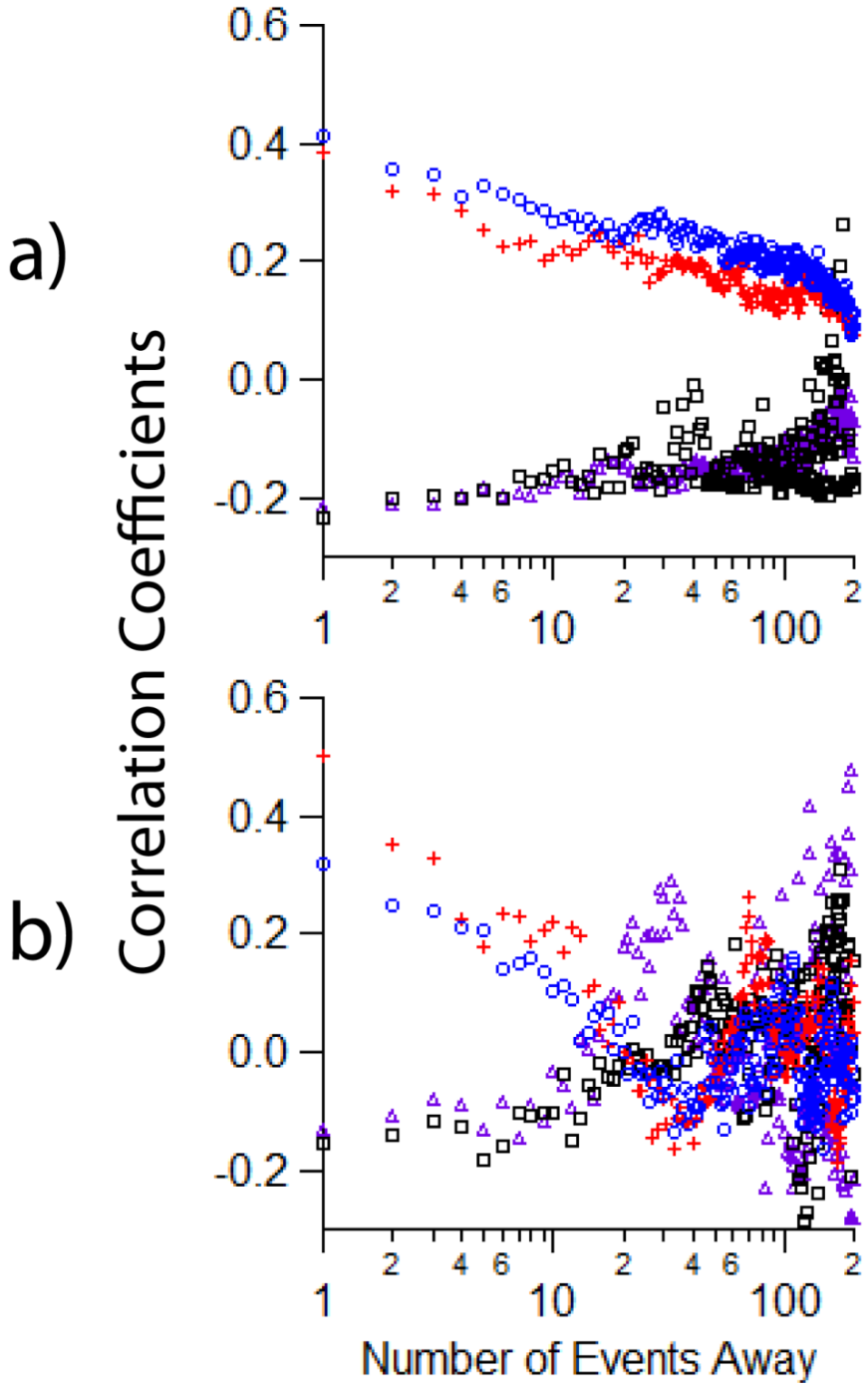

Figure 3.13: Correlation coefficients for *on-on* events (red crosses), *off-off* events (blue circles), *on-off* events (black squares) and *off-on* events (purple triangles) determined as in Figure 3.11 for more distant events, (a) for a cluster and (b) for an individual QD.

indicative of this. Furthermore, our blinking data comes from thresholds based on lifetime data instead of detector noise and is likely not comparable.

3.5 Conclusions from Quantum Dot Cluster Blinking

This work has examined the prediction that the fluctuations of *high*/*low* blinking states in clusters are controlled by the *on*/*off* state of a single, low band gap QD due to energy transfer from donor QDs in the cluster. Additionally, we examined the assumption that the QDs in the cluster exhibit the same blinking statistics typical of an individual isolated QD. Defining an intensity threshold for *high*/*low* blinking corresponding to low emission intensity and short photoluminescence lifetime has allowed us to measure the *high*/*low* event times and blinking statistics for the clusters. Based on the positive correlation between fluorescence lifetime and intensity of the cluster observed in the FLIDs, and the observation of *high/low* blinking in lifetime trajectories, we deduce that the *high*/*low* state is controlled by the *on*/*off* state of a single acceptor QD. The fact that the observed blinking statistics and memory of clusters exhibit the properties characteristic of individual QDs supports the assumption that the blinking properties of the QDs in the cluster are not greatly influenced by their presence in a cluster, even though the QDs are close enough to permit energy transfer on nanosecond time scales.

Chapter 3 References

(1) Chen, Y.; Vela, J.; Htoon, H.; Casson, J. L.; Werder, D. J.; Bussian, D. A.; Klimov, V. I.; Hollingsworth, J. A. "Giant" Multishell CdSe Nanocrystal Quantum Dots with Suppressed Blinking. *J. Am. Chem. Soc.* **2008**, *130*, 5026.

(2) Wang, X. Y.; Ren, X. F.; Kahen, K.; Hahn, M. A.; Rajeswaran, M.; Maccagnano-Zacher, S.; Silcox, J.; Cragg, G. E.; Efros, A. L.; Krauss, T. D. Non-Blinking Semiconductor Nanocrystals. *Nature* **2009**, *459*, 686-689.

(3) Ghosh, Y.; Mangum, B. D.; Casson, J. L.; Williams, D. J.; Htoon, H.; Hollingsworth, J. A. New Insights into the Complexities of Shell Growth and the Strong Influence of Particle Volume in Nonblinking "Giant" Core/Shell Nanocrystal Quantum Dots. *J. Am. Chem. Soc.* **2012**, *134*, 9634-9643.

(4) Kuno, M.; Fromm, D. P.; Hamann, H. F.; Gallagher, A.; Nesbitt, D. J. Nonexponential "Blinking" Kinetics of Single CdSe Quantum Dots: A Universal Power Law Behavior. *J. Chem. Phys.* **2000**, *112*, 3117-3120.

(5) Kuno, M.; Fromm, D. P.; Hamann, H. F.; Gallagher, A.; Nesbitt, D. J. "On"/"Off" Fluorescence Intermittency of Single Semiconductor Quantum Dots. *J. Chem. Phys.* **2001**, *115*, 1028-1040.

(6) Shimizu, K. T.; Neuhauser, R. G.; Leatherdale, C. A.; Empedocles, S. A.; Woo, W. K.; Bawendi, M. G. Blinking Statistics in Single Semiconductor Nanocrystal Quantum Dots. *Phys. Rev. B* **2001**, *63*, 205316.

(7) Kuno, M.; Fromm, D. P.; Johnson, S. T.; Gallagher, A.; Nesbitt, D. J. Modeling Distributed Kinetics in Isolated Semiconductor Quantum Dots. *Phys. Rev. B* **2003**, *67*, 125304.

(8) Stefani, F. D.; Zhong, X. H.; Knoll, W.; Han, M. Y.; Kreiter, M. Memory in Quantum-Dot Photoluminescence Blinking. *New J. Phys.* **2005**, *7*, 197.

(9) Knappenberger, K. L.; Wong, D. B.; Romanyuk, Y. E.; Leone, S. R. Excitation Wavelength Dependence of Fluorescence Intermittency in CdSe/ZnS Core/Shell Quantum Dots. *Nano Lett.* **2007**, *7*, 3869-3874.

(10) Frantsuzov, P.; Kuno, M.; Janko, B.; Marcus, R. A. Universal Emission Intermittency in Quantum Dots, Nanorods and Nanowires. *Nat. Phys.* **2008**, *4*, 519-522.

(11) Lee, S. F.; Osborne, M. A. Brightening, Blinking, Bluing and Bleaching in the Life of a Quantum Dot: Friend or Foe? *ChemPhysChem* **2009**, *10*, 2174-2191.

(12) Vela, J.; Htoon, H.; Chen, Y. F.; Park, Y. S.; Ghosh, Y.; Goodwin, P. M.; Werner, J. H.; Wells, N. P.; Casson, J. L.; Hollingsworth, J. A. Effect of Shell Thickness and Composition on Blinking

Suppression and the Blinking Mechanism in 'Giant' CdSe/CdS Nanocrystal Quantum Dots. *J. Biophotonics* **2010**, *3*, 706-717.

(13) Volkan-Kacso, S.; Frantsuzov, P. A.; Janko, B. Correlations Between Subsequent Blinking Events in Single Quantum Dots. *Nano Lett.* **2010**, *10*, 2761-2765.

(14) Galland, C.; Ghosh, Y.; Steinbruck, A.; Sykora, M.; Hollingsworth, J. A.; Klimov, V. I.; Htoon, H. Two Types of Luminescence Blinking Revealed by Spectroelectrochemistry of Single Quantum Dots. *Nature* **2011**, *479*, 203-207.

(15) Kukura, P.; Celebrano, M.; Renn, A.; Sandoghdar, V. Imaging a Single Quantum Dot When It Is Dark. *Nano Lett.* **2009**, *9*, 926-929.

(16) Pelton, M.; Smith, G.; Scherer, N. F.; Marcus, R. A. Evidence for a Diffusion-Controlled Mechanism for Fluorescence Blinking of Colloidal Quantum Dots. *Proc. Natl. Acad. Sci. U. S. A.* **2007**, *104*, 14249-14254.

(17) Jha, P. P.; Guyot-Sionnest, P. Trion Decay in Colloidal Quantum Dots. *ACS Nano* **2009**, *3*, 1011-1015.

(18) Li, S.; Steigerwald, M. L.; Brus, L. E. Surface States in the Photoionization of High-Quality CdSe Core/Shell Nanocrystals. *ACS Nano* **2009**, *3*, 1267-1273.

(19) Zhao, J.; Nair, G.; Fisher, B. R.; Bawendi, M. G. Challenge to the Charging Model of Semiconductor-Nanocrystal Fluorescence Intermittency from Off-State Quantum Yields and Multiexciton Blinking. *Phys. Rev. Lett.* **2010**, *104*, 157403.

(20) Rosen, S.; Schwartz, O.; Oron, D. Transient Fluorescence of the Off State in Blinking CdSe/CdS/ZnS Semiconductor Nanocrystals Is Not Governed by Auger Recombination. *Phys. Rev. Lett.* **2010**, *104*, 157404.

(21) Hohng, S.; Ha, T. Near-Complete Suppression of Quantum Dot Blinking in Ambient Conditions. *J. Am. Chem. Soc.* **2004**, *126*, 1324-1325.

(22) Hammer, N. I.; Early, K. T.; Sill, K.; Odoi, M. Y.; Emrick, T.; Barnes, M. D. Coverage-Mediated Suppression of Blinking in Solid State Quantum Dot Conjugated Organic Composite Nanostructures. *J. Phys. Chem. B* **2006**, *110*, 14167-14171.

(23) Efros, A. L.; Rosen, M. Random Telegraph Signal in the Photoluminescence Intensity of a Single Quantum Dot. *Phys. Rev. Lett.* **1997**, *78*, 1110-1113.

(24) Verberk, R.; van Oijen, A. M.; Orrit, M. Simple Model for the Power-Law Blinking of Single Semiconductor Nanocrystals. *Phys. Rev. B* **2002**, *66*, 233202.

(25) Lane, L. A.; Smith, A. M.; Lian, T.; Nie, S. Compact and Blinking-Suppressed Quantum Dots for Single-Particle Tracking in Live Cells. *J. Phys. Chem. B* **2014**, Article ASAP.

(26) van Schooten, K. J.; Boehme, C.; Lupton, J. M. Coherent Magnetic Resonance of Nanocrystal Quantum-Dot Luminescence as a Window to Blinking Mechanisms. *ChemPhysChem* **2014**, *15*, 1737-1746.

(27) Cirillo, M.; Aubert, T.; Gomes, R.; Van Deun, R.; Emplit, P.; Biermann, A.; Lange, H.; Thomsen, C.; Brainis, E.; Hens, Z. "Flash" Synthesis of CdSe/CdS Core-Shell Quantum Dots. *Chem. Mater.* **2014**, *26*, 1154-1160.

(28) Frantsuzov, P. A.; Marcus, R. A. Explanation of Quantum Dot Blinking Without the Long-Lived Trap Hypothesis. *Phys. Rev. B* **2005**, *72*, 155321.

(29) Park, S. J.; Link, S.; Miller, W. L.; Gesquiere, A.; Barbara, P. F. Effect of Electric Field on the Photoluminescence Intensity of Single CdSe Nanocrystals. *Chem. Phys.* **2007**, *341*, 169-174.

(30) Yu, M.; Van Orden, A. Enhanced Fluorescence Intermittency of CdSe-ZnS Quantum-Dot Clusters. *Phys. Rev. Lett.* **2006**, *97*, 237402.

(31) Shepherd, D. P.; Whitcomb, K. J.; Milligan, K. K.; Goodwin, P. M.; Gelfand, M. P.; Van Orden, A. Fluorescence Intermittency and Energy Transfer in Small Clusters of Semiconductor Quantum Dots. *J. Phys. Chem. C* **2010**, *114*, 14831-14837.

(32) Kolodny, L. A.; Willard, D. M.; Carillo, L. L.; Nelson, M. W.; Van Orden, A. Spatially Correlated Fluorescence/AFM of Individual Nanosized Particles and Biomolecules. *Anal. Chem.* **2001**, *73*, 1959-1966.

(33) Wang, S.; Querner, C.; Fischbein, M. D.; Willis, L.; Novikov, D. S.; Crouch, C. H.; Drndic, M. Blinking Statistics Correlated with Nanoparticle Number. *Nano Lett.* **2008**, *8*, 4020-4026.

(34) Frantsuzov, P. A.; Volkan-Kacso, S.; Janko, B. Model of Fluorescence Intermittency of Single Colloidal Semiconductor Quantum Dots Using Multiple Recombination Centers. *Phys. Rev. Lett.* **2009**, *103*, 207402.

Chapter 4

Antibunching in Quantum Dot Clusters

This chapter is based on work published in a special issue of the Journal of Physical Chemistry B titled “Photon Antibunching in Small Clusters of CdSe/ZnS Core/Shell Quantum Dots.” I was the lead author in this work with co-authors Jessica Geisenhoff, Duncan Ryan, Martin Gelfand, and Alan Van Orden. Figures, tables, and text are adapted with permission from American Chemical Society. Copyright 2014 American Chemical Society. In this work I designed an experiment to observe the correlated photon histogram from small clusters of quantum dots. I collected correlated photon histograms and time-tagged time resolved photon data from individual quantum dots and small quantum dot clusters. I was able to configure our experimental setup to collect this data, which it is not regularly designed to do because of limitations to the photon counting hardware. This allowed me to observe the antibunching phenomena in individual quantum dots as well as in quantum dot clusters. This phenomenon is well known in individual quantum dots but, to my knowledge, is the first observation of antibunching from multiple quantum dots. I modeled the antibunching as an effect of the energy transfer which successfully reproduced the antibunching observed in clusters using parameters determined from the fluorescence of the cluster. This work contributes significantly to the field of single molecule spectroscopy as well as energy transfer in quantum dots. The best identifier of a single emitter in fluorescence measurements has traditionally been antibunching; however, this work has found antibunching from multiple emitters in close proximity. The antibunching in quantum dot clusters shows that there is a high degree of energy transfer especially in small clusters. This indicates that all quantum dots in these clusters have at least one acceptable donor or acceptor, otherwise the antibunching in clusters would only be observed in some small clusters. Some large clusters did not show a high degree antibunching due to the possibility of multiple local acceptors that were too far from each other to transfer energy.

4.1 Introduction to Antibunching and the Interaction of Energy Transfer with Antibunching

Quantum dots have been extensively studied using single molecule techniques, revealing such phenomena as fluorescence intermittency[1-12] (also known as blinking) and antibunching.[13-18] The origin of blinking in QDs is still somewhat a matter of debate. Many researchers believe that blinking arises from fluctuations in the local environment which open (and close) efficient non-radiative decay channels involving surface states.[8,9,11,12,19-21] Antibunching in QDs, however, is understood quite well. Photon antibunching is the low probability of observing the emission of two photons at the same time from a single emitter such as a QD or fluorescent dye. In nanostructures such as QDs, multiple excitations result in auto-annihilation from fast Auger processes[13,14,18] unlike in a fluorescent dye where the dye is unable to absorb photons while in the excited state.[22-24] Both of these mechanisms result in an antibunched photon signal.

For the past several years our group has studied small clusters of close-proximity CdSe/ZnS QDs with single-molecule techniques, revealing fluorescence behaviors—specifically intensity autocorrelations, fluorescence decay histograms, and fluorescence lifetime-intensity distributions that are distinct from individual QDs and multiple, isolated QDs.[25-27] We have also shown that the complicated fluorescence trajectories of QD clusters can be described by "*high/low*" blinking which has similar statistical properties to the "*on/off*" blinking of individual QDs.[27]

The distinct fluorescence behaviors in small clusters of CdSe/ZnS QDs can be well accounted for by an energy transfer model.[26] Colloidal QD synthesis results in some dispersion in QD band gaps because of their size dependent properties. We make the reasonable hypothesis that in a cluster, larger QDs with smaller band gaps absorb energy from smaller QDs with larger band gaps. The energy transfer process is typically much faster than radiative decay and most of the excitations in a small cluster make their way to the QD with smallest band gap (the "acceptor") in the cluster.[26,28] Thus the fluorescence

intensity of the entire cluster is modulated by the *on*/*off* behavior of the acceptor, resulting in *high*/*low* blinking in clusters that is analogous to *on*/*off* blinking in individual QDs.[27]

Energy transfer between QDs has been well studied in systems where there are distinct donor and acceptor QDs,[29-39] as well as in nominally monodisperse close proximity arrangements of QDs.[28,34,35,40-45] These studies have examined large assemblies of interacting QDs using ensemble averaged spectroscopic methods. While other groups have used single molecule spectroscopy techniques to investigate small individual groupings of nanoparticles and nanorods,[45-49] our focus is the consequence of energy transfer on the unique spectroscopic behavior of such clusters.[25-27]

As a consequence of the energy transfer we hypothesize that multiple excitations of separate QDs in a cluster are likely to all transfer to the acceptor, such that fluorescence from a cluster of QDs should be antibunched relative to the fluorescence from the same number of well separated QDs. In this work we carry out antibunching measurements on individual CdSe/ZnS core/shell QDs, multiple well-separated QDs, and QD clusters comprising multiple QDs in close proximity. We have modeled the data using parameters derived from experimental intensity traces and fluorescence decay histograms. In the case of small compact clusters the energy transfer model yields predictions for the degree of antibunching in reasonable quantitative agreement with the experimental results. Some of the largest clusters we have examined have weaker antibunching than our minimal energy transfer model suggests. This is to be expected, since in a sufficiently large cluster the energy transfer rate between some QDs could be slow compared to the radiative decay rate. Thus there can be more than one acceptor QD, with different portions of the cluster channeling energy to different acceptors.

4.2 Experimental Methods Specific to Quantum Dot Cluster Antibunching

Samples were prepared from a 5mg/mL solution of CdSe/ZnS core/shell (QSO-560 Ocean Nanotech, Springdale, Arkansas) QDs with 560nm peak emission. The stabilizing ligand was octadecylamine. Samples with only individual isolated QDs were prepared by diluting the original

solution by a factor of 2.5 x 10^7 in spectrophotometric grade toluene (Sigma Aldrich, St. Louis, Missouri) and spin casting ~30 µL onto freshly cleaved mica (described below) at 5000 rpm with a Chemat KW-4A spin coater (Northridge California). Methanol was used to cluster individual QDs as in previous studies by slowly precipitating the QDs into clusters.[25-27] Methanol precipitates the QDs by making the solution more polar such that the nonpolar ligands are attracted to other ligands on other QDs. Such clustering is reversible and has been used to purify QD samples by crashing QDs out of solution and resuspending them.[50] Samples containing a mixture of QD clusters and individual isolated QDs were prepared at 1-4 times the concentration of individual QD samples and then incubated with 5-10 µL of methanol (Alfa Aesar, Ward Hill, Massachusetts) per mL of QD dilution for ~10 minutes. Samples made for observation of individual QDs or clusters have very low surface coverage (approximately 5 QDs/clusters in a 20 × 20 μm^2 area). High density QD samples for non-interacting multiple QD measurements were diluted by a factor of 2.5-5 × 10^5 with no methanol. All samples were dried in a vacuum desiccator for 0.5 h before optical measurements.

Mica was employed as a substrate for its combination of flatness and optical transparency, both of which are required for the correlated atomic force microscopy (AFM) and optical measurements in this work. Very thin mica surfaces (V1 highest grade, TED Pella, Redding, California) were prepared and glued to 25×25 mm^2 glass coverslips with low fluorescence optical adhesive (Norland Optical, Cranbury, New Jersey). The surface of the mica was freshly cleaved and treated in a vacuum desiccator with (3-aminopropyl) triethoxysilane (Alfa Aeser, Ward Hill, Massachusetts) before QD deposition.

A diagram of the experimental apparatus is shown in Figure 4.1a. Optical measurements were made with an inverted microscope (Ziess Axiovert S100 2TV, Oberkochen, Germany). Samples were mounted onto a model NIS-30 SC-100/208 piezoelectric scanning stage (Nanonics, Jerusalem, Israel). A 453 nm LDH-P-C 450B laser head and PDL 800-B driver pulsed laser system (Picoquant, Berlin, Germany) was used to excite samples at 5 or 10 MHz and a ~70 ps pulse width. The 0,0 mode of the diode laser was selected with a single mode 5405-XP optical fiber (Thorlabs, Newton, New Jersey).

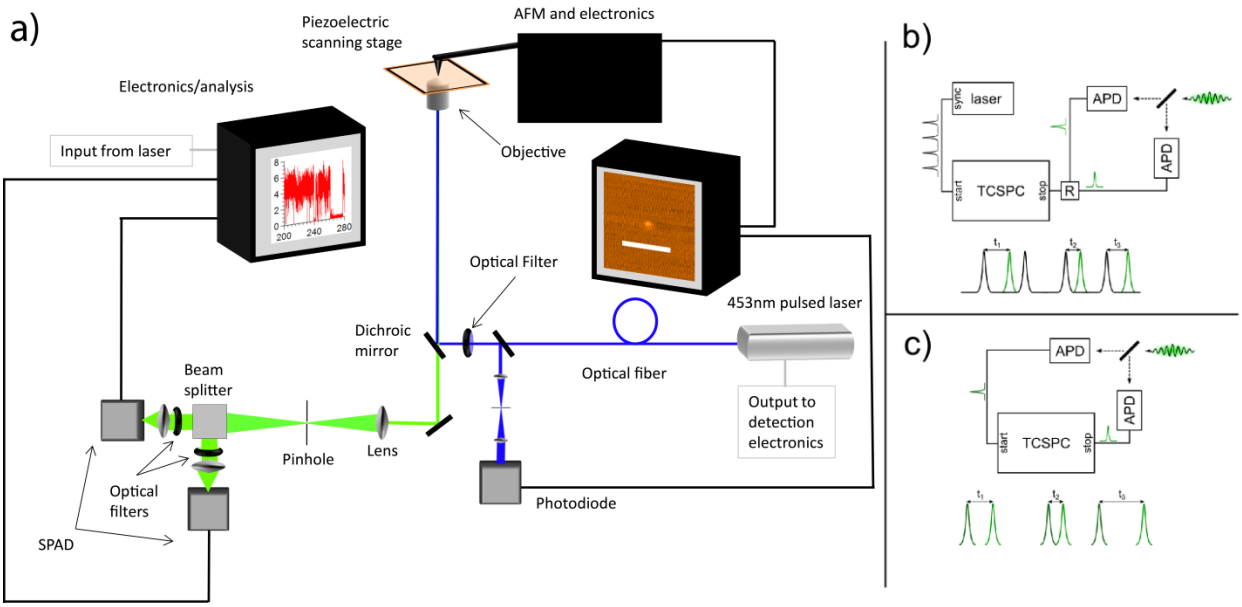

Figure 4.1: Experimental diagram for collection of correlated fluorescence and AFM. Fluorescence traces and lifetime measurements were made with the setup wiring as in a) and b). Antibunching measurements were taken with the wiring shown in c) and all other components unchanged.

The average power was 25 nW, or ~15 W/cm^2 in the excitation region. The beam was focused to a diffraction limited excitation region (~ 0.5 μm diameter) on the surface of the mica through a Zeiss Fluar 1.3 numerical aperture/40× objective. Fluorescence was collected through the same objective and filtered from the excitation beam with a dichroic mirror (Part number Z450rdc, Chroma, Rockingham Vermont). The fluorescence was then focused through a 50 μm pinhole and split with a 50/50 beamsplitter through 565/40 nm band pass filters (part number D565/40m, Chroma, Rockingham, Vermont) and focused onto two avalanche photodiode detectors (Tau-SPAD 50, Picoquant, Berlin, Germany). The samples were raster scanned by the stage with in house programmed software to make a 20×20 μm^2 fluorescence map. The stage was then moved to a fluorescent point where optical measurements were performed.

Fluorescence intensity and lifetime data were collected for five minutes using the configuration in Figure 4.1b with a 10 MHz laser pulse frequency. Signals from the detectors were collected with a photon counting card (PicoQuant Time Harp 200, Berlin, Germany) mounted in a PC. The hardware clock starts when signaled by a TTL pulse from either detector and stops when signaled by the laser sync output. Coincident photon measurements were then collected for ~1 hour by replacing the laser sync signal with a detector NIM pulse output through a 180 ns delay and disconnecting that detector's TTL output. In this Hanbury Brown-Twiss interferometer configuration (Figure 4.1c), the hardware clock is started by one detector and stopped by the other. The measurement records a histogram of delay times between the start and stop signals. The full range of the histogram created is 570 ns with a resolution of 144 ps. Start signals that do not occur within 570 ns of a stop signal are not recorded by the hardware, so useful simultaneous intensity traces cannot be obtained. After the coincident photon measurement, another five-minute intensity/lifetime measurement was made with the laser output and detector TTL pulse reconnected. Fluorescence data were processed with Picoquant's Symphotime (V. 5.3.2.2) software for fluorescence traces and lifetime measurements. Coincident photon data was collected with the Symphotime software and processed with in house programmed Igor Pro 6.34A software.

After fluorescence measurements were carried out, we engaged an AFM (Digital Instruments Bioscope) mounted above the piezo scanning stage and operated by Nanoscope V5.12 software (Digital Instruments). Topographical images were collected from the excitation region in tapping mode with OTESPA AFM probes (40 N/m force constant 270-350 kHz tapping frequency, Bruker). Images were flattened and subjected to a lowpass filter using the Nanoscope V5.12 software. We determined particle effective AFM volumes using in house programmed Igor Pro software.

The topographical images were correlated with the excitation region of the optical microscope using the backscattered excitation beam. We collected the laser light scattered from the surface and AFM probe and spatially filtered the reflection through a 100 μm pinhole. The signal was amplified with a lock-in amplifier (Stanford Research Systems SR844 RF) at the drive frequency of the AFM. The amplified signal allowed us to collect a backscatter image of the excitation beam on the surface and topographical image at the same time and of the same area.[51] We used the backscatter image of the focused laser beam to find the QD or QD cluster observed in the optical measurements and obtain a topographical image. Figure 4.2 shows a series of images that illustrate this process. We obtained a correlated 500×500 nm (256×256 points resolution) image for each QD and cluster in this work.

4.3 Antibunching in Small Quantum Dot Clusters and Comparisons with the Model Predictions

In the present work we have collected fluorescence intensity, lifetime, and antibunching data from individual isolated QDs, well separated groups of QDs, and small clusters of close proximity QDs using single molecule confocal microscopy with pulsed excitation and time tagged photon collection. Fluorescence measurements were correlated with topographical images of the excitation region using spatially correlated atomic force microscopy. Clusters of quasi-spherical CdSe/ZnS core/shell QDs stabilized with octadecylamine ligands in toluene were formed by adding methanol to cause clustering as in previous work.[25-27] After a short time, the solution was spin cast on a thin optically transparent mica surface. These samples are a mixture of individual QDs and clusters which are fully resolved by the

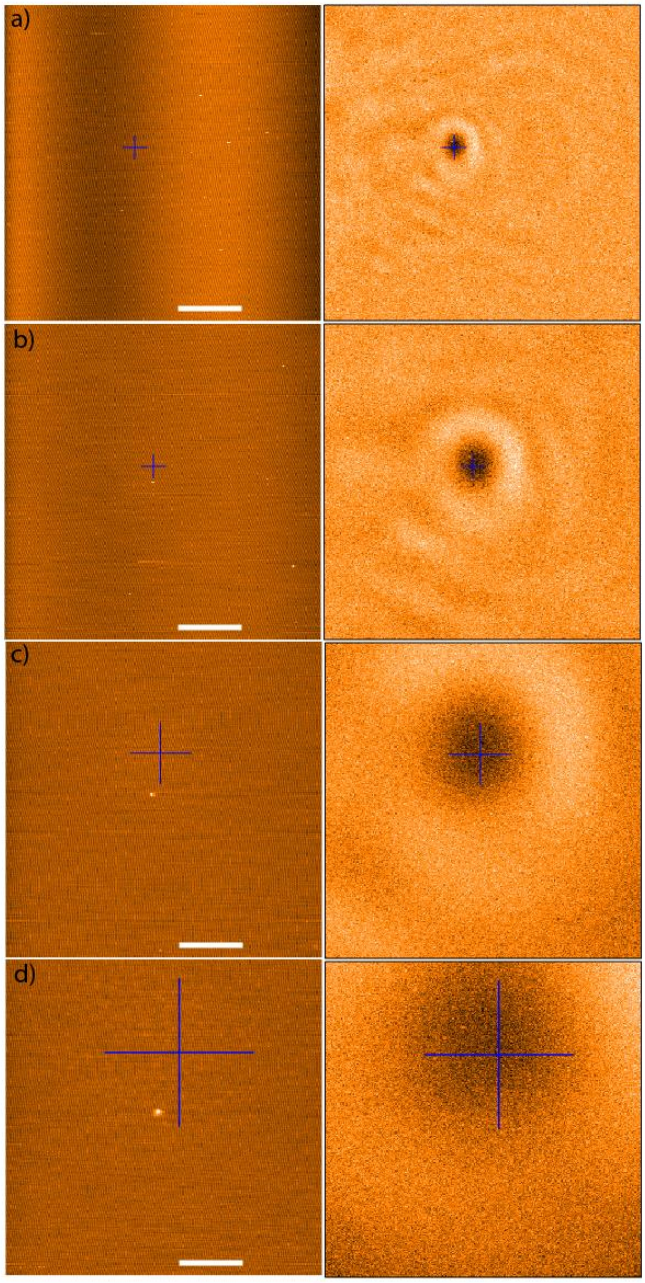

Figure 4.2: AFM images (left) and backscatter images (right) of the excitation region containing a cluster. To find particles in the excitation region, we start with a wide image such as a) and then continue to zoom in on the excitation region. The image scale bars are a) 2µm, b) 1µm, c) 400nm, and d) 200nm.

confocal microscope with confirmation from AFM. We use fluorescence intensity, fluorescence decay histograms, and AFM to distinguish clusters from individual QDs.

Most fluorescent particles observed in optical measurements reported here were determined to be either individual QDs or clusters using the effective AFM volume of the particle from the correlated AFM image. We use the effective AFM volume because the QDs are smaller than the typical radius of curvature for the AFM probes (~7 nm). We can use the effective volume to distinguish individual QDs from clusters, but we are not able to determine the exact number of QDs in the cluster. To determine the effective AFM volume we set the image baseline for each image by fitting a histogram of the image pixel Z heights to a Gaussian. The baseline was defined as three times the width above the center of the Gaussian fit. For each particle, we sum the Z heights in the AFM image that are above the baseline to obtain the effective AFM volume. The volumes are summarized in Table 4.1 for individual QDs, and Table 4.2 for QD clusters.

Samples that only contain individual QDs (no MeOH and thus no clustering) are compared with clustered samples which contain both individual QDs and clusters of varying sizes. Some fluorescent particles can be classified as either an individual QD or cluster unambiguously from the effective AFM volume. Particles with volumes great than 600 nm^3 were classified as clusters, while those with volumes below 200 nm^3 were classified as individual QDs. For ambiguous particles (200-600 nm^3) we used fluorescence data (intensity and decay histograms) to identify particles as a cluster or individual QD. The fluorescence decays can be fit to bi-exponentials where A_{short} is the amplitude of the shorter lifetime and A_{long} is the amplitude of the longer lifetime. The short lifetime component is defined as $A_{short}/(A_{short} + A_{long})$. Previous work[26] has shown that the short lifetime component is generally larger in clusters than in isolated QDs. Particles with maximum normalized intensities greater than 0.5 kHz/nW or short-lifetime component greater than 0.14 were classified as clusters. Results are summarized in Tables 4.1 and 4.2. Importantly, no more than one QD or cluster is found in the excitation region for the individual QD/cluster measurements.

Table 4.1: Individual QD AFM data, measured CPH *A*/*B* ratios, and fluorescence data. QDs marked with a dagger on the maximum intensity were found in samples with clusters.

Effective Volume (nm^3)	452	89	130	152	204	143	193	139	162	515	298	122
Area (nm^2)	337	237	179	195	296	195	144	197	139	319	397	210
CPH Peak Ratio A/B	-0.06	0.00	0.06	0.03	0.03	0.04	0.04	0.03	0.04	0.04	0.03	0.05
Short Lifetime Component	0.08	0.13	0.11	0.20	0.11	0.14	0.13	0.09	0.08	0.07	0.02	0.00
Max Intensity (kHz/nW)	†0.18	0.18	0.22	0.24	0.24	0.28	0.32	†0.33	0.35	0.40	0.41	0.47

Table 4.2: QD cluster AFM data, fluorescence data, measured CPH *A*/*B* ratio, calculated peak ratio (*A*/*B*) for a 2, 3, and 4 QD cluster and *r* parameter. The clusters marked with an asterisk on the *r* value have CPH ratios much higher than predicted by the model, which we attribute to multiple acceptor dots resulting from large size and geometries unfavorable to energy transfer.

Effective Volume (nm^3)	Area (nm^2)	Short Lifetime Component	Max Intensity (kHz/nW)	CPH Peak Ratio A/B	Simulated 4QD A/B	Simulated 3QD A/B	Simulated 2QD A/B	k_T/k_E (model parameter: *r*)
873	483	0.24	0.44	0.07	0.10	0.09	0.07	12.9
1178	620	0.18	0.50	0.08	0.11	0.10	0.07	11.2
348	275	0.22	0.84	0.14	0.12	0.11	0.08	10.1
577	312	0.28	0.55	0.08	0.13	0.11	0.08	9.5
230	328	0.18	0.65	0.15	0.17	0.15	0.11	6.8
1217	531	0.11	0.62	0.18	0.17	0.15	0.11	6.5
878	742	0.19	0.69	0.31	0.18	0.16	0.12	*6.2
1398	620	0.17	0.60	0.15	0.18	0.16	0.12	6.1
629	418	0.23	0.52	0.13	0.19	0.17	0.13	5.8
553	513	0.2	0.32	0.12	0.20	0.18	0.14	5.2
497	427	0.39	0.36	0.14	0.21	0.19	0.14	4.9
514	336	0.25	0.76	0.26	0.22	0.19	0.15	4.7
1007	624	0.30	0.46	0.20	0.24	0.22	0.16	4.0
480	493	0.74	1.02	0.33	0.27	0.23	0.18	3.5
3078	1521	0.30	0.62	0.61	0.29	0.25	0.19	*3.1
2474	949	0.59	0.50	0.28	0.31	0.27	0.21	2.7
1671	966	0.41	1.07	0.53	0.32	0.28	0.21	*2.6

We now discuss the coincident photon histogram (CPH) of individual isolated QDs and describe the features in the CPH. All individual QDs show the expected low coincident photon signal around zero delay which is the hallmark of antibunching[13] (Figure 4.3a). However, the coincident photon signal is non zero, which has been attributed to the small but finite probability that a biexciton may yield two photons.[18] The peak centered at zero delay is denoted the zero delay peak (ZDP). A few nanoseconds on either side of zero delay is an artifact that is due to fluorescence from one detector triggering the other. The fluorescence from the detector avalanche is called afterglow and is reduced by the two band pass filters in front of each detector but is not completely eliminated. However, this artifact can be useful in identifying the ZDP, as it only occurs around zero delay. There are also peaks at intervals separated by multiples of the laser pulse period *T* (one such peak is visible in Figure 4.3). These are "separate pulse peaks" (SPPs), which, like the ZDP, decay exponentially on either side with the time constant of the fluorescence decay. Separate pulse peaks result from pairs of photons associated with excitations from different laser pulses. As an approximation the CPH is fit to the function:

$$Ae^{\frac{-|t|}{\tau_E}} + B(e^{\frac{-|t-T|}{\tau_E}} + e^{\frac{-|t+T|}{\tau_E}} + e^{\frac{-|t-2T|}{\tau_E}} + \cdots) \qquad \text{Equation 4.1}$$

where *A* is the amplitude of the ZDP, *B* is the amplitude of the SPPs, τ_E is the decay lifetime, and *t* is the time between coincident photon arrivals. Additional terms may be included to account for other SPPs in the full range of the CPH. To determine the zero-delay point we use the instrument response to a small amount of attenuated laser signal (Figure 4.4) as well as detector afterglow. The time intervals affected by afterglow are determined by inspection of individual QD CPHs and are not included in the fits to Equation 4.1 for any of the CPHs. The maximum likelihood estimation method was used to determine the best fit. It is worth noting that a simple least squares fit did not produce very different results.

Optical measurements of multiple non-interacting QDs were made on high surface density samples of individual QDs (Figure 4.3b). These measurements show the expected larger ZDPs in their

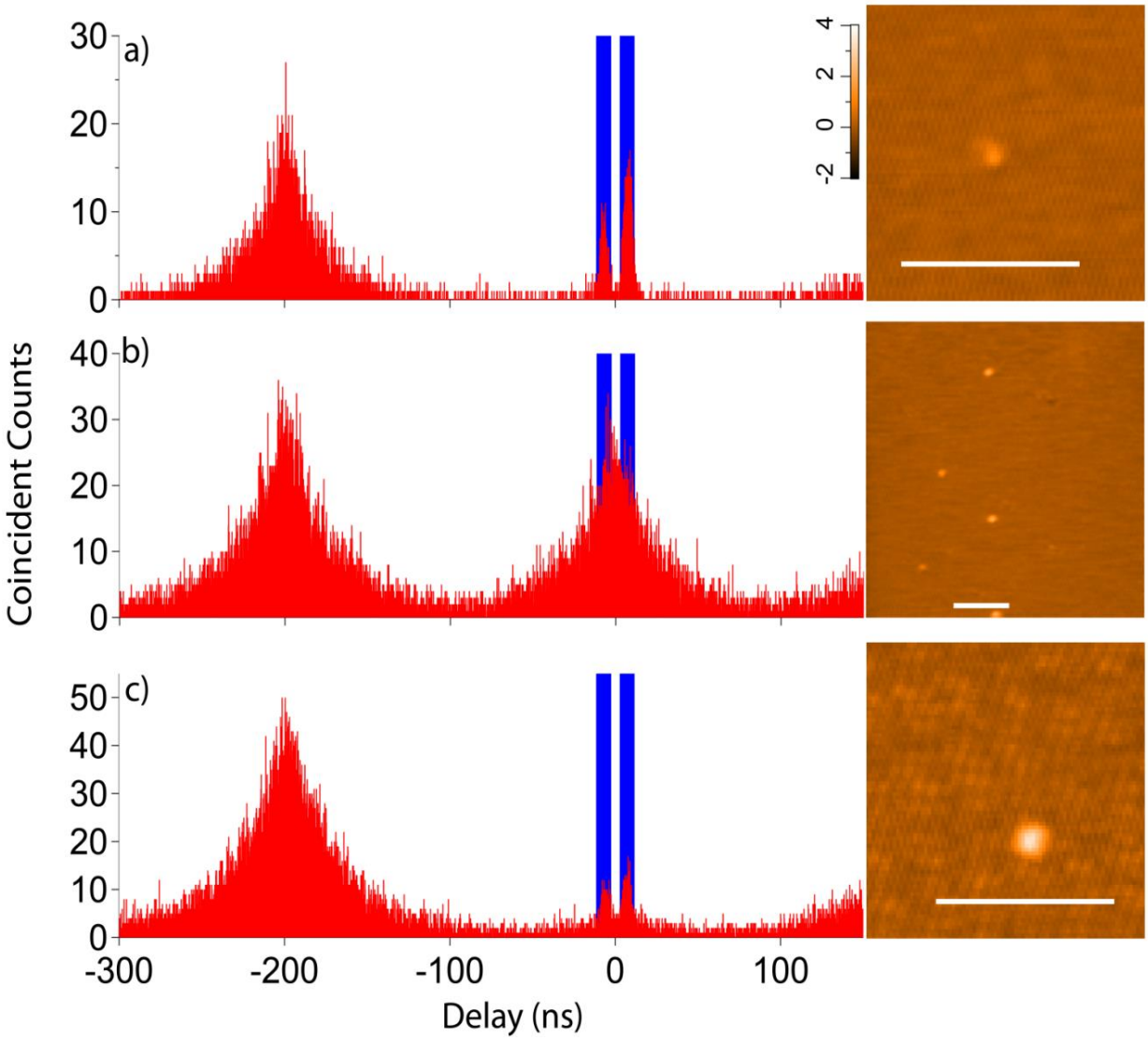

Figure 4.3: Coincident photon histogram (CPH) measurements taken at a 5MHz pulse rate from (a) an isolated QD, (b), multiple isolated QDs, and (c) a cluster of QDs. The insets show AFM images of the QDs found in the excitation area (all scale bars 100 nm). The blue areas of the CPH, which have significant contributions from afterglow, are omitted from further analysis.

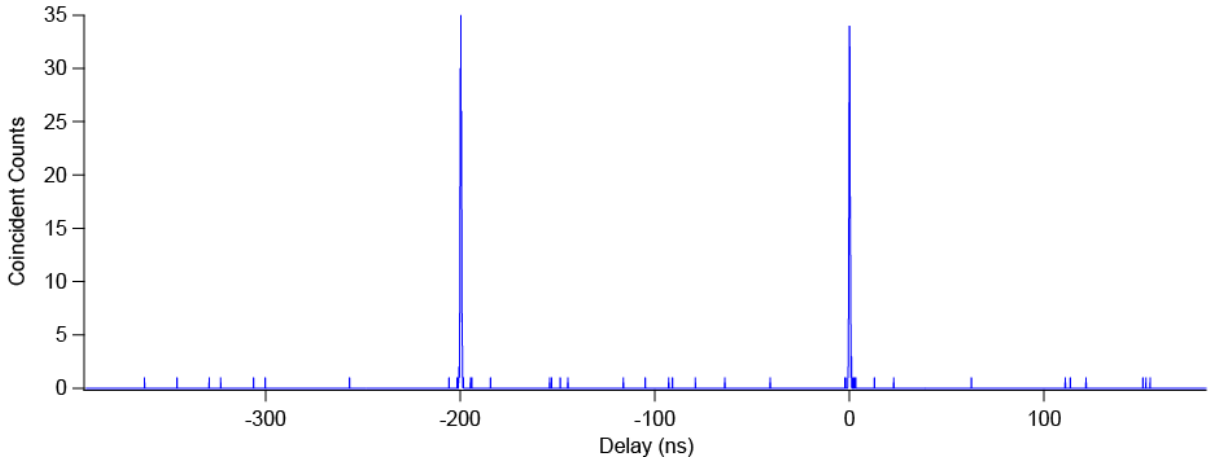

Figure 4.4 Instrument response function taken in the configuration (Figure 4.1c) for collecting the coincident photon histogram. The 560 nm bandpass filters are also replaced with neutral density filters to attenuate laser signal. No antibunching is expected from the laser signal so a peak at the 0 delay present at the same height as the peak from a separate pulse. This is used to determine the 0 delay point for samples.

CPHs because there are multiple independent emitters in the excitation region. Individual QDs show antibunching because multiple excitons on one QD annihilate each other, but multiple QDs can absorb separately from the same pulse and emit separately, resulting in coincident photon counts from a single pulse. The relative heights of the ZDP and the SPP are dependent on the number of QDs in the excitation region, the intensity of illumination at each QD, and the fraction of time each QD spends in the *on* state. Consider a situation where there are two QDs in the probe region, equally illuminated and both are in the *on* state. The signal from separate pulses can occur when either QD absorbs and emits. The ZDP signal results only when both QDs absorb and emit, which is half as likely as either QD absorbing and emitting on separate pulses assuming low excitation probability. Thus, in this situation, the amplitude of the ZDP would be half the amplitude of the SPPs. When one of the two QDs is in the *off* state the resulting CPH will look like a single QD. The overall CPH of the 2 QDs will be a weighted average of the two situations depending on the *on*/*off* times observed. Figure 4.5 shows 2 individual QDs found in the excitation region. This situation was observed by chance, but illustrates the situation of 2 non-interacting QDs nonetheless. Larger collections of non-interacting QDs result in ZDPs with amplitudes closer to the SPPs since the probability of exciting separate emitters when two excitations are generated during one pulse is increased for each *on* QD in the probe region.

The key experimental results are the CPHs of clusters of close proximity QDs (Figure 4.3c). For most clusters, the ZDP is far smaller than expected even for just two non-interacting QDs (Table 4.2, Figure 4.5).We suggest that energy transfer among QDs in close proximity quenches emission from multiple absorptions. We will now describe in detail how a minimal, phenomenological energy transfer model[26] can be used to calculate the ZDP to SPP ratio (A/B from data fits) in terms of just a few parameters, and how those parameters can be mostly determined experimentally, leading to a coherent account of the CPH and other fluorescence data. We will begin by considering the model and its consequences, and then discuss how the results of the calculations can be compared with the experimental data.

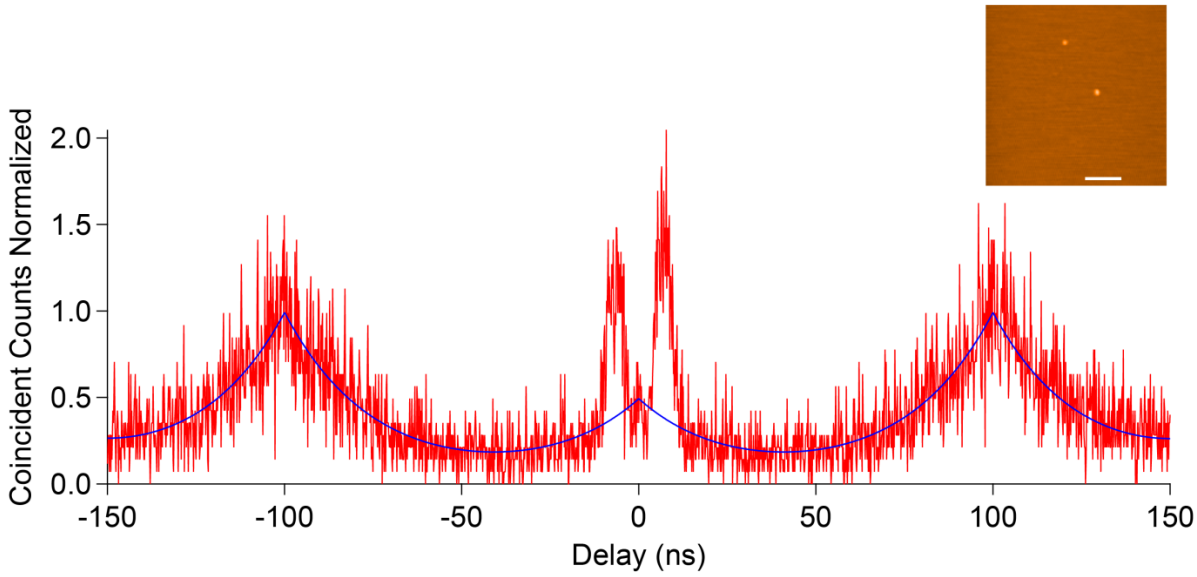

Figure 4.5: Normalized CPH of 2 QDs found in the excitation region collected at 10MHz with the calculated $r = 0$ data for 2 QDs (F = 0.90). The inset is the AFM image of the QDs in the excitation region (Scale Bar = 100nm).

We denote the number of QDs in a cluster as *N*. We assume, as in our earlier work, that the QDs have mostly identical properties; in particular that they each have the same optical absorption cross-section, the same radiative decay rate k_E, the same probability *F* of being in the *on* state during the course of a measurement, and that they blink independently of the other QDs in the cluster. The only way in which the QDs are assumed to differ is in their band gaps; it is assumed that nonradiative energy transfer is possible from a given QD to any QD with a smaller band gap at a rate k_T. It is useful to define the rate ratio $r = k_T/k_E$, and to note that average *r* for the clusters studied in this work is ~6.

There are some new assumptions relevant to CPH measurements. We assume that a doubly-excited *on* QD becomes singly-excited at a rate fast compared to k_E and k_T via loss to Auger processes: that is, we neglect the small but finite biexciton yield reported by Nair *et al*.[18] We also assume that the excitation probability of each QD in any pulse is very small (in our experiments it is approximately 0.75%, see Equations 4.2-4.4) so that we can neglect the possibility of triple-excitation in a single pulse, and also neglect all contributions to the SPPs except those arising from single excitations. The probability of excitation for a single QD is determined from the following calculations. The average power in the confocal region is

$$\frac{P_0}{Area} = P_A \qquad \text{Equation 4.2}$$

$$(P_A)\frac{\lambda}{hc} = F_l \qquad \text{Equation 4.3}$$

$$P_{abs} = (\sigma_{QD})\left(\frac{F_l}{f}\right) \qquad \text{Equation 4.4}$$

where P_0 is the average power going into the objective, the Area is the spot area in cm^2 (assuming .25μm radius), P_A is the intensity, λ is the excitation wavelength, *h* is Planck's constant, *c* is the speed of light, F_l is the fluence, P_{abs} is the probability of absorption per pulse, σ_{QD} is the absorptive cross section, and *f* is the pulse frequency. We take σ_{QD} to be approximately $10^{-16}cm^2$ from Lounis et al.[13] since our excitation

wavelength and QD emission are similar to their work. Using the parameters detailed in the experimental section we determine the probability of excitation in one QD per pulse to be 0.75%.

At any instant, some of the QDs in a cluster under illumination may be *on*, and others may be *off*. There are 2^N "states" of the cluster defined by the *on*/*off* status of its constituent QDs, and following our simple assumptions the probability of a state with M *on* QDs is $F^M(1\text{-}F)^{N\text{-}M}$. Calculating the A/B ratio in the context of the model requires calculating the contributions to the ZDP and the SPPs for every state of the cluster. The calculations of the ZDP amplitudes in turn require the consideration of all cases where two *on* QDs are excited, while for the SPP amplitudes we consider cases where just one *on* QD is excited. Excitations of QDs in the *off* state are not recoverable. We will present a complete derivation of A/B from the model only for the case of $N = 2$. For $N = 3$ we will describe in detail the case of one interesting state, and otherwise we will just present the results for A/B. Note that the assumption of a single energy transfer rate is geometrically implausible for a cluster with $N > 4$, so we only carry out calculations for $N = 2$, 3, and 4. Although we can distinguish individual QDs from clusters by a combination of effective volume from AFM and fluorescence data, it is difficult to obtain definitive information about the number of QDs in a cluster. The effective volumes obtained for clusters (Table 4.2) are, on average, less than 4 times larger than the values for individual QDs in Table 4.1, so we believe the assumption that $N = 2$, 3 or 4 is reasonable in most cases (with some exceptions to be discussed below).

For $N = 2$, there are 4 states, which we identify by listing whether each QD is *on* or *off*, in order of decreasing energy gap (donor/acceptor): (i) *on*/*on*, probability F^2, (ii) *off*/*on*, probability $F(1\text{-}F)$, (iii) *on*/*off*, probability $F(1\text{-}F)$, and (iv) *off*/*off*, probability $(1\text{-}F)^2$. Following the terminology of our previous work,[27] the first two are "*high*" states of the cluster and the last two are "*low*" states. For state (iv) there is no emission at all. States (ii) and (iii) cannot emit two photons from one laser pulse. Their contribution to the SPP is proportional to the square of the quantum yield for single excitations which is equal to $(0.5)^2$ for state (ii) and $[0.5/(1+r)]^2$ for state (iii). We do not consider the excitation probability per QD per pulse and the collection efficiency because we assume these parameters to be the same for every state. State (i)

is the most interesting. Its quantum yield for single excitations is 1. Double excitations can be either both on the same QD (with probability 0.5) or on different QDs (probability 0.5). In the former case, only a single photon is emitted. In the latter case, we need to consider the dynamics of the excitations; Figure 4.6a summarizes the kinetic equations in graphical form. Solving these equations (see Eq 4.5-4.15) leads to the result that two-photon emission takes place with probability 2/(2+*r*). Complete derivations of the 2 photon yield from the state shown in Figure 4.6a is shown below. First are the derivations for the state populations and second photon yields for the cases presented in Figure 4.6. States in square brackets can be identified in Figure 4.6a (Here state refers to the specific arrangement of excited QDs in the cluster, rather than the arrangement of *on*/*off* QDs.). The equations for changes in populations can be read directly from the diagram and are as follows

$$\frac{d[P_{DE}]}{dt} = -(2k_E + k_T)[P_{DE}] \qquad \text{Equation 4.5}$$

$$\frac{d[P_{SE1*}]}{dt} = k_E[P_{DE}] - k_E[P_{SE1*}] \qquad \text{Equation 4.6}$$

$$\frac{d[P_{SE2}]}{dt} = k_E[P_{DE}] - (k_E + k_T)[P_{SE2}] \qquad \text{Equation 4.7}$$

$$\frac{d[P_{SE1}]}{dt} = k_T[P_{SE2}] - k_E[P_{SE1}] \qquad \text{Equation 4.8}$$

$$\frac{d[Ph_2]}{dt} = k_E([P_{SE1*}] + [P_{SE2}] + [P_{SE1}]) \qquad \text{Equation 4.9}$$

Equation 4.5 can be solve immediately to yield

$$[P_{DE}]_{(t)} = [P_{DE}]_{(0)} e^{-(2k_E+k_T)t} \ . \qquad \text{Equation 4.10}$$

and the result can be inserted into 4.6 and 4.7, allowing them to be solved and giving

$$[P_{SE1*}]_{(t)} = [P_{DE}]_{(0)} \frac{k_E}{(k_E+k_T)} \left(e^{-k_E t} - e^{-(2k_E+k_T)t} \right) \qquad \text{Equation 4.11}$$

$$[P_{SE2}]_{(t)} = [P_{DE}]_{(0)} \left(e^{-(k_E+k_T)t} - e^{-(2k_E+k_T)t} \right) . \qquad \text{Equation 4.12}$$

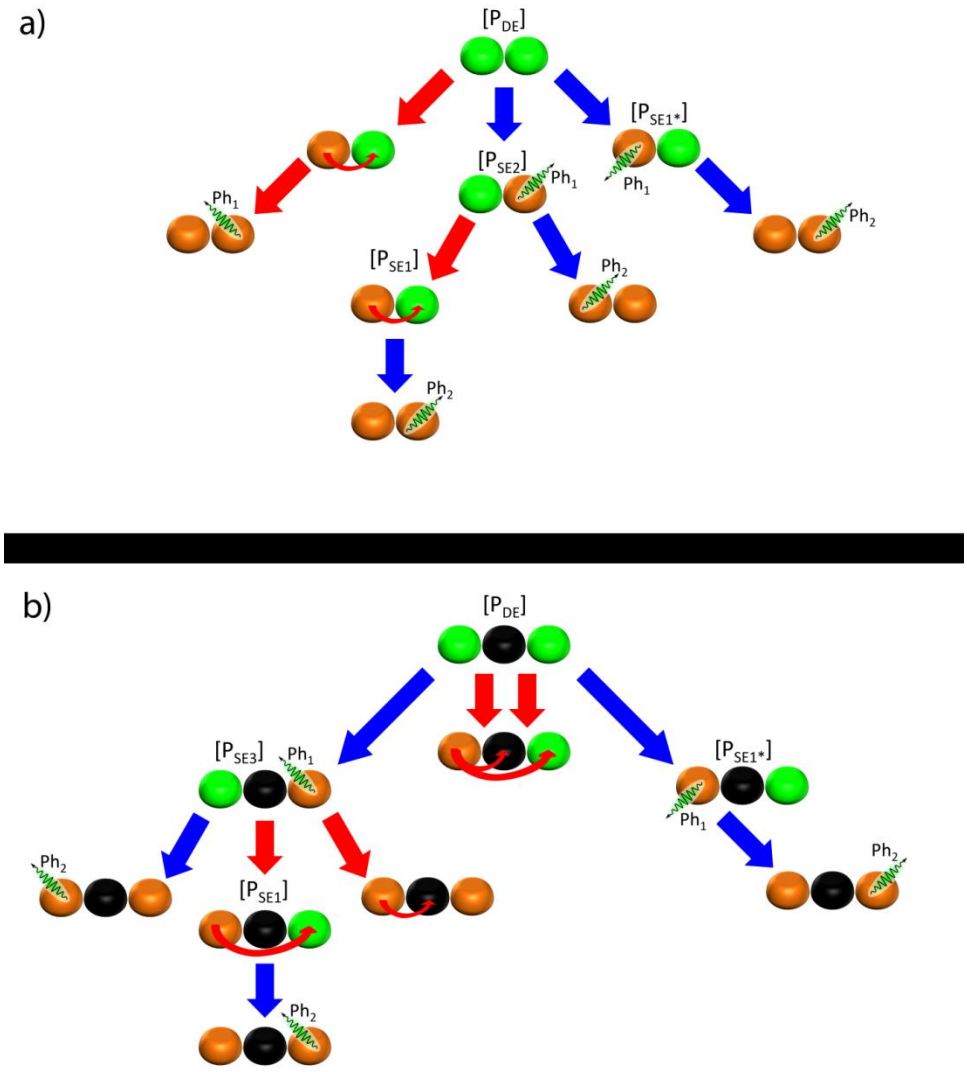

Figure 4.6: A schematic depicting the model predicted pathways to photon emission or excitation loss in a) 2 QD cluster and b) 3 QD cluster with one QD in the *off* state and two excitations. The QDs are arranged from largest band gap (left) to smallest (right), not reflecting actual geometries. Green QDs have an exciton, gold QDs are in the *on* state with no exciton and the black QD is in the *off* state. Blue arrows indicate photon emission at the rate k_E and red arrows indicate energy transfer at the rate k_T. The sub-states are identified; $[P_{DE}]$ is the initial double exciton state, $[P_{SE1}]$ is a state with single exciton on the acceptor QD resulting from energy transfer, $[P_{SE1*}]$ is a state with a single exciton on the acceptor resulting from emission, $[P_{SE2}]$ is a state with a single exciton on the 2nd lowest band gap QD, $[P_{SE3}]$ is a state with a single exciton on the 3rd lowest band gap QD, Ph_1 is the emission of the first photon from the system, and Ph_2 is the emission of a second photon from the system. Curved red arrows show the direction of the exciton transfer.

Inserting these last two into 4.8 allows for its solution, with the result

$$[P_{SE1}]_{(t)} = [P_{DE}]_{(0)}\left(\frac{k_E\, e^{-k_E t}}{(k_E+k_T)} - e^{-(k_E+k_T)t} - \frac{k_T e^{-(2k_E+k_T)t}}{k_E+k_T}\right) \quad \text{Equation 4.13}$$

and now 4.9 can be solved to obtain

$$[Ph_2]_{(t)} = [P_{DE}]_{(0)}\left(\frac{2k_E}{2k_E+k_T} - \frac{2e^{-k_E t}}{(k_E+k_T)} + \frac{2k_E k_T e^{-(2k_E+k_T)t}}{(2k_E+k_T)(k_E+k_T)}\right). \quad \text{Equation 4.14}$$

Evaluating 4.14 at infinite time gives the two-photon quantum yield $2k_E/(2k_E+k_T)$ or $2/(2+r)$. Putting together all of the contributions described above gives the SPP amplitude for the two QD cluster proportional to

$$SPP \cong F^2 + \left(\frac{F(1-F)}{4}\right)\left(1 + \frac{1}{(1+r)^2}\right) \quad \text{Equation 4.15}$$

and the ZDP amplitude proportional to

$$ZDP \cong \frac{F^2}{2}\left(\frac{2}{2+r}\right) \quad \text{Equation 4.16}$$

and the ratio of the ZDP to the SPP is

$$\frac{A}{B} = \frac{1}{(2+r)\left[1+\frac{1}{4}\left(\frac{1}{F}-1\right)\left(1+\frac{1}{(1+r)^2}\right)\right]} \quad \text{Equation 4.17}$$

A few facts about this result are worth noting. For typical values of *r*, the contribution of state (iii) to the SPP is small relative to the contribution of state (ii). As a function of *F*, the maximum value of *A*/*B* is attained when *F*=1, and even for *F* as small as 3/4 the value of *A*/*B* is still nearly 12/13 of that maximum value.

The case *F* = 1, where only the all-*on* state needs to be considered, is readily generalized to any number of QDs in a cluster, leading to

$$\frac{A}{B} = \left(\frac{N-1}{N}\right)\left(\frac{2}{2+r}\right)$$ Equation 4.18

The first factor comes from the probability that two excitations are initially on different QDs. Equation 4.18 is always the maximum *A*/*B* as a function of *F*. It is also a good approximation to the exact result of the model calculation for any $F \approx 1$. The $r = 0$ limit of Equation 18 recovers the expected result for isolated QDs, namely that *A*/*B* is given by the probability that two excitations are initially on different QDs. The $r = 0$ limit for arbitrary *F* can also be evaluated for any *N*, with the result

$$\frac{A}{B} = \frac{(N-1)F}{1+(N-1)F}$$ Equation 4.19

For $N > 2$ and $F < 1$ the calculations for *A/B* are more involved. As an example, consider the probability of two-photon emission from a three-QD cluster in the state *on*/*off*/*on* when the two *on* QDs are excited. The kinetic equations are summarized graphically in Figure 4.6b. Compared to the two-QD *on*/*on* state there are more routes for energy loss. The two-photon emission probability (P_{DEm}) derivation is shown below in equations 4.20-4.30. The equations governing the sub-state populations of the three QD cluster state in Figure 4.6b are

$$\frac{d[P_{DE}]}{dt} = -(2k_E + 2k_T)[P_{DE}]$$ Equation 4.20

$$\frac{d[P_{SE1*}]}{dt} = k_E[P_{DE}] - k_E[P_{SE1*}]$$ Equation 4.21

$$\frac{d[P_{SE3}]}{dt} = k_E[P_{DE}] - (k_E + 2k_T)[P_{SE1*}]$$ Equation 4.22

$$\frac{d[P_{SE1}]}{dt} = k_T[P_{SE3}] - k_E[P_{SE1}]$$ Equation 4.23

$$\frac{d[Ph_2]}{dt} = k_E([P_{SE1*}] + [P_{SE3}] + [P_{SE1}])$$ Equation 4.24

Again these can be solved one at a time, starting with 4.20 and working downward, with the results

$$[P_{DE}]_{(t)} = [P_{DE}]_{(0)}e^{-2(k_E+k_T)t}$$ Equation 4.25

$$[P_{SE1*}]_{(t)} = [P_{DE}]_{(0)} \frac{k_E}{(k_E+2k_T)} \left(e^{-k_E t} - e^{-2(k_E+2k_T)t} \right)$$ Equation 4.26

$$[P_{SE3}]_{(t)} = [P_{DE}]_{(0)} \left(e^{-(k_E+2k_T)t} - e^{-2(k_E+k_T)t} \right)$$ Equation 4.27

$$[P_{SE1}]_{(t)} = [P_{DE}]_{(0)} \left(\frac{k_E\, e^{-k_E t}}{2(k_E+2k_T)} - \frac{e^{-(k_E+2k_T)t}}{2} - \frac{(k_E)^2 e^{-2(k_E+k_T)t}}{k_E+2k_T} \right)$$ Equation 4.28

$$[Ph_2]_{(t)} = [P_{DE}]_{(0)} \frac{k_E}{2(k_E+2k_T)} \left(\frac{2k_E+3k_T}{k_E+k_T} - 3e^{-k_E t} - e^{-(k_E+2k_T)t} + \frac{(2k_E+k_T)e^{-(2k_E+k_T)t}}{(k_E+k_T)} \right)$$ Equation 4.29

Evaluating 4.29 at infinite time and replacing k_T/k_E with r gives the two-photon quantum yield equivalent to

$$P_{DEm} = \frac{(2+3r)}{2(1+r)(1+2r)},$$ Equation 4.30

resulting in a P_{DEm} that is smaller than the *on*/*on* case of the two QD cluster. This is a representative calculation for one of the 2^3 states of a three QD cluster. We have carried out similar calculations for every state of 3 and 4-QD clusters (Tables 4.3 and 4.4). The general prediction for *A*/*B* of a cluster with N members is

$$\frac{A}{B} = \frac{\sum_{n=1}^{2^N} (P_n P_{DE,n})}{\sum_{n=1}^{2^N} (P_n P_{SE,n}^2)}$$ Equation 4.31

where 2^N is the total number of states, P_n is the probability of the state n, $P_{DE,n}$ is the average two photon probability of the state, and $P_{SE,n}$ is the average single photon probability calculated in Tables 4.3 and 4.4.

Let us now consider how to compare experimental CPH data for QD clusters with the results of the model calculations. The model parameters are *N*, *r*, and *F*. We estimate *F* by examining the fluorescence trajectories for each individual QD presented in Table 4.1. These trajectories yielded a mean *F* value of 0.90 with a standard deviation of 0.04. A sample of an individual QD intensity trajectory and histogram with *on*/*off* threshold is presented in Figure 4.7. Although there was undoubtedly selection bias towards QDs with larger *F* values, we believe *F*=0.90 is a plausible estimate. Furthermore, as we have

Table 4.3: States of a 2 and 3 QD cluster, probability of being in that state given the *on* time fraction F, and the contributions to the SPP and ZDP for that state normalized to QY=1 for the all *on* state case. The states are B for *on* (bright) and D for *off* (dark) and arranged in decreasing energy. For example, the DB state for a 2 QD cluster below has the acceptor in the *on* state and the donor in the *off* state. The first state listed for each cluster is the all *on* state and last listed is the all *off* state.

N = 2 Cluster			
State	Probability of State	Average single photon emission probability	Average two photon emission probability
BB	F^2	1	$\frac{1}{2}\left(\frac{2k_E}{2k_E+k_T}\right)$
DB	F(1-F)	$\frac{1}{2}$	0
BD	F(1-F)	$\frac{1}{2}\frac{k_E}{k_E+k_T}$	0
DD	$(1-F)^2$	0	0
N = 3 Cluster			
BBB	F^3	1	$\frac{2}{3}\left(\frac{2k_E}{2k_E+k_T}\right)$
DBB	$F^2(1-F)$	$\frac{2}{3}$	$\frac{2}{9}\left(\frac{2k_E}{2k_E+k_T}\right)$
BDB	$F^2(1-F)$	$\frac{1}{3}\left(\frac{2k_E+3k_T}{k_E+2k_T}\right)$	$\frac{2}{9}\left(\frac{k_E(2k_E+3k_T)}{2(k_E+2k_T)(k_E+k_T)}\right)$
BBD	$F^2(1-F)$	$\frac{1}{3}\left(\frac{2k_E}{k_E+k_T}\right)$	$\frac{2}{9}\left(\frac{2k_E^2}{(k_E+k_T)(2k_E+3k_T)}\right)$
DBD	$F(1-F)^2$	$\frac{1}{3}\left(\frac{k_E}{k_E+k_T}\right)$	0
BDD	$F(1-F)^2$	$\frac{1}{3}\left(\frac{k_E}{k_E+2k_T}\right)$	0
DDB	$F(1-F)^2$	$\frac{1}{3}$	0
DDD	$(1-F)^3$	0	0

Table 4.4: States of 4 QD cluster, probability of being in that state given the *on* time fraction F, and the contributions to the SPP and ZDP for that state normalized to QY=1 for the all *on* state case. The states are B for *on* (bright) and D for *off* (dark) and arranged in decreasing energy. For example, the DBDD state for a 4 QD cluster below has the acceptor in the highest band gap QD in the *off* state, the second highest band gap QD in the *on* state, the third highest band gap QD in the *off* state, and the acceptor (lowest band gap QD) in the *off* state. The first state is the all *on* state and last state is the all *off* state.

N = 4 Cluster			
State	Probability of state	Average single photon emission probability	Average two photon emission probability
BBBB	F^4	1	$\frac{3}{4}\left(\frac{2k_E}{2k_E+k_T}\right)$
DBBB	$F^3(1-F)$	$\frac{3}{4}$	$\frac{3}{8}\left(\frac{2k_E}{2k_E+k_T}\right)$
BDBB	$F^3(1-F)$	$\frac{1}{4}\left(\frac{3k_E+8k_T}{k_E+3k_T}\right)$	$\frac{6k_E^2+25k_Ek_T+17k_T^2}{4(k_E+3k_T)(2k_E+k_T)(2k_E+3k_T}$
BBDB	$F^3(1-F)$	$\frac{1}{4}\left(\frac{3k_E+4k_T}{k_E+2k_T}\right)$	$\frac{k_E(3k_E^2+11k_Ek_T+10k_T^2)}{4(k_E+2k_T)(k_E+k_T)(2k_E+5k_T)}$
BBBD	$F^3(1-F)$	$\frac{3}{4}\left(\frac{k_E}{k_E+k_T}\right)$	$\frac{6k_E^2}{8(k_E+k_T)(2k_E+3k_T)}$
DDBB	$F^2(1-F)^2$	$\frac{1}{2}$	$\frac{1}{8}\left(\frac{2k_E}{2k_E+k_T}\right)$
DBDB	$F^2(1-F)^2$	$\frac{2k_E+3k_T}{4(k_E+2k_T)}$	$\frac{1}{8}\left(\frac{k_E(2k_E+3k_T)}{2(k_E+2k_T)(k_E+k_T)}\right)$
BDDB	$F^2(1-F)^2$	$\frac{2k_E+4k_T}{4(k_E+3k_T)}$	$\frac{1}{8}\left(\frac{2k_E(k_E+2k_T)}{(2k_E+2k_T)(k_E+3k_T)}\right)$
DBBD	$F^2(1-F)^2$	$\frac{1}{4}\left(\frac{2k_E}{k_E+k_T}\right)$	$\frac{1}{8}\left(\frac{2k_E^2}{(k_E+k_T)(2k_E+3k_T)}\right)$
BDBD	$F^2(1-F)^2$	$\frac{k_E(2k_E+5k_T)}{4(k_E+k_T)(k_E+k_T)}$	$\frac{k_E^2(k_E+k_T)}{16(k_E+k_T)(k_E+2k_T)(k_E+3k_T)}$
BBDD	$F^2(1-F)^2$	$\frac{2k_E}{4(k_E+2k_T)}$	$\frac{1}{8}\left(\frac{k_E^2}{(k_E+2k_T)^2}\right)$
DDDB	$F(1-F)^3$	$\frac{1}{4}$	0
DDBD	$F(1-F)^3$	$\frac{1}{4}\left(\frac{k_E}{k_E+k_T}\right)$	0
DBDD	$F(1-F)^3$	$\frac{1}{4}\left(\frac{k_E}{k_E+2k_T}\right)$	0
BDDD	$F(1-F)^3$	$\frac{1}{4}\left(\frac{k_E}{k_E+3k_T}\right)$	0
DDDD	$(1-F)^4$	0	0

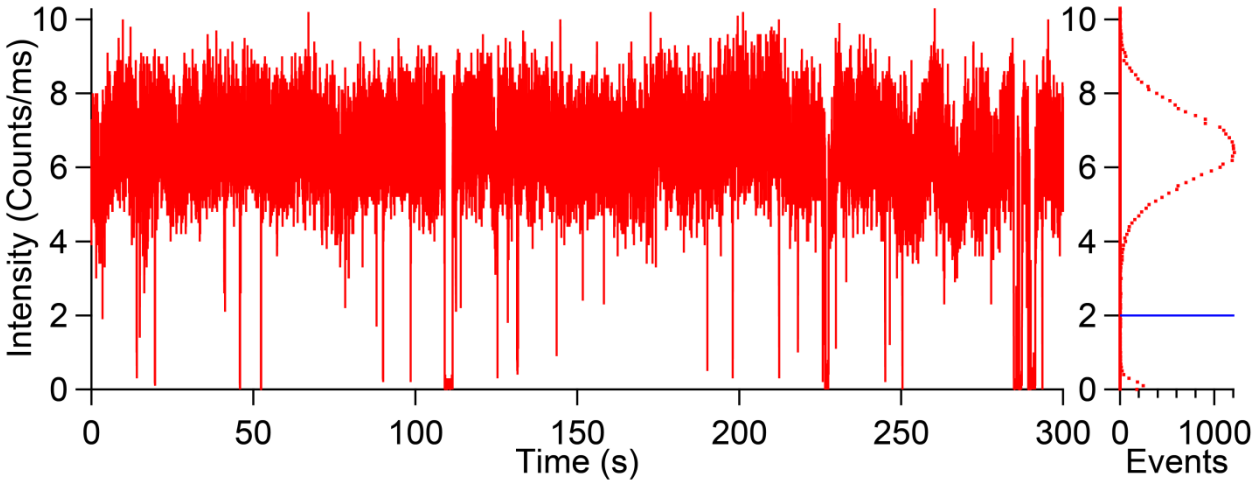

Figure 4.7: Intensity trajectory and histogram for an individual QD. The *on*/*off* threshold is the horizontal blue line in histogram. The amount of time above the threshold divided by the total time of the measurement give the F parameter (0.97 for this trajectory).

noted above in a few special cases, the model results for A/B are generally insensitive to F when its value is not too far from 1.

The ratio of rates $r = k_T/k_E$ in a cluster is fixed by the fluorescence decay histogram for the cluster. As discussed in our previous work,[26] the decay histograms are described well by biexponential decay, with the long lifetime, $\tau_L \approx 1/k_E$, and the short lifetime, $\tau_S \approx 1/(k_E+k_T)$. Thus after fitting the fluorescence decay histograms (Figure 4.8) obtained in two 5-min measurements before and after the CPH measurements we extract the value $r \approx \tau_L/\tau_S$-1. Typical values for τ_L and τ_S are 25 ns and 4ns respectively. The parameter N remains undetermined, so we present the model results of A/B for N = 2,3, and 4 for comparison with the CPH measurements in Table 4.2.

In most cases, the calculated values of the model represent the data very well. One such instance is presented in Figure 4.9. We obtain an A/B ratio of 0.15 for this cluster. The calculated r = 0 CPH, simulating no energy transfer, for the two and four QD cases give A/B ratios of 0.47 and 0.73 respectively, which are far above the measured value. The calculated A/B ratios allowing for energy transfer, using r = 6.1 as obtained from fluorescence data for this cluster, for a two and four QD cluster are 0.12 and 0.18, respectively. Extraordinary conditions would need to hold for the cluster to be represented well under the assumption of no energy transfer: the constituents would have to be in the *off* state 82% of the time (*i.e.*, F = 0.18) to obtain A/B = 0.15 with N = 2. This would be difficult to reconcile with the intensity data from this cluster, which was approximately 2-3 times brighter than individual QDs and not significantly weighted toward the cluster *low* state. Note that a previous study indicated that the blinking behavior of colloidal QDs was not affected by the presence of neighbors in a cluster.[27] In contrast, the energy transfer model accurately describes the observed cluster CPH data, assuming N = 2 to 4, without contradicting other observations.

There are a few cluster CPHs that do not match the predictions of the model. One of these is presented in Figure 4.10. These clusters are exceptionally large, with particularly larger area than the

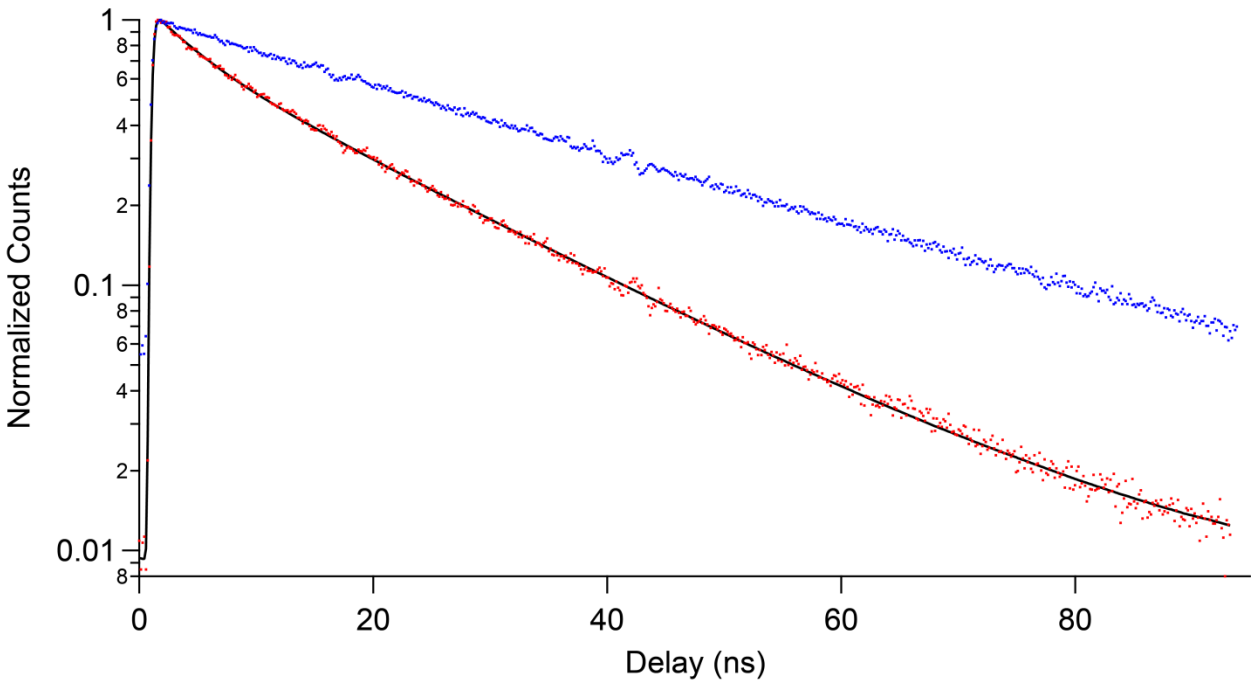

Figure 4.8: Normalized fluorescence decay of an individual QD (blue) and a cluster (red) with a biexponential fit for the cluster (black) showing the relatively large short lifetime component in clusters of QDs. The two lifetimes from the fit were τ_s = 4.8 ns and τ_L = 23.7 ns. The r parameter as calculated from these values is τ_L/τ_s -1 = 4.0.

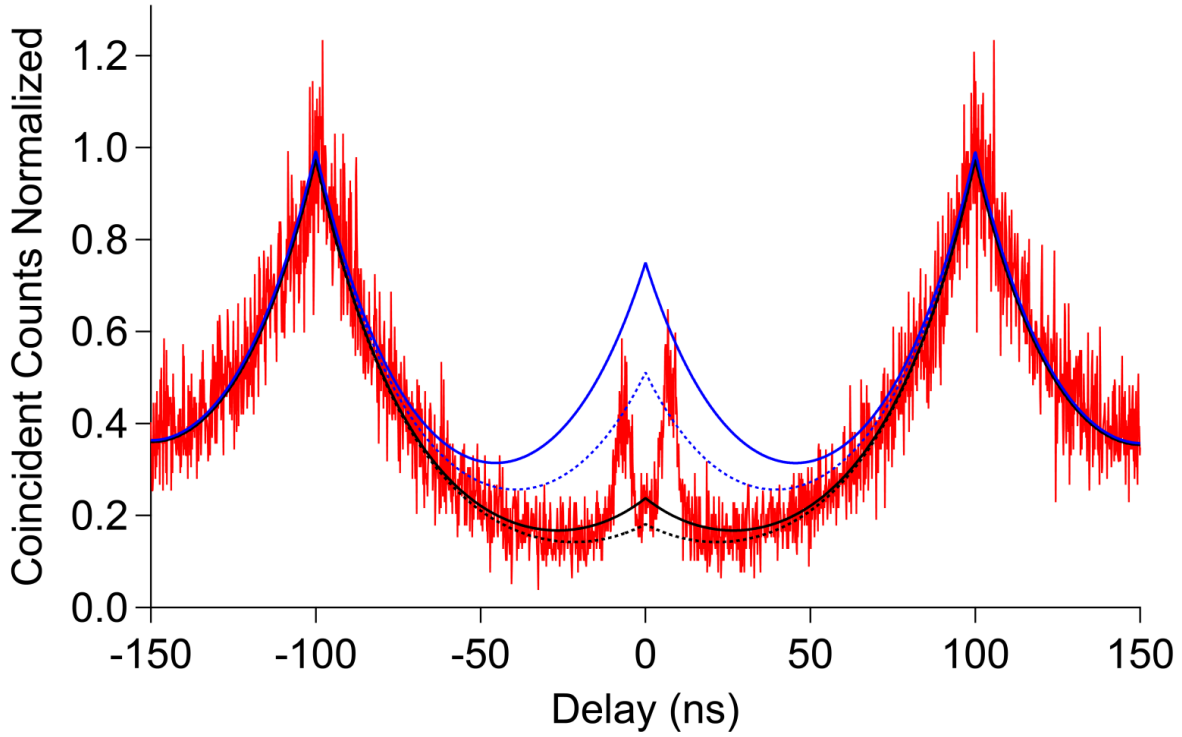

Figure 4.9: Normalized CPH data from a cluster and calculated CPHs. The data were taken at a 10 MHz pulse rate on a cluster (red) and were normalized to the fit amplitude of the SPP. The model parameters were $F = 0.9$ for all calculations, $r = 0$ to simulate non-interacting QDs (blue lines) and $r = 6.1$ to simulate energy transfer (black lines). The fluorescence decay for calculated CPHs was determined from the CPH fit of the data. Solid lines are calculated results for a 4 QD cluster and dotted lines for a 2 QD cluster. The r parameter was obtained from fluorescence measurements before and after the CPH was collected.

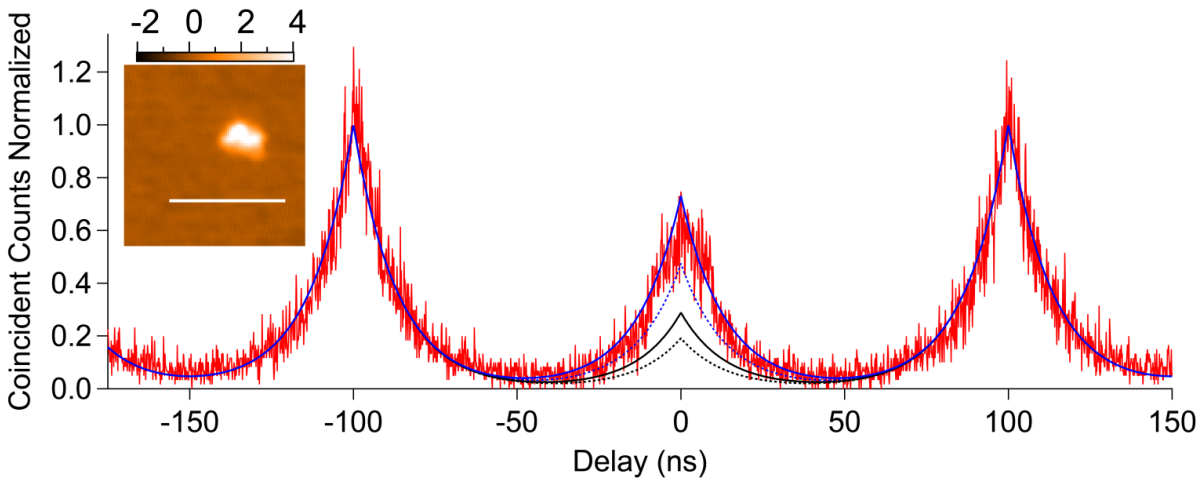

Figure 4.10: Normalized CPH data from a large cluster with calculated CPHs. The data were taken at 10 MHz pulse rate on a large cluster (red) and normalized to the fit amplitude. The model parameters were F = 0.9 for all calculations, r = 0 to simulate non-interacting QDs (blue lines) and r = 3.1 to simulate energy transfer (black lines). The fluorescence decay for calculated CPHs was determined from the CPH fit of the data. Solid lines are calculated results for a 4 QD cluster and dotted lines for a 2 QD cluster. The inset is the AFM image of the large cluster with a 100 nm scale bar. The CPH is much higher than the energy transfer model predicts because the size of the cluster allows for multiple acceptor QDs.

clusters that match the model predictions well. The model considers clusters with QDs that are able to transfer energy to all lower-band gap QDs at the same rate. We postulate that in the large clusters, two or more relatively low band gap QDs are too far from each other for fast energy transfer. This separation reduces the likelihood that two excitons will end up on the same QD and annihilate each other, and the CPH thus will be similar to that of multiple isolated QDs. The effect is not just dependent on size and not expected in all large clusters: A cluster would need to be large enough and have geometry and acceptor positions such that energy is funneled to separate parts of the cluster. The larger a cluster is, the more likely it is that multiple local acceptors will be present.

4.4 Conclusions from Antibunching in Quantum Dot Clusters

This work has examined clusters of close proximity QDs and found antibunching in the coincident photon histograms: the ratio of zero-delay peak to separate-pulse peak amplitudes is less than one would obtain for two isolated QDs in the excitation region. We find that these small compact QD clusters exhibit photon antibunching that is more characteristic of a single emitter than multiple QDs, hence antibunching may not serve as a single, definitive test that an individual QD has been observed. These results can be rationalized within a simple model of energy transfer, in which excitons on separate QDs can transfer to the same QD resulting in the loss of one exciton to fast Auger processes, or an exciton can transfer to an *off* QD. Either process would lead to a reduced signal at zero delay in the coincident photon histogram. The same model has been used to describe other features of small QD cluster fluorescence[26,27] and describes the data presented here in a coherent manner, with exceptions that can be rationalized on physical grounds. At this time, the case for energy transfer in small clusters of nominally monodisperse QDs appears to be incontrovertible. However, these results do not constrain the mechanism of energy transfer, which is yet to be determined. The mechanism of inter-QD energy transfer often invoked by others in studies involving ensembles of monodisperse QDs[28,34,35,40-42] is Förster resonance energy transfer. Our estimates of QD proximity and transfer times presented in this work (<10

nm and typically 2-6 ns), and elsewhere,[26,27] are consistent with a Förster like mechanism, but do not preclude other mechanisms such as Dexter electron transfer.

Chapter 4 References

(1) Kuno, M.; Fromm, D. P.; Hamann, H. F.; Gallagher, A.; Nesbitt, D. J. Nonexponential "Blinking" Kinetics of Single CdSe Quantum Dots: A Universal Power Law Behavior. *J. Chem. Phys.* **2000**, *112*, 3117-3120.

(2) Kuno, M.; Fromm, D. P.; Hamann, H. F.; Gallagher, A.; Nesbitt, D. J. "On"/"Off" Fluorescence Intermittency of Single Semiconductor Quantum Dots. *J. Chem. Phys.* **2001**, *115*, 1028-1040.

(3) Shimizu, K. T.; Neuhauser, R. G.; Leatherdale, C. A.; Empedocles, S. A.; Woo, W. K.; Bawendi, M. G. Blinking Statistics in Single Semiconductor Nanocrystal Quantum Dots. *Phys. Rev. B* **2001**, *63*, 205316.

(4) Kuno, M.; Fromm, D. P.; Johnson, S. T.; Gallagher, A.; Nesbitt, D. J. Modeling Distributed Kinetics in Isolated Semiconductor Quantum Dots. *Phys. Rev. B* **2003**, *67*, 125304.

(5) Stefani, F. D.; Zhong, X. H.; Knoll, W.; Han, M. Y.; Kreiter, M. Memory in Quantum-Dot Photoluminescence Blinking. *New J. Phys.* **2005**, *7*, 197.

(6) Knappenberger, K. L.; Wong, D. B.; Romanyuk, Y. E.; Leone, S. R. Excitation Wavelength Dependence of Fluorescence Intermittency in CdSe/ZnS Core/Shell Quantum Dots. *Nano Lett.* **2007**, *7*, 3869-3874.

(7) Frantsuzov, P.; Kuno, M.; Janko, B.; Marcus, R. A. Universal Emission Intermittency in Quantum Dots, Nanorods and Nanowires. *Nat. Phys.* **2008**, *4*, 519-522.

(8) Lee, S. F.; Osborne, M. A. Brightening, Blinking, Bluing and Bleaching in the Life of a Quantum Dot: Friend or Foe? *ChemPhysChem* **2009**, *10*, 2174-2191.

(9) Rosen, S.; Schwartz, O.; Oron, D. Transient Fluorescence of the Off State in Blinking CdSe/CdS/ZnS Semiconductor Nanocrystals Is Not Governed by Auger Recombination. *Phys. Rev. Lett.* **2010**, *104*, 157404.

(10) Volkan-Kacso, S.; Frantsuzov, P. A.; Janko, B. Correlations Between Subsequent Blinking Events in Single Quantum Dots. *Nano Lett.* **2010**, *10*, 2761-2765.

(11) Zhao, J.; Nair, G.; Fisher, B. R.; Bawendi, M. G. Challenge to the Charging Model of Semiconductor-Nanocrystal Fluorescence Intermittency from Off-State Quantum Yields and Multiexciton Blinking. *Phys. Rev. Lett.* **2010**, *104*, 157403.

(12) Galland, C.; Ghosh, Y.; Steinbruck, A.; Sykora, M.; Hollingsworth, J. A.; Klimov, V. I.; Htoon, H. Two Types of Luminescence Blinking Revealed by Spectroelectrochemistry of Single Quantum Dots. *Nature* **2011**, *479*, 203-207.

(13) Lounis, B.; Bechtel, H. A.; Gerion, D.; Alivisatos, P.; Moerner, W. E. Photon Antibunching in Single Cdse/Zns Quantum Dot Fluorescence. *Chem. Phys. Lett.* **2000**, *329*, 399-404.

(14) Messin, G.; Hermier, J. P.; Giacobino, E.; Desbiolles, P.; Dahan, M. Bunching and Antibunching in The Fluorescence of Semiconductor Nanocrystals. *Opt. Lett.* **2001**, *26*, 1891-1893.

(15) Santori, C.; Pelton, M.; Solomon, G.; Dale, Y.; Yamamoto, E. Triggered Single Photons From a Quantum Dot. *Phys. Rev. Lett.* **2001**, *86*, 1502-1505.

(16) Zwiller, V.; Blom, H.; Jonsson, P.; Panev, N.; Jeppesen, S.; Tsegaye, T.; Goobar, E.; Pistol, M. E.; Samuelson, L.; Bjork, G. Single Quantum Dots Emit Single Photons at a Time: Antibunching Experiments. *Appl. Phys. Lett.* **2001**, *78*, 2476-2478.

(17) Michler, P.; Imamoglu, A.; Mason, M. D.; Carson, P. J.; Strouse, G. F.; Buratto, S. K. Quantum Correlation Among Photons from a Single Quantum Dot at Room Temperature. *Nature* **2000**, *406*, 968-970.

(18) Nair, G.; Zhao, J.; Bawendi, M. G. Biexciton Quantum Yield of Single Semiconductor Nanocrystals from Photon Statistics. *Nano Lett.* **2011**, *11*, 1136-1140.

(19) Pelton, M.; Smith, G.; Scherer, N. F.; Marcus, R. A. Evidence for a Diffusion-Controlled Mechanism for Fluorescence Blinking of Colloidal Quantum Dots. *Proc. Natl. Acad. Sci. U. S. A.* **2007**, *104*, 14249-14254.

(20) Frantsuzov, P. A.; Volkan-Kacso, S.; Janko, B. Model of Fluorescence Intermittency of Single Colloidal Semiconductor Quantum Dots Using Multiple Recombination Centers. *Phys. Rev. Lett.* **2009**, *103*, 207402.

(21) Vela, J.; Htoon, H.; Chen, Y. F.; Park, Y. S.; Ghosh, Y.; Goodwin, P. M.; Werner, J. H.; Wells, N. P.; Casson, J. L.; Hollingsworth, J. A. Effect of Shell Thickness and Composition on Blinking Suppression and the Blinking Mechanism in 'Giant' CdSe/CdS Nanocrystal Quantum Dots. *J. Biophotonics* **2010**, *3*, 706-717.

(22) Basche, T.; Moerner, W. E.; Orrit, M.; Talon, H. Photon Antibunching in the Fluorescence of a Single Dye Molecule Trapped in a Solid. *Phys. Rev. Lett.* **1992**, *69*, 1516-1519.

(23) Ambrose, W. P.; Goodwin, P. M.; Enderlein, J.; Semin, D. J.; Martin, J. C.; Keller, R. A. Fluorescence Photon Antibunching from Single Molecules on a Surface. *Chem. Phys. Lett.* **1997**, *269*, 365-370.

(24) Weston, K. D.; Dyck, M.; Tinnefeld, P.; Muller, C.; Herten, D. P.; Sauer, M. Measuring the Number of Independent Emitters in Single-Molecule Fluorescence Images and Trajectories Using Coincident Photons. *Anal. Chem.* **2002**, *74*, 5342-5349.

(25) Yu, M.; Van Orden, A. Enhanced Fluorescence Intermittency of CdSe-ZnS Quantum-Dot Clusters. *Phys. Rev. Lett.* **2006**, *97*, 237402.

(26) Shepherd, D. P.; Whitcomb, K. J.; Milligan, K. K.; Goodwin, P. M.; Gelfand, M. P.; Van Orden, A. Fluorescence Intermittency and Energy Transfer in Small Clusters of Semiconductor Quantum Dots. *J. Phys. Chem. C* **2010**, *114*, 14831-14837.

(27) Whitcomb, K. J.; Ryan, D. P.; Gelfand, M. P.; Van Orden, A. Blinking Statistics of Small Clusters of Semiconductor Nanocrystals. *J. Phys. Chem. C* **2013**, *117*, 25761-25768.

(28) Tang, Z. Y.; Ozturk, B.; Wang, Y.; Kotov, N. A. Simple Preparation Strategy and One-Dimensional Energy Transfer in CdTe Nanoparticle Chains. *J. Phys. Chem. B* **2004**, *108*, 6927-6931.

(29) Kagan, C. R.; Murray, C. B.; Nirmal, M.; Bawendi, M. G. Electronic Energy Transfer in CdSe Quantum Dot Solids. *Phys. Rev. Lett.* **1996**, *76*, 1517-1520.

(30) Wargnier, R.; Baranov, A. V.; Maslov, V. G.; Stsiapura, V.; Artemyev, M.; Pluot, M.; Sukhanova, A.; Nabiev, I. Energy Transfer in Aqueous Solutions of Oppositely Charged CdSe/ZnS Core/Shell Quantum Dots and in Quantum Dot-Nanogold Assemblies. *Nano Lett.* **2004**, *4*, 451-457.

(31) Franzl, T.; Shavel, A.; Rogach, A. L.; Gaponik, N.; Klar, T. A.; Eychmuller, A.; Feldmann, J. High-Rate Unidirectional Energy Transfer in Directly Assembled CdTe Nanocrystal Bilayers. *Small* **2005**, *1*, 392-395.

(32) Guo, L.; Krauss, T. D.; Poitras, C. B.; Lipson, M.; Teng, X. W.; Yang, H. Energy Transfer Between Colloidal Semiconductor Nanocrystals in an Optical Microcavity. *Appl. Phys. Lett.* **2006**, *89*, 061104.

(33) Mork, A. J.; Weidman, M. C.; Prins, F.; Tisdale, W. A. Magnitude of the Forster Radius in Colloidal Quantum Dot Solids. *J. Phys. Chem. C* **2014**, *118*, 13920-13928.

(34) Achermann, M.; Petruska, M. A.; Crooker, S. A.; Klimov, V. I. Picosecond Energy Transfer in Quantum Dot Langmuir-Blodgett Nanoassemblies. *J. Phys. Chem. B* **2003**, *107*, 13782-13787.

(35) Crooker, S. A.; Hollingsworth, J. A.; Tretiak, S.; Klimov, V. I. Spectrally Resolved Dynamics of Energy Transfer in Quantum-Dot Assemblies: Towards Engineered Energy Flows in Artificial Materials. *Phys. Rev. Lett.* **2002**, *89*, 186802.

(36) Franzl, T.; Koktysh, D. S.; Klar, T. A.; Rogach, A. L.; Feldmann, J.; Gaponik, N. Fast energy transfer in layer-by-layer assembled CdTe nanocrystal bilayers. *Appl. Phys. Lett.* **2004**, *84*, 2904-2906.

(37) Kagan, C. R.; Murray, C. B.; Bawendi, M. G. Long-range resonance transfer of electronic excitations in close-packed CdSe quantum-dot solids. *Phys. Rev. B* **1996**, *54*, 8633-8643.

(38) Kim, D.; Okahara, S.; Nakayama, M.; Shim, Y. Experimental verification of Forster energy transfer between semiconductor quantum dots. *Phys. Rev. B* **2008**, *78*, 153301.

(39) Lunz, M.; Bradley, A. L.; Chen, W. Y.; Gun'ko, Y. K. Two-Dimensional Forster Resonant Energy Transfer in a Mixed Quantum Dot Monolayer: Experiment and Theory. *J. Phys. Chem. C* **2009**, *113*, 3084-3088.

(40) Koole, R.; Liljeroth, P.; Donega, C. D.; Vanmaekelbergh, D.; Meijerink, A. Electronic Coupling and Exciton Energy Transfer in CdTe Quantum-Dot Molecules. *J. Am. Chem. Soc.* **2006**, *128*, 10436-10441.

(41) Clark, S. W.; Harbold, J. M.; Wise, F. W. Resonant Energy Transfer in PbS Quantum Dots. *J. Phys. Chem. C* **2007**, *111*, 7302-7305.

(42) Bose, R.; McMillan, J. F.; Gao, J.; Rickey, K. M.; Chen, C. J.; Talapin, D. V.; Murray, C. B.; Wong, C. W. Temperature-Tuning of Near-Infrared Monodisperse Quantum Dot Solids at 1.5 μm for Controllable Forster Energy Transfer. *Nano Lett.* **2008**, *8*, 2006-2011.

(43) Williams, K. J.; Tisdale, W. A.; Leschkies, K. S.; Haugstad, G.; Norris, D. J.; Aydil, E. S.; Zhu, X. Y. Strong Electronic Coupling in Two-Dimensional Assemblies of Colloidal PbSe Quantum Dots. *ACS Nano* **2009**, *3*, 1532-1538.

(44) Koole, R.; Luigjes, B.; Tachiya, M.; Pool, R.; Vlugt, T. J. H.; Donega, C. D. M.; Meijerink, A.; Vanmaekelbergh, D. Differences in cross-link chemistry between rigid and flexible dithiol molecules revealed by optical studies of CdTe quantum dots. *J. Phys. Chem. C* **2007**, *111*, 11208-11215.

(45) Xu, X. X.; Stottinger, S.; Battagliarin, G.; Hinze, G.; Mugnaioli, E.; Li, C.; Mullen, K.; Basche, T. Assembly and Separation of Semiconductor Quantum Dot Dimers and Trimers. *J. Am. Chem. Soc.* **2011**, *133*, 18062-18065.

(46) Querner, C.; Wang, S.; Healy, K.; Fairfield, J. A.; Fischbein, M. A.; Drndic, M. Fluorescence Dynamics of Semiconductor Nanorod Clusters Studied by Correlated Atomic Force, Transmission Electron, and Fluorescence Microscopy. *J. Phys. Chem. C* **2008**, *112*, 19945-19956.

(47) Wang, S.; Querner, C.; Fischbein, M. D.; Willis, L.; Novikov, D. S.; Crouch, C. H.; Drndic, M. Blinking Statistics Correlated with Nanoparticle Number. *Nano Lett.* **2008**, *8*, 4020-4026.

(48) Wang, S.; Querner, C.; Dadosh, T.; Crouch, C. H.; Novikov, D. S.; Drndic, M. Collective Fluorescence Enhancement in Nanoparticle Clusters. *Nat Commun* **2011**, *2*, 364.

(49) Kang, H.; Clarke, M. L.; Lacerda, S. H. D.; Karim, A.; Pease, L. F.; Hwang, J. Multimodal Optical Studies of Single and Clustered Colloidal Quantum Dots for the Long-Term Optical Property Evaluation of Quantum Dot-Based Molecular Imaging Phantoms. *Biomed. Opt. Express* **2012**, *3*, 1312-1325.

(50) Danek, M.; Jensen, K. F.; Murray, C. B.; Bawendi, M. G. Synthesis of luminescent thin-film CdSe/ZnSe quantum dot composites using CdSe quantum dots passivated with an overlayer of ZnSe. *Chem. Mater.* **1996**, *8*, 173-180.

(51) Kolodny, L. A.; Willard, D. M.; Carillo, L. L.; Nelson, M. W.; Van Orden, A. Spatially Correlated Fluorescence/AFM of Individual Nanosized Particles and Biomolecules. *Anal. Chem.* **2001**, *73*, 1959-1966.

Chapter 5

Conclusions and Future Work

My major contributions to the field of single molecule study of quantum dot interactions are the validations of the independent unaltered blinking assumption in the energy transfer model and the observation of antibunching in small clusters as described by our energy transfer model. Each of these accomplishments has broad implications to the field of optoelectronics, imaging, and single molecule studies when quantum dots are used in these applications. Future work should be directed at interrogating the mechanism using single molecule work to either confirm the Förster mechanism that others have implicated or discover other factors in the energy transfer between nominally monodisperse quantum dot clusters. There are two current efforts in our group to do this, both impacted by my work. One attempt involves single molecule fluorescence correlated with transmission electron microscopy. The other entails creating well controlled clusters of known size and geometry for single molecule study. My work allows more confident analysis of fluorescence via antibunching which aids these efforts greatly.

5.1 Conclusions

Individual QD blinking is well known and studied but the blinking behavior of close proximity QDs has not been extensively investigated and no comprehensive study on the blinking memory, threshold effects, or *off* statistics had been done on small clusters of QDs until my 2013 work.[1] The finding that QD blinking is unaltered by the proximity of other QDs is not obvious, especially considering the work by the Drndic group on CdSe nanorods[2,3] which showed altered blinking when nanorods grouped together. My work also indicates that the mechanism of energy transfer does not interact with the mechanism of blinking by showing that the blinking statistics of the cluster are very similar to individual QD blinking. This implies that the close proximity of other QDs in the broad category of optoelectronics does not affect the blinking, and therefore potential energy loss possibilities in close

packed architectures in solar applications,[4,5] lasing,[6,7] and photodetectors[8,9] which typically use QD films. The energy transfer itself, however, can lead to more loss possibilities when energy from a QD is transferred to an *off* QD but the probability that the QD will be *off* is unaffected. Applications that extract or separate excitons much faster than the transfer time, as in some solar applications, should not be affected by the energy transfer. Other applications, primarily lasing and imaging, that use the emission of the QDs will be affected because the emission is typically much slower than the transfer which allows for energy to transfer to *off* QDs and is then lost.

My work on the antibunched fluorescence from multiple emitters[10] has wide ranging impacts on any research that studies fluorescence from individual QDs where close proximity QD clusters are possible. Antibunching is thought of the single conclusive evidence that an individual emitter is present in the excitation region. Antibunching has typically been a reliable indicator of an individual emitter for dyes and QDs because the 0 delay peak ratio or the magnitude of the 2nd order autocorrelation at 0 delay is below ½ for any individual emitter. Antibunching has been used in this way in very important work on QD blinking[11] and has been the subject of study recently in QDs.[12-14] In my 2014 work on cluster antibunching we see antibunching from multiple QD emitters confirmed by correlated AFM measurements. We are able to predict the degree of antibunching relatively well considering the number of QDs in the cluster isn't known exactly. The clusters can be distinguished from individual QDs in my work; however, the clusters would easily be mistaken for individual QDs with the above criteria. In fact, the degree of antibunching in small clusters of QDs is more characteristic of an individual emitter than multiple emitters.

The antibunching in small clusters of QDs also has implications for energy transfer among nominally monodisperse QDs as well. Each small cluster observed showed significant antibunching that was predictable using the fluorescence lifetime of the cluster. These predictions are made with the assumptions of the energy transfer model, namely, that energy transfer can occur from any QD in the cluster to any QD with a lower band gap and that there are no QDs that cannot transfer to a lower band

gap QD except the lowest band gap QD, the acceptor. This assumption conflicts with the predictions of Crooker et al.[15] in which energy transfer among nominally monodisperse QDs was found to occur between QDs with at least a 55 meV band gap disparity. Our results are surprising because Crooker's work makes logical sense. The FRET mechanism requires spectral overlap between the donor and acceptor. Although there is dispersion in the energies of QDs in a given sample, not all clusters should have QDs that have another QD to donate energy to. The only exceptions to the model observed in my work are in exceptionally large clusters where multiple local acceptors are presumed to be too far away to interact. If energy transfer can only occur between band gaps with a 55 meV disparity, then smaller clusters should be more likely to have a pair of low band gap QDs that cannot transfer to each other because of a lack of spectral overlap, and therefore, should not exhibit the degree of antibunching that all small QD clusters do in my work. The mechanism Crooker et al. implicate in their study is Förster resonance energy transfer (FRET) mechanism. In my work, the AFM correlation is able to distinguish individual QDs from clusters, but has never been able to observe individual members of a cluster nor the distances between QDs, and therefore, we have not been able to provide evidence for a specific mechanism for the energy transfer observed. Our observations are not in contradiction with FRET given the rates and distances known, but the efficiency observed is nonetheless surprising given the monodispersity and small cluster sizes.

5.2 Future Directions

Recent work by Mork et al.[16] has indicated that FRET with the assumption of random dipole orientations and dipole only coupling does not describe energy transfer between different sized donors and acceptors. This finding is despite previous work indicating that the FRET mechanism assuming random dipole interactions described energy transfer among QDs well,[15,17-23] however, in their work[16] careful measurements were performed with high resolution transmission electron microscopy (TEM) on mixed films of donors and acceptors. Their main finding was that the FRET transfer rate was approximately an order of magnitude faster than predicted by assuming random dipole orientation. This

may be related to the surprisingly efficient energy transfer we see that results in all clusters showing antibunching. It is also a phenomenon that may be better suited to single molecule measurements. Ensemble measurements obtain average information over many systems probed at once. Sample through-put is relatively high, but if the sample properties are not well controlled, e.g. the distance between QDs, the ensemble averaging will make obtaining specific information about the mechanism difficult. Single molecule measurements remove the need for sample control by measuring a very small sample very well.

The next set of experiments on nominally monodisperse QD clusters should be to determine the mechanism of energy transfer by obtaining the distance dependence of the energy transfer rate. The FRET mechanism has a $1/r^6$ (r is the center to center distance) dependence of the transfer efficiency. If we were able to measure the distance between QDs in variety of clusters and the FRET efficiency with the correlated fluorescence measurements we would be able to determine the distance dependence and confirm the Förster mechanism as the energy transfer mechanism. We would also be able to determine the Förster radius and therefore, the FRET parameters to possibly corroborate the findings of Mork et al.[16] or the traditional random dipole assumptions of others.[15,17-23]

We are currently able to collect such data in principle. The Drndic group has done fluorescence correlated TEM experiments on CdSe nanorod clusters,[2,3] which were found by correlating fluorescence from a gold patterned TEM grid with a TEM image. Our instrument could correlate fluorescence from an area on a TEM grid using the AFM to mark (rip) the grid around a fluorescence measurement and find the QD cluster in the area near the marks in the TEM. The antibunching signal, fluorescence intensity, autocorrelation, and lifetime of the fluorescence are able to distinguish clusters from individual QDs before a TEM measurement, which is the more challenging measurement. My antibunching work can also give a reasonable estimate of the cluster size without AFM correlation, allowing suitable clusters to be found spectroscopically before attempts at TEM correlation making such a project much more feasible.

Another experimental goal in progress, primarily by Duncan Ryan, is clusters of known size and geometry, e.g. 2 QD dimers, using an established centrifugation technique for single molecule study. The work by Wu et al.[24] has shown that these dimers could be prepared in high yield with this technique, but the measurements on the system in their work were ensemble measurements. Such dimers would provide us with a well-known system to study with single molecule techniques that would not only allow us to interrogate the energy transfer mechanism, but also answer one more key question; does the identity of the acceptor remain the same? The work by Neuhauser et al.[25] showed spectral drift in individual QDs which raises the question of how much the energy transfer rate fluctuates and can a QD drift enough to change from acceptor to donor? With a well characterized dimer, the distance between QDs can be determined from an ensemble measurement, the orientation assumed to be constant, and the energy transfer rate can be measured with single molecule fluorescence lifetime to determine if this rate fluctuates over time. This can be better determined in a dimer because there are fewer fluorescence states of the cluster. A dimer only has one fluorescent *low* state and the energy transfer rate of this state is unambiguous since the ratio of donor to acceptor is fixed at 1:1 and the high and low states can be easily identified so the consistency of the rate can as a function of time can be examined clearly.

Chapter 5 References

(1) Whitcomb, K. J.; Ryan, D. P.; Gelfand, M. P.; Van Orden, A. Blinking Statistics of Small Clusters of Semiconductor Nanocrystals. *J. Phys. Chem. C* **2013**, *117*, 25761-25768.

(2) Wang, S.; Querner, C.; Fischbein, M. D.; Willis, L.; Novikov, D. S.; Crouch, C. H.; Drndic, M. Blinking Statistics Correlated with Nanoparticle Number. *Nano Lett.* **2008**, *8*, 4020-4026.

(3) Wang, S. Y.; Querner, C.; Dadosh, T.; Crouch, C. H.; Novikov, D. S.; Drndic, M. Collective Fluorescence Enhancement in Nanoparticle Clusters. *Nat. Commun.* **2011**, *2*, 364.

(4) Kamat, P. V. Quantum Dot Solar Cells. The Next Big Thing in Photovoltaics. *J. Phys. Chem. Lett.* **2013**, *4*, 908-918.

(5) Nozik, A. J.; Beard, M. C.; Luther, J. M.; Law, M.; Ellingson, R. J.; Johnson, J. C. Semiconductor Quantum Dots and Quantum Dot Arrays and Applications of Multiple Exciton Generation to Third-Generation Photovoltaic Solar Cells. *Chem. Rev.* **2010**, *110*, 6873-6890.

(6) Chen, Y. J.; Herrnsdorf, J.; Guilhabert, B.; Zhang, Y. F.; Watson, I. M.; Gu, E. D.; Laurand, N.; Dawson, M. D. Colloidal Quantum Dot Random Laser. *Opt. Express* **2011**, *19*, 2996-3003.

(7) Dang, C.; Roh, K.; Lee, J.; Breen, C.; Steckel, J. S.; Coe-Sullivan, S.; Nurmikko, A. Red, Green, and Blue Laser Action in Solid Colloidal Quantum Dot Films. *2012 12th Ieee Conference on Nanotechnology (Ieee-Nano)* **2012**.

(8) Clifford, J. P.; Konstantatos, G.; Johnston, K. W.; Hoogland, S.; Levina, L.; Sargent, E. H. Fast, Sensitive and Spectrally Tuneable Colloidal Quantum-Dot Photodetectors. *Nat. Nanotechnol.* **2009**, *4*, 40-44.

(9) Konstantatos, G.; Clifford, J.; Levina, L.; Sargent, E. H. Sensitive Solution-Processed Visible-Wavelength Photodetectors. *Nat. Photonics* **2007**, *1*, 531-534.

(10) Whitcomb, K. J.; Geisenhoff, J. Q.; Ryan, D. P.; Gelfand, M. P.; Van Orden, A. Photon Antibunching in Small Clusters of CdSe/ZnS Core/Shell Quantum Dots. *J. Phys. Chem. B* **2014**, *Article ASAP*.

(11) Galland, C.; Ghosh, Y.; Steinbruck, A.; Sykora, M.; Hollingsworth, J. A.; Klimov, V. I.; Htoon, H. Two Types of Luminescence Blinking Revealed by Spectroelectrochemistry of Single Quantum Dots. *Nature* **2011**, *479*, 203-207.

(12) Nair, G.; Zhao, J.; Bawendi, M. G. Biexciton Quantum Yield of Single Semiconductor Nanocrystals from Photon Statistics. *Nano Lett.* **2011**, *11*, 1136-1140.

(13) Galland, C.; Ghosh, Y.; Steinbruck, A.; Hollingsworth, J. A.; Htoon, H.; Klimov, V. I. Lifetime Blinking in Nonblinking Nanocrystal Quantum Dots. *Nat. Commun.* **2012**, *3*, 908.

(14) Park, Y. S.; Ghosh, Y.; Chen, Y.; Piryatinski, A.; Xu, P.; Mack, N. H.; Wang, H. L.; Klimov, V. I.; Hollingsworth, J. A.; Htoon, H. Super-Poissonian Statistics of Photon Emission from Single CdSe-CdS Core-Shell Nanocrystals Coupled to Metal Nanostructures. *Phys. Rev. Lett.* **2013**, *110*, 117401.

(15) Crooker, S. A.; Hollingsworth, J. A.; Tretiak, S.; Klimov, V. I. Spectrally Resolved Dynamics of Energy Transfer in Quantum-Dot Assemblies: Towards Engineered Energy Flows in Artificial Materials. *Phys. Rev. Lett.* **2002**, *89*, 186802.

(16) Mork, A. J.; Weidman, M. C.; Prins, F.; Tisdale, W. A. Magnitude of the Forster Radius in Colloidal Quantum Dot Solids. *J. Phys. Chem. C* **2014**, *118*, 13920-13928.

(17) Kagan, C. R.; Murray, C. B.; Bawendi, M. G. Long-range resonance transfer of electronic excitations in close-packed CdSe quantum-dot solids. *Phys. Rev. B* **1996**, *54*, 8633-8643.

(18) Kagan, C. R.; Murray, C. B.; Nirmal, M.; Bawendi, M. G. Electronic Energy Transfer in CdSe Quantum Dot Solids. *Phys. Rev. Lett.* **1996**, *76*, 1517-1520.

(19) Achermann, M.; Petruska, M. A.; Crooker, S. A.; Klimov, V. I. Picosecond Energy Transfer in Quantum Dot Langmuir-Blodgett Nanoassemblies. *J. Phys. Chem. B* **2003**, *107*, 13782-13787.

(20) Franzl, T.; Koktysh, D. S.; Klar, T. A.; Rogach, A. L.; Feldmann, J.; Gaponik, N. Fast energy transfer in layer-by-layer assembled CdTe nanocrystal bilayers. *Appl. Phys. Lett.* **2004**, *84*, 2904-2906.

(21) Franzl, T.; Shavel, A.; Rogach, A. L.; Gaponik, N.; Klar, T. A.; Eychmuller, A.; Feldmann, J. High-Rate Unidirectional Energy Transfer in Directly Assembled CdTe Nanocrystal Bilayers. *Small* **2005**, *1*, 392-395.

(22) Kim, D.; Okahara, S.; Nakayama, M.; Shim, Y. Experimental verification of Forster energy transfer between semiconductor quantum dots. *Phys. Rev. B* **2008**, *78*, 153301.

(23) Lunz, M.; Bradley, A. L.; Chen, W. Y.; Gun'ko, Y. K. Two-Dimensional Forster Resonant Energy Transfer in a Mixed Quantum Dot Monolayer: Experiment and Theory. *J. Phys. Chem. C* **2009**, *113*, 3084-3088.

(24) Xu, X. X.; Stottinger, S.; Battagliarin, G.; Hinze, G.; Mugnaioli, E.; Li, C.; Mullen, K.; Basche, T. Assembly and Separation of Semiconductor Quantum Dot Dimers and Trimers. *J. Am. Chem. Soc.* **2011**, *133*, 18062-18065.

(25) Neuhauser, R. G.; Shimizu, K. T.; Woo, W. K.; Empedocles, S. A.; Bawendi, M. G. Correlation Between Fluorescence Intermittency and Spectral Diffusion in Single Semiconductor Quantum Dots. *Phys. Rev. Lett.* **2000**, *85*, 3301-3304.